KEK-TH-1426

Tau and muon lepton flavor violations in the littlest Higgs model with T parity

Toru Goto,[1,*] Yasuhiro Okada,[1,2,†] and Yasuhiro Yamamoto[1,2,‡]

[1] *KEK Theory Center, Institute of Particle and Nuclear Studies, KEK, Tsukuba, Ibaraki 305-0801, Japan*

[2] *Department of Particle and Nuclear Physics, The Graduate University for Advanced Studies (Sokendai), Tsukuba, Ibaraki 305-0801, Japan*

(Dated: April 27, 2011)

Abstract

Lepton flavor violation in τ and μ processes is studied in the littlest Higgs model with T parity. We consider various asymmetries defined in polarized τ and μ decays. Correlations among branching ratios and asymmetries are shown in the following lepton flavor violation processes: $\mu^+ \to e^+\gamma$, $\mu^+ \to e^+e^+e^-$, $\mu^- A \to e^- A$ (A = Al, Ti, Au and Pb), $\tau^+ \to \mu^+\gamma$, $\tau^+ \to \mu^+\mu^+\mu^-$, $\tau^+ \to \mu^+e^+e^-$, $\tau^+ \to \mu^+ P$ ($P = \pi^0$, η and η'), $\tau^+ \to \mu^+ V$ ($V = \rho^0$, ω and ϕ), $\tau^+ \to e^+\gamma$, $\tau^+ \to e^+e^+e^-$, $\tau^+ \to e^+\mu^+\mu^-$, $\tau^+ \to e^+ P$, $\tau^+ \to e^+ V$, $\tau^+ \to \mu^+\mu^+e^-$ and $\tau^+ \to e^+e^+\mu^-$. It is shown that large parity asymmetries and time-reversal asymmetries are allowed in $\mu^+ \to e^+e^+e^-$. For τ lepton flavor violation processes, sizable asymmetries are possible reflecting characteristic chirality structure of lepton flavor violating interactions in this model.

*E-mail address:tgoto@post.kek.jp

†E-mail address:yasuhiro.okada@kek.jp

‡E-mail address:yamayasu@post.kek.jp

I. INTRODUCTION

Although the standard model (SM) is successful in describing almost all experimental results of high energy physics in terms of gauge theory, the dynamics responsible for the elerctroweak symmetry breaking is unknown. In the minimal version of the Higgs sector, one Higgs doublet field is introduced as an effective description of the dynamics below some cutoff scale Λ . Constraints from electroweak precision measurements indicate that Λ is at least beyond 3 TeV. On the other hand, this scale already introduces a fine-tuning problem of the Higgs mass term at the $O(1)$ % level. This is called a little hierarchy problem [1].

Little Higgs models [2] were proposed as a solution to the little hierarchy problem. In these models, the Higgs doublet field appears as pseudo Nambu-Goldstone (NG) bosons of new strong dynamics at the cutoff scale. A remarkable property is that the one-loop quadratic divergence to the renormalization of the Higgs mass term is cancelled by a proper choice of global and local symmetries, so that the cutoff scale can be pushed to $O(10)$TeV without a severe fine-tuning. A simple case is called the littlest Higgs model [3] where the Higgs field is realized as a part of the NG bosons associated with the global symmetry breaking of SU(5) to SO(5) and the gauge symmetry is $[\mathrm{SU}(2)\times\mathrm{U}(1)]^2$. Then the quadratic divergence of the Higgs mass term in the SM is cancelled by the extra gauge bosons and the heavy partner of the top quark. Subsequent studies [4], however, showed that these heavy partners need to be heavier than several TeV to satisfy severe constraints imposed by precise electroweak measurements, hence reintroducing some degree of the fine-tuning problem. In the littlest Higgs model with T parity (LHT) [5], the model is extended to have a Z_2 parity so that the heavy gauge bosons assigned to be T-odd particles do not directly couple with a pair of the SM fermions, and the phenomenological constraints are somewhat relaxed.

Flavor physics provides an interesting possibility to explore the LHT. In order to assign T parity, we need to introduce extra fermions (T-odd fermions) which are left-handed SU(2) doublets. Then, the flavor transition can arise in the vertices of heavy gauge bosons, T-odd fermions and ordinary SM fermions. There are two 3×3 unitary matrices describing these flavor transitions associated with quark and lepton sectors besides the ordinary flavor mixing matrices in the quark and lepton sectors i.e. the Cabibbo-Kobayashi-Maskawa (CKM) [6] and Pontecorvo-Maki-Nakagawa-Sakata (PMNS) [7] matrices. These matrices are new sources of flavor changing neutral current (FCNC) processes in the quark sector and

lepton flavor violating (LFV) processes in the charged lepton sector. In the early literature on this subject various observable quantities of FCNC and LFV processes were calculated in the LHT and showed that the effects of T-odd partners can be sizable and the correlations among various observable quantities can be different from other new physics model such as supersymmetric (SUSY) models [8–12]. It was pointed out later that calculations missed a type of diagrams and the logarithmic dependences on the cutoff scale in the FCNC and LFV amplitudes disappear thanks to new contributions [13, 14], thus reducing theoretical ambiguity associated with the physics at the ultraviolet cutoff scale. Branching ratios of various FCNC and LFV processes were reevaluated including the new contributions [15, 16]. The qualitative feature turned out to be similar to the previous calculation though there were sizable changes at the quantitative level.

In this paper, we present the results of further studies in tau and muon LFV processes. In addition to branching fractions, we also study observables defined with the help of polarizations of the initial muon and tau lepton [17, 18]. Polarized muon experiments can be done using surface muon beams that are 100% polarized in the opposite direction of the μ^+ momentum. In fact, a $\mu^+ \to e^+\gamma$ experiment with initial muon polarization is under consideration [19]. In the tau pair production at e^+ e^- colliders, the polarization information can be obtained by taking an angular correlation with tau decays on the opposite side [18]. The study of polarized tau decays is also being considered for the $\tau^+ \to \mu^+\mu^+\mu^-$ process at the CERN Large Hadron Collider (LHC) where we can utilize the tau polarization from W decays [20]. In the following, we consider the processes $\mu^+ \to e^+\gamma$, $\mu^+ \to e^+e^+e^-$, $\mu^- A \to e^- A$ (A = Al, Ti, Au and Pb), $\tau^+ \to \mu^+\gamma$, $\tau^+ \to \mu^+\mu^+\mu^-$, $\tau^+ \to \mu^+e^+e^-$, $\tau^+ \to \mu^+ P$ ($P = \pi^0$, η and η'), $\tau^+ \to \mu^+ V$ ($V = \rho^0$, ω and ϕ), $\tau^+ \to e^+\gamma$, $\tau^+ \to e^+e^+e^-$, $\tau^+ \to e^+\mu^+\mu^-$, $\tau^+ \to e^+ P$, $\tau^+ \to e^+ V$, $\tau^+ \to \mu^+\mu^+e^-$ and, $\tau^+ \to e^+e^+\mu^-$. We define a parity asymmetry in two-body decays and two parity and one time-reversal asymmetries in three-body decays. In addition, we can define forward-backward asymmetry and forward-backward-angular asymmetries in the cases of $\tau^+ \to \mu^+e^+e^-$ and $\tau^+ \to e^+\mu^+\mu^-$. We show that the parity asymmetries of two-body decays reflect the characteristic chirality structure of the LFV interactions. For three-body decays, we find that there are useful relations among various asymmetries. We calculate the rates of μ-e conversions for different muonic atoms and show that the ratios of the conversion rates can vary within 1 order of magnitude over most of the LHT model parameter space. These features, as well as correlations of various branching ratios, can be

useful in discriminating different new physics models.

This paper is organized as follows: Section II is a brief review of the LHT. LFV processes are classified and various asymmetries are defined in Sec. III. Numerical results on the various observable quantities are shown in Sec. IV. Section V is the conclusion. Appendix A shows the general formulae of branching ratios and asymmetries for the processes studied. Functions for the Wilson coefficients are given in Appendix B. Useful formulae to perform the consistency test of the LHT are presented in Appendix C.

II. THE LITTLEST HIGGS MODEL WITH T PARITY

In this section we review the LHT in order to fix the notations we use in this paper. We use the Lagrangian given in Ref. [10] with corrections discussed in Refs. [13, 14].

A. Gauge and Higgs sectors

Gauge and Higgs sectors of the littlest Higgs model are described as a nonlinear σ model with the spontaneous global symmetry breaking from SU(5) to SO(5) with scalar fields, Σ, which is transformed as **15** representation of the SU(5). The vacuum expectation value of the scalar fields, Σ_0, which breaks the global SU(5) symmetry is

$$\Sigma_0 = \begin{pmatrix} 0 & 0 & 0 & 1 & 0 \\ 0 & 0 & 0 & 0 & 1 \\ 0 & 0 & 1 & 0 & 0 \\ 1 & 0 & 0 & 0 & 0 \\ 0 & 1 & 0 & 0 & 0 \end{pmatrix}. \tag{1}$$

Generators of the unbroken SO(5) symmetry, T^a, and the broken ones of SU(5)/SO(5), X^a, satisfy the following relations,

$$\Sigma_0 T^a \Sigma_0 = -(T^a)^T, \qquad \Sigma_0 X^a \Sigma_0 = (X^a)^T. \tag{2}$$

The Lagrangian of the NG bosons and gauge fields is given by

$$\mathcal{L}_{\text{NG-gauge}} = \frac{f^2}{8}\text{tr}[(D^\mu\Sigma)^\dagger D_\mu \Sigma] + \sum_{i=1,2}\left(-\frac{1}{2}\text{tr}[W_i{}^{\mu\nu}W_{i\mu\nu}] - \frac{1}{4}B_i{}^{\mu\nu}B_{i\mu\nu}\right), \tag{3}$$

where f is the decay constant of the nonlinear σ model and the NG boson field is written as follows,

$$\Sigma = \xi\Sigma_0\xi^T = \xi^2\Sigma_0, \quad \xi = e^{i\Pi/f}, \tag{4}$$

$$\Pi = \pi^a X^a = \begin{pmatrix} -\frac{\omega^0}{2} - \frac{\eta}{2\sqrt{5}} & -\frac{\omega^+}{\sqrt{2}} & -i\frac{\pi^+}{\sqrt{2}} & -i\phi^{++} & -i\frac{\phi^+}{\sqrt{2}} \\ -\frac{\omega^+}{\sqrt{2}} & \frac{\omega^0}{2} - \frac{\eta}{2\sqrt{5}} & \frac{v+h+i\pi^0}{2} & -i\frac{\phi^+}{\sqrt{2}} & \frac{-i\phi^0+\phi^{\rm P}}{\sqrt{2}} \\ i\frac{\pi^-}{\sqrt{2}} & \frac{v+h-i\pi^0}{2} & \frac{2\eta}{\sqrt{5}} & -i\frac{\pi^+}{\sqrt{2}} & \frac{v+h+i\pi^0}{2} \\ i\phi^{--} & i\frac{\phi^-}{\sqrt{2}} & i\frac{\pi^-}{\sqrt{2}} & -\frac{\omega^0}{2} - \frac{\eta}{2\sqrt{5}} & -\frac{\omega^-}{\sqrt{2}} \\ i\frac{\phi^-}{\sqrt{2}} & \frac{i\phi^0+\phi^{\rm P}}{\sqrt{2}} & \frac{v+h-i\pi^0}{2} & -\frac{\omega^+}{\sqrt{2}} & \frac{\omega^0}{2} - \frac{\eta}{2\sqrt{5}} \end{pmatrix}. \tag{5}$$

Fourteen NG bosons are denoted by h, $\pi^{\pm,0}$, $\omega^{\pm,0}$, η, $\phi^{\pm,0}$, ϕ^P, and $\phi^{\pm\pm}$. As explained later, $H = (-i\pi^+/\sqrt{2}, (v+h+i\pi^0)/2)^T$ is identified as the SM Higgs doublet. v is the electroweak symmetry breaking vacuum expectation value, $v = 246$ GeV. $W_i^{a\mu}$ and B_i^μ $(i = 1, 2)$ are gauge fields of the $\mathrm{SU}(2)_i \times \mathrm{U}(1)_i$, which are subgroups of the SU(5). The generators of the gauged subgroups are

$$Q_1^a = \frac{1}{2}\begin{pmatrix} \sigma^a & 0 & 0 \\ 0 & 0 & 0 \\ 0 & 0 & 0 \end{pmatrix}, \qquad Y_1 = \frac{1}{10}\mathrm{diag}\,(3, 3, -2, -2, -2), \tag{6}$$

$$Q_2^a = \frac{1}{2}\begin{pmatrix} 0 & 0 & 0 \\ 0 & 0 & 0 \\ 0 & 0 & -\sigma^{aT} \end{pmatrix}, \qquad Y_2 = \frac{1}{10}\mathrm{diag}\,(2, 2, 2, -3, -3), \tag{7}$$

where σ^a (a =1, 2, 3) are the Pauli matrices. The covariant derivative of Σ is defined as

$$D_\mu\Sigma = \partial_\mu\Sigma - \sqrt{2}i\sum_{j=1,2}\Big(gW_{j\mu}^a(Q_j^a\Sigma + \Sigma Q_j^{aT}) + g'B_{j\mu}(Y_J\Sigma + \Sigma Y_j)\Big), \tag{8}$$

where g and g' are gauge coupling constants of $\mathrm{SU}(2)_L \times \mathrm{U}(1)_Y$.

The Lagrangian (3) has a discrete symmetry under the following Z_2 transformation, which is called T parity [5].

$$W_1^{a\mu} \leftrightarrow W_2^{a\mu}, \qquad B_1^\mu \leftrightarrow B_2^\mu, \tag{9}$$

$$\Pi \leftrightarrow -\Omega\Pi\Omega, \qquad \Omega = \mathrm{diag}\,(1, 1, -1, 1, 1). \tag{10}$$

The T parity eigenstates of the gauge bosons are

$$W_L^{\pm,3\mu} = \frac{W_1^{\pm,3\mu} + W_2^{\pm,3\mu}}{\sqrt{2}}, \quad B_L^\mu = \frac{B_1^\mu + B_2^\mu}{\sqrt{2}} \qquad \text{(T-even)}, \tag{11}$$

$$W_H^{\pm,3\mu} = \frac{W_1^{\pm,3\mu} - W_2^{\pm,3\mu}}{\sqrt{2}}, \quad B_H^\mu = \frac{B_1^\mu - B_2^\mu}{\sqrt{2}} \qquad \text{(T-odd)}, \tag{12}$$

where $W_j^{\pm\mu} = (W_j^{1\mu} \mp i W_j^{2\mu})/\sqrt{2}$ $(j = 1, 2)$. As for the NG boson fields, we can show from Eqs. (5) and (10) that h, $\pi^{\pm,0}$ are T-even particles and the others are T-odd particles. $W_H^{\pm,3\mu}$ and B_H^μ receive mass of the order of f from the gauge symmetry breaking $[\mathrm{SU}(2)\times\mathrm{U}(1)]^2 \to \mathrm{SU}(2)_L\times\mathrm{U}(1)_Y$ by absorbing $\omega^{\pm,0}$ and η. After the electroweak symmetry breaking, $\pi^{\pm,0}$ are absorbed by the SM gauge fields, $W_L^{\pm,3\mu}$ and B_L^μ. Mass eigenstates of the neutral gauge bosons are defined by

$$Z_L^\mu = W_L^{3\mu}\cos\theta_W - B_L^\mu \sin\theta_W, \qquad A_L^\mu = W_L^{3\mu}\sin\theta_W + B_L^\mu\cos\theta_W, \tag{13}$$

$$Z_H^\mu = W_H^{3\mu}\cos\theta_H - B_H^\mu \sin\theta_H, \qquad A_H^\mu = W_H^{3\mu}\sin\theta_H + B_H^\mu\cos\theta_H, \tag{14}$$

where Z_L^μ and A_L^μ are the SM Z boson and photon. θ_W is the weak mixing angle determined as $\sin\theta_W = g'/\sqrt{g^2+g'^2}$. The mixing angle of the T-odd gauge bosons is given by

$$\tan 2\theta_H = -\frac{g g' c_v^2 s_v^2}{g^2 - \frac{1}{5}g'^2 - \frac{1}{2}(g^2 - g'^2)c_v^2 s_v^2}, \tag{15}$$

where $c_v = \cos(v/(\sqrt{2}f))$ and $s_v = \sin(v/(\sqrt{2}f))$. Expanding in terms of v^2/f^2, we obtain

$$\sin\theta_H = -\frac{gg'}{g^2 - \frac{1}{5}g'^2}\frac{v^2}{4f^2} + O(\frac{v^4}{f^4}), \tag{16}$$

$$\cos\theta_H = 1 + O(\frac{v^4}{f^4}). \tag{17}$$

Gauge boson masses are given as

$$m_{W_L}^2 = \frac{g^2 f^2}{2} s_v^2, \qquad m_{Z_L}^2 = \frac{m_{W_L}^2}{\cos^2\theta_W}, \tag{18a}$$

$$m_{W_H}^2 = g^2 f^2 \left(1 - \frac{s_v^2}{2}\right), \tag{18b}$$

$$\begin{aligned} m_{Z_H}^2 &= \frac{g^2 f^2}{c_H^2 - s_H^2}\left[\left(1 - \frac{c_v^2 s_v^2}{2}\right)c_H^2 - \frac{g'^2}{5g^2}\left(1 - \frac{5}{2}c_v^2 s_v^2\right)s_H^2\right] \\ &= m_{W_H}^2 + O(\frac{v^4}{f^2}), \end{aligned} \tag{18c}$$

$$\begin{aligned} m_{A_H}^2 &= \frac{g'^2 f^2}{5(c_H^2 - s_H^2)}\left[\left(1 - \frac{5}{2}c_v^2 s_v^2\right)c_H^2 - \frac{5g^2}{g'^2}\left(1 - \frac{c_v^2 s_v^2}{2}\right)s_H^2\right] \\ &= \frac{g'^2 f^2}{5}\left(1 - \frac{5v^2}{4f^2} + O(\frac{v^4}{f^4})\right), \end{aligned} \tag{18d}$$

where $s_H = \sin\theta_H$ and $c_H = \cos\theta_H$. We consider terms up to $O(v^4/f^4)$ so that we neglect the difference between m_{W_H} and m_{Z_H} in our analysis.

B. Fermion sector

The fermion sector of the LHT consists of three families of quark and lepton fields $q_{1,2}$, $\ell_{1,2}$, u_R, d_R, ν_R, e_R, q_{HR} and ℓ_{HR} for each generation, and a set of the "top-partner" fermions, $t'_{1,2}$ and $t'_{1R,2R}$. Following the procedure given in Ref. [13], we assign gauge charges of the fermion fields as summarized in Table I. The kinetic terms of left-handed fermions are given by

$$\begin{aligned}\mathcal{L}_{\text{left}} =&\bar{\Psi}_1\gamma^\mu\left(i\partial_\mu - \sqrt{2}gQ_1^aW_{1\mu}^a - \sqrt{2}g'B_{1\mu}Y_1^{\Psi_1} - \sqrt{2}g'B_{2\mu}Y_2^{\Psi_1}\right)P_L\Psi_1\\ &+\bar{\Psi}_2\gamma^\mu\left(i\partial_\mu + \sqrt{2}gQ_2^{aT}W_{2\mu}^a - \sqrt{2}g'B_{1\mu}Y_1^{\Psi_2} - \sqrt{2}g'B_{2\mu}Y_2^{\Psi_2}\right)P_L\Psi_2\,,\end{aligned} \tag{19}$$

where these fermions are introduced as incomplete multiplets of the SU(5),

$$\Psi_1 = \begin{pmatrix} -i\sigma^2\ell_1 \\ 0 \\ 0 \end{pmatrix}, \quad \Psi_2 = \begin{pmatrix} 0 \\ 0 \\ -i\sigma^2\ell_2 \end{pmatrix} \tag{20}$$

and $P_L = \frac{1-\gamma_5}{2}$. Under the T parity, they transform as

$$\Psi_1 \leftrightarrow -\Sigma_0\Psi_2. \tag{21}$$

Thus the SM leptons and the T-odd leptons are given as the T parity eigenstates,

$$\ell_L = \frac{\ell_1 - \ell_2}{\sqrt{2}} \quad \text{(T-even)}, \tag{22}$$

$$\ell_H = \frac{\ell_1 + \ell_2}{\sqrt{2}} \quad \text{(T-odd)}, \tag{23}$$

respectively. The right-handed SM fermions are introduced in the same manner as in the SM.

The right-handed T-odd leptons are introduced as a nonlinear representation of the SU(5),

$$\Psi_R = \begin{pmatrix} \tilde{\psi}_R \\ \chi_R \\ -i\sigma^2\ell_{HR} \end{pmatrix}, \tag{24}$$

	$\mathrm{SU}(2)_1$	$\mathrm{SU}(2)_2$	Y_1	Y_2
$q_1 = \begin{pmatrix} u_1 \\ d_1 \end{pmatrix}$	**2**	**1**	$\frac{1}{30}$	$\frac{4}{30}$
$q_2 = \begin{pmatrix} u_2 \\ d_2 \end{pmatrix}$	**1**	**2**	$\frac{4}{30}$	$\frac{1}{30}$
t'_1	**1**	**1**	$\frac{16}{30}$	$\frac{4}{30}$
t'_2	**1**	**1**	$\frac{4}{30}$	$\frac{16}{30}$
$\ell_1 = \begin{pmatrix} \nu_1 \\ e_1 \end{pmatrix}$	**2**	**1**	$-\frac{3}{10}$	$-\frac{2}{10}$
$\ell_2 = \begin{pmatrix} \nu_2 \\ e_2 \end{pmatrix}$	**1**	**2**	$-\frac{2}{10}$	$-\frac{3}{10}$

	$\mathrm{SU}(2)_1$	$\mathrm{SU}(2)_2$	Y_1	Y_2
u_R	**1**	**1**	$\frac{1}{3}$	$\frac{1}{3}$
d_R	**1**	**1**	$-\frac{1}{6}$	$-\frac{1}{6}$
t'_{1R}	**1**	**1**	$\frac{16}{30}$	$\frac{4}{30}$
t'_{2R}	**1**	**1**	$\frac{4}{30}$	$\frac{16}{30}$
ν_R	**1**	**1**	0	0
e_R	**1**	**1**	$-\frac{1}{2}$	$-\frac{1}{2}$

TABLE I: Quantum numbers of fermion fields. $Y_{1,2}$ are charges of $\mathrm{U}(1)_{1,2}$. Generation indices are suppressed. For q_{HR} and ℓ_{HR}, see the text.

where upper three components, $\tilde{\psi}_R$ and χ_R, are heavy enough to be neglected in low energy dynamics. Ψ_R changes the sign with the T parity. In order to construct the gauge invariant kinetic term, we define Ψ_R^ξ as

$$\Psi_R^\xi = \xi \Psi_R \tag{25}$$

which transform linearly under the SU(5) transformation. Thus the kinetic term is given by

$$\mathcal{L}_{\mathrm{HR}} = \frac{1}{2}\overline{\Psi_R^\xi}\gamma^\mu \left(i\partial_\mu - \sqrt{2}gW_{1\mu}^a Q_1^a + \sqrt{2}gW_{2\mu}^a Q_2^{aT} - \sqrt{2}g' B_{1\mu} Y_1^{\Psi_R} - \sqrt{2}g' B_{2\mu} Y_2^{\Psi_R} \right) P_R \Psi_R^\xi + (\text{T parity conjuation}), \tag{26}$$

where $Y_1^{\Psi_R} = \frac{1}{10}\mathrm{diag}(3,3,-2,-2,-2)$ and $Y_2^{\Psi_R} = \frac{1}{10}\mathrm{diag}(2,2,2,-3,-3)$. The quark sector is constructed in the same procedure. For the quark sector, $Y_1^{\Psi_R} = \frac{1}{30}\mathrm{diag}(19,19,4,4,4)$ and $Y_2^{\Psi_R} = \frac{1}{30}\mathrm{diag}(16,16,16,1,1)$.

C. The Yukawa sector

The Yukawa couplings of the T-odd fermions are

$$\mathcal{L}_{\text{T-odd-Yukawa}} = -\kappa^{ij} f(\bar{\Psi}_2^i \xi + \bar{\Psi}_1^i \Sigma_0 \Omega \xi^\dagger \Omega) \Psi_R^j + \text{H.c.}, \tag{27}$$

with generation indices, i and j. Thus their masses are given by

$$m_{H\ell}^i = \sqrt{2}\kappa^i f, \tag{28}$$

$$m_{H\nu}^i = \frac{\kappa^i f}{\sqrt{2}}(1 + c_v) = m_{H\ell}^i \left(1 + O\left(\frac{v^2}{f^2}\right)\right), \tag{29}$$

where i is the generation index and κ^i are eigenvalues of the Yukawa coupling matrix, κ^{ij}. We neglect $O(v^2/f^2)$ differences between $m_{H\ell}^i$ and $m_{H\nu}^i$ in the calculation of LFV processes because these differences only contribute to the higher order corrections in the v^2/f^2 expansion. For the SM charged leptons, the gauge invariant Yukawa coupling terms are written as

$$\mathcal{L}_{\text{T-even-Yukawa}} = -\frac{\lambda_{\text{d}}^{ij}}{2\sqrt{2}} f \epsilon_{ab}\epsilon_{xyz} \left[(\bar{\Psi}_2^{Xi})_x (\Sigma)_{ay} (\Sigma)_{bz} - (\bar{\Psi}_1^{Xi}\Sigma_0)_x (\tilde{\Sigma})_{ay} (\tilde{\Sigma})_{bz}\right] e_R^j + \text{H.c.}, \tag{30}$$

where a, $b = (1, 2)$ and x, y, $z = (3, 4, 5)$ are SU(5) indices and i and j are generation indices. The left-handed SM lepton doublets are embedded in SU(5) multiplets Ψ_1^{Xi} and Ψ_1^{Xi} as

$$\Psi_1^{Xi} = \begin{pmatrix} i\tilde{X}\ell_1^i \\ 0 \\ 0 \end{pmatrix}, \quad \Psi_2^{Xi} = \begin{pmatrix} 0 \\ 0 \\ iX\ell_2^i \end{pmatrix}, \tag{31}$$

where X and $\tilde{X}$ are $\text{SU}(2)_i$ singlet scalar fields whose U(1) gauge charges are $(Y_1, Y_2) = (\frac{1}{10}, -\frac{1}{10})$ and $(-\frac{1}{10}, \frac{1}{10})$, respectively. Following Ref. [21], we use $(\Sigma_{33})^{-1/4}$ and its T parity conjugate as X and $\tilde{X}$, respectively.

D. New mixing matrices

As explained in Ref. [8], the mass matrices of the SM fermions and the T-odd fermions are not simultaneously diagonalized in general. Consequently, new mixing matrices are

introduced in the interaction among the T-odd gauge bosons and fermions. We extract the interaction terms of the T-odd W boson and leptons from Eq. (19) as

$$\mathcal{L}_{\rm left} \supset \frac{ig}{\sqrt{2}}(V_{H\ell})_{ij}\bar{\nu}_H^i\gamma_\mu P_L \ell^j W_H^{+\mu} + \frac{ig}{\sqrt{2}}(V_{H\nu})_{ij}\bar{\ell}_H^j\gamma_\mu P_L \nu^j W_H^{-\mu} + \text{H.c.}, \tag{32}$$

where $V_{H\ell}$ and $V_{H\nu}$ are new mixing matrices. These two mixing matrices are related to each other by

$$V_{PMNS} = V_{H\ell}^\dagger V_{H\nu}, \tag{33}$$

where V_{PMNS} is the PMNS matrix [7], because the mass matrices of ℓ_H and ν_H are determined by the same Yukawa coupling matrix κ^{ij}. $V_{H\ell}$ and $V_{H\nu}$ also appear in the interaction of the neutral T-odd gauge bosons and leptons. We parameterize $V_{H\ell}$ as

$$V_{H\ell} = \begin{pmatrix} 1 & 0 & 0 \\ 0 & c_{23}^\ell & s_{23}^\ell e^{-i\delta_{23}^\ell} \\ 0 & -s_{23}^\ell e^{i\delta_{23}^\ell} & c_{23}^\ell \end{pmatrix} \begin{pmatrix} c_{13}^\ell & 0 & s_{13}^\ell e^{-i\delta_{13}^\ell} \\ 0 & 1 & 0 \\ -s_{13}^\ell e^{i\delta_{13}^\ell} & 0 & c_{13}^\ell \end{pmatrix} \begin{pmatrix} c_{12}^\ell & s_{12}^\ell e^{-i\delta_{12}^\ell} & 0 \\ -s_{12}^\ell e^{i\delta_{12}^\ell} & c_{12}^\ell & 0 \\ 0 & 0 & 1 \end{pmatrix}, \tag{34}$$

where $s_{ij}^\ell = \sin\theta_{ij}^\ell$ and $c_{ij}^\ell = \cos\theta_{ij}^\ell$. We take θ_{ij}^ℓ and δ_{ij}^ℓ as input parameters. Notice that there remain three unremovable phases in $V_{H\ell}$ after the phase convention of the PMNS matrix is fixed, as pointed out in Ref. [10]. For the quark sector, we define new mixing matrices V_{Hd} and V_{Hu} in the same way as $V_{H\ell}$ and $V_{H\nu}$. We take V_{Hd} as a matrix parametrized like Eq. (34) and the other mixing matrix, V_{Hu}, is expressed by V_{Hd} and the CKM matrix [6] in the following way:

$$V_{Hu} = V_{Hd}V_{CKM}^\dagger. \tag{35}$$

III. LEPTON FLAVOR VIOLATION IN THE LITTLEST HIGGS MODEL WITH T PARITY

In this section, we present formulae for observables in the LFV processes in the LHT. In contrast to previous works [11, 12, 14–16], we consider various angular distributions in polarized μ and τ decays in addition to the branching ratios and the $\mu - e$ conversion rates in various muonic atoms. Studying the angular distributions is useful to extract information about the chirality structure of the low energy effective Lagrangian.

The LFV processes that we consider in this paper are the following.

- Radiative two-body decays: $\mu^+ \to e^+\gamma$, $\tau^+ \to \mu^+\gamma$ and $\tau^+ \to e^+\gamma$.

- Leptonic three-body decays of μ and τ. We classify these decay modes into three types according to the lepton flavor combination in the final state.

  - Type I: $\mu^+ \to e^+e^+e^-$, $\tau^+ \to \mu^+\mu^+\mu^-$ and $\tau^+ \to e^+e^+e^-$. All the three leptons in the final state have the same flavor.

  - Type II: $\tau^+ \to \mu^+e^+e^-$ and $\tau^+ \to e^+\mu^+\mu^-$. In these processes, the final state consists of a pair of same flavor leptons with opposite charges and another lepton with different flavor. There are no identical particles in the final state.

  - Type III: $\tau^+ \to \mu^+\mu^+e^-$ and $\tau^+ \to e^+e^+\mu^-$. Lepton flavor changes by more than one.

- Semileptonic two-body decay of τ. We consider $\tau^+ \to \mu^+P$ and $\tau^+ \to \mu^+V$ modes, where P and V stand for a pseudoscalar meson (π^0, η or η') and a vector meson (ρ^0, ω or ϕ), respectively, as well as corresponding $\tau^+ \to e^+$ modes. We do not consider $\tau^+ \to \mu^+(e^+)K^{(*)}$ modes, where both quark and lepton flavors are violated.

- $\mu - e$ conversion in a muonic atom. In these processes, $\mu^- A \to e^- A$, we discuss aluminum (Al), titanium (Ti), gold (Au) and lead (Pb) as target atom, A, because the conversion rates depend on target nuclei [22].

In the LHT, LFV processes are induced by loop diagrams with the T-odd gauge bosons and leptons in the internal lines. Contributions of the T-even particles are negligible because they are suppressed by neutrino masses. Since only the left-handed SM (T-even) leptons couple to the T-odd gauge bosons, the low energy effective Lagrangian for LFV has a restricted chirality structure: the lepton flavor changing occurs in the left-handed lepton sector only. In the following subsections, we present the formulae for the effective Lagrangians, branching ratios, and various asymmetries, which can be defined based on angular distributions. Except for the $\mu - e$ conversion, we explicitly show formulae for τ to μ transitions. Those for μ to e and τ to e are obtained by appropriate replacements of flavor indices. For simplicity, we neglect lepton masses in the final states.

In the following, formulae of the low energy effective Lagrangians and the observable quantities are shown based on the LFV interactions relevant to the LHT. Those in the case of the most general low energy effective Lagrangians are given in Appendix A.

A. $\mu^+ \to e^+\gamma$, $\tau^+ \to \mu^+\gamma$ and, $\tau^+ \to e^+\gamma$

The effective Lagrangian for $\tau^+ \to \mu^+\gamma$ in the LHT consists of the following dipole moment type operator.

$$\mathcal{L}_\gamma = -\frac{4G_F}{\sqrt{2}}\left[m_\tau A_R^{\rm LHT}\bar{\tau}_R\sigma^{\mu\nu}\mu_L F_{\mu\nu} + \text{H.c.}\right], \tag{36}$$

where

$$A_R^{\rm LHT} = \frac{e}{(4\pi)^2}\frac{v^2}{8f^2}\sum_l (V_{H\ell})^*_{l3}(V_{H\ell})_{l2}\left(N_{CM}(x_l) + \frac{1}{2}N_{NM}(x_l) + \frac{1}{10}N_{NM}(x'_l)\right), \tag{37}$$

with

$$x_l = \frac{{m^l_{H\ell}}^2}{m^2_{W_H}}, \quad x'_l = \frac{{m^l_{H\ell}}^2}{m^2_{A_H}} = \frac{5}{\tan^2\theta_W}x_l. \tag{38}$$

The functions N_{CM} and N_{NM} are given in Appendix B. The coefficient of the operator with the opposite chirality, $\bar{\tau}_L\sigma^{\mu\nu}\mu_R F_{\mu\nu}$, is suppressed by m_μ/m_τ due to the chirality properties in the interaction of the T-odd gauge bosons.

For a $\tau^+ \to \mu^+\gamma$ decay of a polarized τ^+, we define a decay angle θ as the angle between the spin of τ^+ and the momentum of μ^+ in the rest frame of τ^+. The configuration of spin and momenta are shown in Fig. 1.

The differential branching ratio with respect to $\cos\theta$ is given by

$$\frac{d}{d\cos\theta}\text{Br}(\tau^+ \to \mu^+\gamma)_{\rm LHT} = \tau_\tau\frac{G_F^2 m_\tau^5}{\pi}\left|A_R^{\rm LHT}\right|^2(1-\cos\theta). \tag{39}$$

We define the polarization asymmetry, which characterizes the chirality structure of the effective interaction in (36), as

$$A_\gamma(\tau^+ \to \mu^+\gamma) = \frac{1}{\text{Br}(\tau^+ \to \mu^+\gamma)}\left(\int_0^1 - \int_{-1}^0\right)d\cos\theta\frac{d\text{Br}(\tau^+ \to \mu^+\gamma)}{d\cos\theta}, \tag{40}$$

where the integrated branching ratio is

$$\text{Br}(\tau^+ \to \mu^+\gamma) = \int_{-1}^1 d\cos\theta\frac{d\text{Br}(\tau^+ \to \mu^+\gamma)}{d\cos\theta}. \tag{41}$$

A_γ is a parity odd quantity since $\cos\theta$ is proportional to the inner product $\vec{s}\cdot\vec{p}$, where $\vec{s}$ and $\vec{p}$ are spin of initial τ^+ and spatial momentum of final μ^+, respectively. By substituting (39), we obtain

$$\text{Br}(\tau^+ \to \mu^+\gamma)_{\rm LHT} = \tau_\tau\frac{2G_F^2 m_\tau^5}{\pi}\left|A_R^{\rm LHT}\right|^2, \tag{42}$$

$$A_\gamma(\tau^+ \to \mu^+\gamma)_{\rm LHT} = -\frac{1}{2}. \tag{43}$$

The parameter independent result of A_γ is a consequence of the special chirality structure of the LHT.

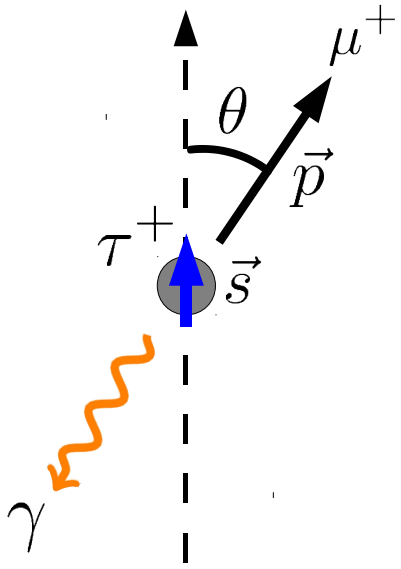

FIG. 1: Configuration of $\tau^+ \to \mu^+\gamma$ decay. The dashed arrow denotes the direction of the τ^+ spin. The solid and the wavy arrows show the directions of momenta of the μ^+ and the photon, respectively. θ is defined as the angle between the directions of the τ^+ spin and the μ^+ momentum.

B. $\mu^+ \to e^+e^+e^-$, $\tau^+ \to \mu^+\mu^+\mu^-$ and $\tau^+ \to e^+e^+e^-$

The effective Lagrangian for type I leptonic three-body decay, $\tau^+ \to \mu^+\mu^+\mu^-$, in the LHT is given as

$$\begin{aligned}\mathcal{L}_{\rm I} = -\frac{4G_F}{\sqrt{2}}\big[&m_\tau A_R^{\rm LHT}\bar{\tau}_R\sigma^{\mu\nu}\mu_L F_{\mu\nu} + g_{Ll}^{\rm I,LHT}(\bar{\tau}_L\gamma^\mu\mu_L)(\bar{\mu}_L\gamma_\mu\mu_L)\\ &+ g_{Lr}^{\rm I,LHT}(\bar{\tau}_L\gamma^\mu\mu_L)(\bar{\mu}_R\gamma_\mu\mu_R) + \text{H.c.}\big],\end{aligned} \tag{44}$$

where

$$g_{Ll}^{\rm I,LHT} = \frac{g^2}{(4\pi)^2}\frac{v^2}{8f^2}\sum_l (V_{H\ell})^*_{l3}(V_{H\ell})_{l2} \times \left(-\sin^2\theta_W P_\gamma(x_l) + \left(-\frac{1}{2}+\sin^2\theta_W\right)P_Z(x_l) + \sum_m (V_{H\ell})^*_{m2}(V_{H\ell})_{m2} B_{(e)}(x_l,x_m)\right), \tag{45}$$

$$g_{Lr}^{\rm I,LHT} = \frac{g^2}{(4\pi)^2}\frac{v^2}{8f^2}\sum_l (V_{H\ell})^*_{l3}(V_{H\ell})_{l2}\,(-\sin^2\theta_W)\big(P_\gamma(x_l) - P_Z(x_l)\big). \tag{46}$$

The functions P_γ, P_Z and $B_{(e)}$ represent contributions of photon penguin, Z penguin and box diagrams, respectively, and are given in Appendix B. $A_R^{\rm LHT}$ is shown in (37).

The spin and momentum configuration of a three-body decay of a polarized τ^+ at rest is determined by two energy variables and two angular variables, as depicted in Fig. 2. The three spatial momenta of the particles in the final state are denoted as $\vec{p}_a$, $\vec{p}_b$, and $\vec{p}_c$. We take z axis in the direction of $\vec{p}_a$ and the decay plane is identified as the z-x plane. The direction of x axis is chosen in such a way that the x component of $\vec{p}_b$ has a positive value. We take the y axis along $\vec{p}_a \times \vec{p}_b$. The direction of the polarization vector of the initial particle is parametrized by the polar and the azimuthal angles θ and ϕ, respectively. For the $\tau^+ \to \mu^+\mu^+\mu^-$ decay, we identify the momentum of μ^- as $\vec{p}_a$. Two μ^+'s are distinguished by their energies. The momentum of the μ^+ with larger (smaller) energy is identified as $\vec{p}_b$ ($\vec{p}_c$).

As for the energy variables, we define

$$x_{b,c} = \frac{2E_{b,c}}{m_\tau}, \tag{47}$$

where $E_{b,c}$ are energies of μ^+'s with momenta $\vec{p}_{b,c}$. E_b is larger than E_c by definition. Possible ranges of $x_{b,c}$ in an approximation of massless final particles are

$$\frac{1}{2} \le x_b \le 1, \qquad 1 - x_b \le x_c \le x_b. \tag{48}$$

However, the $\tau^+ \to \mu^+\mu^+\mu^-$ decay amplitude is singular for $x_b \to 1$, where the invariant mass of the pair of μ^+ (with $\vec{p}_c$) and μ^- is vanishing within the approximation of neglecting the muon mass. The singularity comes from the pole of the photon propagator in the contribution from the dipole moment operator. We introduce a cutoff parameter $0 < \delta \ll 1$ and take the integration interval of x_b as

$$\frac{1}{2} \le x_b \le 1 - \delta, \tag{49}$$

in order to avoid this collinear singularity.

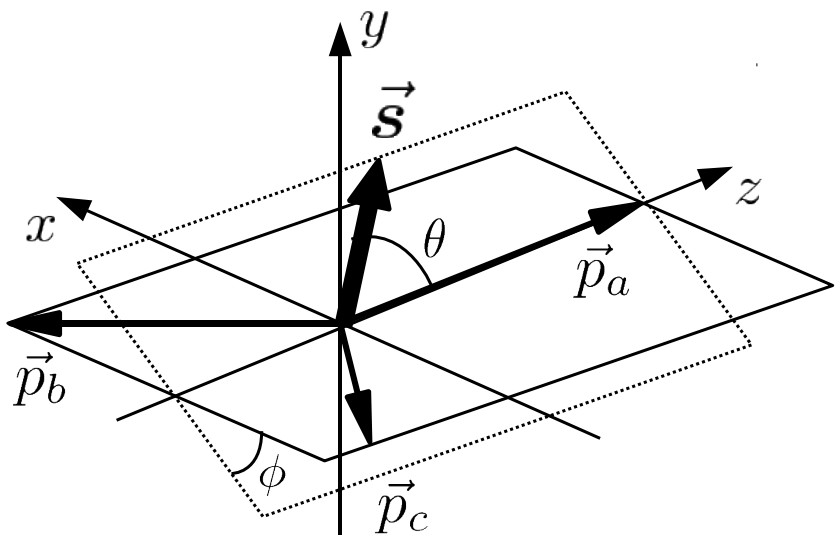

FIG. 2: The spin and momentum configuration of a three-body decay in the rest frame of the initial lepton. The decay plane is identified as the z-x plane where the z axis is taken to be the direction of particle a's momentum. the x axis is defined so that the x component of particle b's momentum is positive. The direction of the initial lepton polarization vector $\vec{s}$ is parametrized by the polar and the azimuthal angles θ and ϕ, respectively.

The δ-dependent branching ratio is calculated by integration over $x_{b,c}$, $\cos\theta$ and ϕ as

$$\mathrm{Br}(\delta) = \int_{-1}^{1} d\cos\theta \int_0^{2\pi} d\phi \int_{1/2}^{1-\delta} dx_b \int_{1-x_b}^{x_b} dx_c \frac{d^4\mathrm{Br}}{dx_b dx_c\, d\phi\, d\cos\theta}. \tag{50}$$

The general formulae of differential branching ratios are shown in Appendix A. We also define the following angular asymmetries:

$$A_Z(\delta) = \frac{1}{\mathrm{Br}(\delta)} \left(\int_0^1 - \int_{-1}^0 \right) d\cos\theta \int_0^{2\pi} d\phi \int_{1/2}^{1-\delta} dx_b \int_{1-x_b}^{x_b} dx_c \frac{d^4\mathrm{Br}}{dx_b dx_c\, d\phi\, d\cos\theta}, \tag{51a}$$

$$A_X(\delta) = \frac{1}{\mathrm{Br}(\delta)} \int_{-1}^{1} d\cos\theta \left(\int_{-\pi/2}^{\pi/2} - \int_{\pi/2}^{3\pi/2} \right) d\phi \int_{1/2}^{1-\delta} dx_b \int_{1-x_b}^{x_b} dx_c \frac{d^4\mathrm{Br}}{dx_b dx_c\, d\phi\, d\cos\theta}, \tag{51b}$$

$$A_Y(\delta) = \frac{1}{\mathrm{Br}(\delta)} \int_{-1}^{1} d\cos\theta \left(\int_0^{\pi} - \int_{-\pi}^0 \right) d\phi \int_{1/2}^{1-\delta} dx_b \int_{1-x_b}^{x_b} dx_c \frac{d^4\mathrm{Br}}{dx_b dx_c\, d\phi\, d\cos\theta}. \tag{51c}$$

The branching ratio and asymmetries in the LHT are expressed as

$$\mathrm{Br}(\tau^+ \to \mu^+\mu^+\mu^-)_{\mathrm{LHT}}(\delta) = \mathrm{Br}(\tau^+ \to \bar{\nu}_\tau e^+ \nu_e) B^{\mathrm{I,LHT}}(\delta), \tag{52}$$

$$B^{\mathrm{I,LHT}}(\delta) = C_{R1}^{\mathrm{I,LHT}} A_1(\delta) + C_{L2}^{\mathrm{I,LHT}} A_2(\delta) + C_{L3}^{\mathrm{I,LHT}} A_3(\delta) + C_{J1}^{\mathrm{I,LHT}} A_4(\delta) + C_{J3}^{\mathrm{I,LHT}} A_5(\delta), \quad (53)$$

$$A_Z^{\mathrm{I,LHT}}(\delta) = \frac{1}{2B^{\mathrm{I,LHT}}(\delta)} \big(C_{R1}^{\mathrm{I,LHT}} B_1(\delta) + C_{L2}^{\mathrm{I,LHT}} B_2(\delta) - C_{L3}^{\mathrm{I,LHT}} A_3(\delta) - C_{J1}^{\mathrm{I,LHT}} A_4(\delta) + C_{J3}^{\mathrm{I,LHT}} A_5(\delta) \big), \quad (54a)$$

$$A_X^{\mathrm{I,LHT}}(\delta) = \frac{1}{2B^{\mathrm{I,LHT}}(\delta)} \big(-C_{R1}^{\mathrm{I,LHT}} C_1(\delta) + C_{L2}^{\mathrm{I,LHT}} C_2(\delta) - C_{J1}^{\mathrm{I,LHT}} C_3(\delta) + C_{J3}^{\mathrm{I,LHT}} C_4(\delta) \big), \quad (54b)$$

$$A_Y^{\mathrm{I,LHT}}(\delta) = \frac{1}{2B^{\mathrm{I,LHT}}(\delta)} \big(-C_{J5}^{\mathrm{I,LHT}} C_3(\delta) + C_{J6}^{\mathrm{I,LHT}} C_4(\delta) \big). \quad (54c)$$

The functions $A_i(\delta)$, $B_i(\delta)$, and $C_i(\delta)$ are given in Appendix A 2. $C_{R1}^{\mathrm{I,LHT}}$, *etc.* are written in terms of the Wilson coefficients in (44) as

$$C_{R1}^{\mathrm{I,LHT}} = \left| e A_R^{\mathrm{LHT}} \right|^2, \quad C_{L2}^{\mathrm{I,LHT}} = \left| g_{Lr}^{\mathrm{I,LHT}} \right|^2, \quad C_{L3}^{\mathrm{I,LHT}} = \left| g_{Ll}^{\mathrm{I,LHT}} \right|^2, \quad (55a)$$

$$C_{J1}^{\mathrm{I,LHT}} = \mathrm{Re}[e A_R^{\mathrm{LHT}} g_{Ll}^{\mathrm{I,LHT}*}], \quad C_{J3}^{\mathrm{I,LHT}} = \mathrm{Re}[e A_R^{\mathrm{LHT}} g_{Lr}^{\mathrm{I,LHT}*}], \quad (55b)$$

$$C_{J5}^{\mathrm{I,LHT}} = \mathrm{Im}[e A_R^{\mathrm{LHT}} g_{Ll}^{\mathrm{I,LHT}*}], \quad C_{J6}^{\mathrm{I,LHT}} = \mathrm{Im}[e A_R^{\mathrm{LHT}} g_{Lr}^{\mathrm{I,LHT}*}]. \quad (55c)$$

As explained in Appendix A 2, A_Z and A_X are parity odd asymmetries and A_Y is a time-reversal asymmetry.

The time-reversal asymmetry A_Y is induced by the CP violation in the effective Lagrangian, since we are considering a theory with CPT invariance. In fact, $C_{J5}^{\mathrm{I,LHT}}$ and $C_{J6}^{\mathrm{I,LHT}}$ are proportional to the Jarlskog invariant [23] defined for $V_{H\ell}$:

$$\begin{aligned} C_{J5,J6}^{\mathrm{I,LHT}} \propto J(V_{H\ell}) &= \mathrm{Im}\left[(V_{H\ell})_{11}^* (V_{H\ell})_{22}^* (V_{H\ell})_{12} (V_{H\ell})_{21} \right] \\ &= c_{12}^\ell c_{13}^{\ell\,2} c_{23}^\ell s_{12}^\ell s_{13}^\ell s_{23}^\ell \sin(\delta_{12}^\ell - \delta_{13}^\ell + \delta_{23}^\ell). \end{aligned} \quad (56)$$

Therefore, a three-generation mixing is necessary for nonvanishing A_Y. Notice that two of three complex phases in $V_{H\ell}$ are removable when T-even neutrino masses are neglected. That is why $J(V_{H\ell})$ depends on only one combination of the phases.

C. $\tau^+ \to \mu^+e^+e^-$ and $\tau^+ \to e^+\mu^+\mu^-$

The effective Lagrangian for a type II trilepton decay $\tau^+ \to \mu^+e^+e^-$ has a similar structure to (44):

$$\begin{aligned}\mathcal{L}_{\rm II} = -\frac{4G_F}{\sqrt{2}}\big[&m_\tau A_R^{\rm LHT}\bar\tau_R\sigma^{\mu\nu}\mu_L F_{\mu\nu} + g_{Ll}^{\rm II,LHT}(\bar\tau_L\gamma^\mu\mu_L)(\bar e_L\gamma_\mu e_L)\\ &+ g_{Lr}^{\rm II,LHT}(\bar\tau_L\gamma^\mu\mu_L)(\bar e_R\gamma_\mu e_R) + \text{H.c.}\big],\end{aligned} \tag{57}$$

where

$$\begin{aligned}g_{Ll}^{\rm II,LHT} = \frac{g^2}{(4\pi)^2}\frac{v^2}{8f^2}\Bigg(&\sum_l (V_{H\ell})^*_{l3}(V_{H\ell})_{l2}\Big[-\sin^2\theta_W P_\gamma(x_l) + \Big(-\frac{1}{2}+\sin^2\theta_W\Big)P_Z(x_l)\Big]\\ &+\sum_{l,m}\Big[(V_{H\ell})^*_{l3}(V_{H\ell})_{l2}(V_{H\ell})^*_{m1}(V_{H\ell})_{m1}\\ &+(V_{H\ell})^*_{l3}(V_{H\ell})_{l1}(V_{H\ell})^*_{m1}(V_{H\ell})_{m2}\Big]B_{(e)}(x_l,x_m)\Bigg),\end{aligned} \tag{58}$$

and $g_{Lr}^{\rm II,LHT} = g_{Lr}^{\rm I,LHT}$. $A_R^{\rm LHT}$ is the same as (37).

Kinematical variables are defined in a similar way to the type I case. For the momentum assignment, we identify particles a, b and c in Fig. 2 as μ^+, e^+ and e^-, respectively [1]. A difference from the type I case is that both $x_b > x_c$ and $x_b < x_c$ are possible in type II modes because there are no identical particles in the final state. Therefore, the range of x_b and x_c are

$$\delta \le x_b \le 1, \qquad 1+\delta - x_b \le x_c \le 1, \tag{59}$$

where the cutoff parameter $0 < \delta \ll 1$ is introduced to avoid the collinear singularity in $x_b + x_c \to 1$.

Formulae for the branching ratio and the angular asymmetries $A_{Z,X,Y}$ in $\tau^+ \to \mu^+e^+e^-$ decay in the LHT are obtained as

$$\text{Br}(\tau^+ \to \mu^+e^+e^-)_{\rm LHT}(\delta) = \text{Br}(\tau^+ \to \bar\nu_\tau e^+\nu_e)B^{\rm II,LHT}(\delta), \tag{60}$$

$$\begin{aligned}B^{\rm II,LHT}(\delta) =& C_{R1}^{\rm II,LHT}D_1(\delta) + (C_{L3}^{\rm II,LHT}+C_{L4}^{\rm II,LHT})D_3(\delta)\\ &+(C_{J1}^{\rm II,LHT}+C_{J3}^{\rm II,LHT})D_4(\delta),\end{aligned} \tag{61}$$

[1] The convention of particle assignment is different from that in Ref. [18]

$$A_Z^{\rm II,LHT}(\delta) = \frac{1}{2B^{\rm II,LHT}}\Big(- C_{R1}^{\rm II,LHT} D_5(\delta) + (C_{L3}^{\rm II,LHT} + C_{L4}^{\rm II,LHT}) D_6(\delta) - \frac{1}{3}(C_{J1}^{\rm II,LHT} + C_{J3}^{\rm II,LHT}) D_4(\delta)\Big), \tag{62a}$$

$$A_X^{\rm II,LHT}(\delta) = \frac{\pi}{2B^{\rm II,LHT}}\big((-C_{L3}^{\rm II,LHT} + C_{L4}^{\rm II,LHT}) E_1(\delta) + (C_{J1}^{\rm II,LHT} - C_{J3}^{\rm II,LHT}) E_2(\delta)\big), \tag{62b}$$

$$A_Y^{\rm II,LHT}(\delta) = \frac{\pi}{2B^{\rm II,LHT}}\big(- (C_{J7}^{\rm II,LHT} - C_{J8}^{\rm II,LHT}) E_3(\delta)\big), \tag{62c}$$

where

$$C_{R1}^{\rm II,LHT} = \left|eA_R^{\rm LHT}\right|^2, \quad C_{L3}^{\rm II,LHT} = \left|g_{Lr}^{\rm II,LHT}\right|^2, \quad C_{L4}^{\rm II,LHT} = \left|g_{Ll}^{\rm II,LHT}\right|^2, \tag{63a}$$

$$C_{J1}^{\rm II,LHT} = {\rm Re}[eA_R^{\rm LHT} g_{Ll}^{\rm II,LHT*}], \quad C_{J3}^{\rm II,LHT} = {\rm Re}[eA_R^{\rm LHT} g_{Lr}^{\rm II,LHT*}], \tag{63b}$$

$$C_{J7}^{\rm II,LHT} = {\rm Im}[eA_R^{\rm LHT} g_{Ll}^{\rm II,LHT*}], \quad C_{J8}^{\rm II,LHT} = {\rm Im}[eA_R^{\rm LHT} g_{Lr}^{\rm II,LHT*}]. \tag{63c}$$

The functions $D_i(\delta)$, $E_i(\delta)$ and $F_i(\delta)$ are given in Appendix A 3.

In the type II decay, another class of asymmetries can be defined. We define the energy asymmetry in $\tau^+ \to \mu^+ e^+ e^-$ as the asymmetry between the partial widths with $E_{e^+} > E_{e^-}$ and $E_{e^+} < E_{e^-}$ in the rest frame of initial τ^+:

$$A_{FB} = \frac{1}{\rm Br}\left(\int_{x_b>x_c} - \int_{x_b<x_c}\right) dx_b dx_c \frac{d^2{\rm Br}}{dx_b dx_c}. \tag{64}$$

This asymmetry is also called as the forward-backward asymmetry, because $x_b > x_c$ ($x_b < x_c$) corresponds to $\vec{p}_{\mu^+}\cdot\vec{p}_{e^-} > 0$ ($\vec{p}_{\mu^+}\cdot\vec{p}_{e^-} < 0$) in the rest frame of the $e^+\,e^-$ pair. Furthermore, we define the following asymmetries combining asymmetric integrations over (x_b, x_c) and ($\cos\theta$, ϕ):

$$A_{ZFB} = \frac{1}{{\rm Br}(\delta)}\left(\int_0^1 - \int_{-1}^0\right) d\cos\theta \int_0^{2\pi} d\phi \left(\int_{x_b>x_c} - \int_{x_b<x_c}\right) dx_b dx_c \frac{d^4{\rm Br}}{dx_b dx_c\, d\phi\, d\cos\theta}, \tag{65a}$$

$$A_{XFB} = \frac{1}{{\rm Br}(\delta)}\int_{-1}^1 d\cos\theta \left(\int_{-\pi/2}^{\pi/2} - \int_{\pi/2}^{3\pi/2}\right) d\phi \left(\int_{x_b>x_c} - \int_{x_b<x_c}\right) dx_b dx_c \frac{d^4{\rm Br}}{dx_b dx_c\, d\phi\, d\cos\theta}, \tag{65b}$$

$$A_{YFB} = \frac{1}{{\rm Br}(\delta)}\int_{-1}^1 d\cos\theta \left(\int_0^{\pi} - \int_{-\pi}^0\right) d\phi \left(\int_{x_b>x_c} - \int_{x_b<x_c}\right) dx_b dx_c \frac{d^4{\rm Br}}{dx_b dx_c\, d\phi\, d\cos\theta}. \tag{65c}$$

In the LHT, we obtain

$$A_{FB}^{\rm II,LHT}(\delta) = \frac{1}{B^{\rm II,LHT}}\bigg(-\frac{1}{4}(C_{L3}^{\rm II,LHT} - C_{L4}^{\rm II,LHT})D_2(\delta) + \frac{1}{2}(C_{J1}^{\rm II,LHT} - C_{J3}^{\rm II,LHT})D_4(\delta)\bigg), \tag{66a}$$

$$A_{ZFB}^{\rm II,LHT}(\delta) = \frac{1}{2B^{\rm II,LHT}}\bigg(\frac{1}{4}(C_{L3}^{\rm II,LHT} - C_{L4}^{\rm II,LHT})D_2(\delta) - \frac{1}{2}(C_{J1}^{\rm II,LHT} - C_{J3}^{\rm II,LHT})D_4(\delta)\bigg), \tag{66b}$$

$$A_{XFB}^{\rm II,LHT}(\delta) = \frac{1}{2B^{\rm II,LHT}}\bigg(C_{R1}^{\rm II,LHT}E_4(\delta) + \frac{4}{3}(C_{L3}^{\rm II,LHT} + C_{L4}^{\rm II,LHT})E_1(\delta) + \frac{4}{3}(C_{J1}^{\rm II,LHT} + C_{J3}^{\rm II,LHT})E_2(\delta)\bigg), \tag{66c}$$

$$A_{YFB}^{\rm II,LHT}(\delta) = \frac{1}{2B^{\rm II,LHT}}\bigg(-\frac{4}{3}(C_{J7}^{II} + C_{J8}^{II})E_3(\delta)\bigg), \tag{66d}$$

where the functions $G_i(\delta)$ and $H_i(\delta)$ are given in Appendix A 3.

D. $\tau^+ \to \mu^+\mu^+e^-$ and $\tau^+ \to e^+e^+\mu^-$

The type III leptonic decay modes, such as $\tau^+ \to \mu^+\mu^+e^-$, are those in which the lepton flavor changes by two. At the one-loop level, only the box diagrams contribute to these decay modes. The effective Lagrangian for $\tau^+ \to \mu^+\mu^+e^-$ is

$$\mathcal{L}_{\rm III} = -\frac{4G_F}{\sqrt{2}}\big[g_{Ll}^{\rm III,LHT}(\bar{\tau}_L\gamma^\mu\mu_L)(\bar{e}_L\gamma_\mu\mu_L) + \text{H.c.}\big], \tag{67}$$

where

$$g_{Ll}^{\rm III,LHT} = \frac{g^2}{(4\pi)^2}\frac{v^2}{8f^2}\sum_{l,m}(V_{H\ell})_{l3}^*(V_{H\ell})_{l2}(V_{H\ell})_{m1}^*(V_{H\ell})_{m2}B_{(e)}(x_l, x_m). \tag{68}$$

The kinematics of the type III decay is treated in a way similar to the type I case. For $\tau^+ \to \mu^+\mu^+e^-$ mode, e^- and one of the μ^+'s, which has a larger energy in the rest frame of τ^+, is identified as particles a and b in Fig. 2, respectively. We define the angular asymmetries A_Z, A_X and A_Y by (51a), (51b) and (51c), respectively. The forward-backward type asymmetries are not defined because there are identical particles in the final state as in the type I case.

The branching ratio in the LHT is written as

$$\frac{\text{Br}(\tau^+ \to \mu^+\mu^+e^-)_{\rm LHT}(\delta)}{\text{Br}(\tau^+ \to \bar{\nu}_\tau e^+\nu_e)} = C_{L3}^{\rm III,LHT}A_3(\delta), \tag{69}$$

where

$$C_{L3}^{\mathrm{III,LHT}} = \left| g_{Ll}^{\mathrm{III,LHT}} \right|^2 \tag{70}$$

and $A_3(\delta)$ is given in Appendix A 2. Since the differential width is written in terms of one combination of the Wilson coefficient, $C_{L3}^{\mathrm{III,LHT}}$, the angular asymmetries are determined independently of the input parameters:

$$A_Z^{\mathrm{III,LHT}} = -\frac{1}{2}, \qquad A_X^{\mathrm{III,LHT}} = 0, \qquad A_Y^{\mathrm{III,LHT}} = 0, \tag{71}$$

E. $\tau^+ \to \mu^+\pi, \eta, \eta'$ and $\tau^+ \to e^+\pi, \eta, \eta'$

The effective Lagrangian for semileptonic $\tau \to \mu$ decay processes are written as

$$\begin{aligned}\mathcal{L}_{\mathrm{had}} = -\frac{4G_F}{\sqrt{2}}\Big[& m_\tau A_R^{\mathrm{LHT}} \bar{\tau}_R \sigma^{\mu\nu} \mu_L F_{\mu\nu} \\ & + \sum_{q=u,d,s} \left(g_{Ll(q)}^{\mathrm{LHT}} (\bar{\tau}_L \gamma^\mu \mu_L)(\bar{q}_L \gamma_\mu q_L) + g_{Lr(q)}^{\mathrm{LHT}} (\bar{\tau}_L \gamma^\mu \mu_L)(\bar{q}_R \gamma_\mu q_R) \right) + \mathrm{H.c.} \Big].\end{aligned} \tag{72}$$

The Wilson coefficients are given as

$$\begin{aligned} g_{Ll(q)}^{\mathrm{LHT}} = & \frac{g^2}{(4\pi)^2} \frac{v^2}{8f^2} \sum_l (V_{H\ell})_{l3}^* (V_{H\ell})_{l2} \\ & \times \left(Q_q \sin^2\theta_W P_\gamma(x_l) + (T_q^3 - Q_q \sin^2\theta_W) P_Z(x_l) + \sum_m (V_{Hq})_{m1}^* (V_{Hq})_{m1} B_{(q)}(x_l, x_m) \right), \end{aligned} \tag{73}$$

$$g_{Lr(q)}^{\mathrm{LHT}} = \frac{g^2}{(4\pi)^2} \frac{v^2}{8f^2} \sum_l (V_{H\ell})_{l3}^* (V_{H\ell})_{l2}\, Q_q \sin^2\theta_W \big(P_\gamma(x_l) - P_Z(x_l) \big), \tag{74}$$

where T_q^3 and Q_q are the weak isospin and the electromagnetic charge for quarks, respectively. A_R^{LHT} is given in (37).

For the two-body decay process $\tau^+ \to \mu^+ P$, where P stands for a neutral pseudoscalar meson π^0, η or η', the differential branching ratio is written as

$$\frac{d\mathrm{Br}(\tau^+ \to \mu^+ P)_{\mathrm{LHT}}}{d\cos\theta} = \tau_\tau \frac{G_F^2 m_\tau^3}{8\pi} \left(1 - \frac{m_P^2}{m_\tau^2} \right)^2 \left| G_{RP}^{\mathrm{LHT}} \right|^2 (1 + \cos\theta), \tag{75}$$

where the decay angle θ is defined in the same way as in the $\tau^+ \to \mu^+\gamma$ case. The effective coupling G_{RP}^{LHT} for $P = \pi^0$ and $P = \eta$ are written in terms of the Wilson coefficients in (72)

as

$$G_{R\pi}^{\rm LHT} = \frac{f_\pi}{2\sqrt{2}}\left(g_{Lr(u)}^{\rm LHT} - g_{Lr(d)}^{\rm LHT} - g_{Ll(u)}^{\rm LHT} + g_{Ll(d)}^{\rm LHT}\right), \tag{76}$$

$$G_{R\eta}^{\rm LHT} = \frac{1}{2}\left(\frac{f_\eta^q}{\sqrt{2}}(g_{Lr(u)}^{\rm LHT} + g_{Lr(d)}^{\rm LHT} - g_{Ll(u)}^{\rm LHT} - g_{Ll(d)}^{\rm LHT}) + f_\eta^s(g_{Lr(d)}^{\rm LHT} - g_{Ll(d)}^{\rm LHT})\right). \tag{77}$$

f_π, f_η^q and f_η^s are the decay constants of the pseudoscalar mesons that are defined in Appendix A 5. The effective coupling for $\tau^+ \to \mu^+\eta'$ is obtained by replacing the subscript η with η' in the expression of $G_{R\eta}$. Formulae for the branching ratio and the polarization asymmetry A_P are derived from (75) as

$$\mathrm{Br}(\tau^+ \to \mu^+ P)_{\rm LHT} = \tau_\tau \frac{G_F^2 m_\tau^3}{4\pi}\left(1 - \frac{m_P^2}{m_\tau^2}\right)^2 |G_{RP}|^2, \tag{78}$$

$$A_P(\tau^+ \to \mu^+ P)_{\rm LHT} = \frac{1}{2}. \tag{79}$$

A_P is purely determined by the chirality structure of the effective Lagrangian (72) and independent of the values of the input parameters.

F. $\tau^+ \to \mu^+\rho,\omega,\phi$ and $\tau^+ \to e^+\rho,\omega,\phi$

The semileptonic two-body decay $\tau^+ \to \mu^+ V$, where V denotes a neutral vector meson ρ^0, ω, or ϕ are also described by the effective Lagrangian (72). The branching ratio and the polarization asymmetry A_V, which is defined similarly to A_γ and A_P, are written as

$$\mathrm{Br}(\tau^+ \to \mu^+ V)_{\rm LHT} = \tau_\tau \frac{G_F^2 m_\tau^3}{\pi}\left(1 - \frac{m_V^2}{m_\tau^2}\right)^2 B_V^{\rm LHT}, \tag{80}$$

$$B_V^{\rm LHT} = |G_{RAV}|^2\left(2 + \frac{m_V^2}{m_\tau^2}\right) + |G_{LV}|^2\frac{m_\tau^2 + 2m_V^2}{4m_V^2} - 3\mathrm{Re}[G_{RAV}G_{LV}^*], \tag{81}$$

$$A_V(\tau^+ \to \mu^+ V)_{\rm LHT} = \frac{1}{2B_V^{\rm LHT}} \times\left(|G_{RAV}|^2\left(2 - \frac{m_V^2}{m_\tau^2}\right) + |G_{LV}|^2\left(\frac{m_\tau^2 - 2m_V^2}{4m_V^2}\right) + \mathrm{Re}[G_{RAV}G_{LV}^*]\right). \tag{82}$$

The effective coupling constants for $V = \rho^0$, ω and ϕ are

$$G^{\rm LHT}_{RA\rho} = \frac{f_\rho}{\sqrt{2}}\frac{m_\tau}{m_\rho} e A^{\rm LHT}_R, \tag{83a}$$

$$G^{\rm LHT}_{L\rho} = \frac{f_\rho m_\rho}{2\sqrt{2} m_\tau}\left(g^{\rm LHT}_{Ll(u)} - g^{\rm LHT}_{Ll(d)} + g^{\rm LHT}_{Lr(u)} - g^{\rm LHT}_{Lr(d)}\right), \tag{83b}$$

$$G^{\rm LHT}_{RA\omega} = \frac{f_\omega}{3\sqrt{2}}\frac{m_\tau}{m_\omega} e A^{\rm LHT}_R, \tag{83c}$$

$$G^{\rm LHT}_{L\omega} = \frac{f_\omega m_\omega}{2\sqrt{2} m_\tau}\left(g^{\rm LHT}_{Ll(u)} + g^{\rm LHT}_{Ll(d)} + g^{\rm LHT}_{Lr(u)} + g^{\rm LHT}_{Lr(d)}\right), \tag{83d}$$

$$G^{\rm LHT}_{RA\phi} = \frac{f_\phi}{3}\frac{m_\tau}{m_\phi} e A^{\rm LHT}_R, \tag{83e}$$

$$G^{\rm LHT}_{L\phi} = -\frac{f_\phi m_\phi}{2 m_\tau}\left(g^{\rm LHT}_{Ll(s)} + g^{\rm LHT}_{Lr(s)}\right), \tag{83f}$$

where the decay constants $f_{\rho,\omega,\phi}$ are defined in Appendix A 5.

G. $\mu - e$ conversion

The effective Lagrangian for the coherent $\mu - e$ conversion processes has the same structure as (72).

$$\mathcal{L}_{\rm had} = -\frac{4G_F}{\sqrt{2}}\Big[m_\mu A^{\rm LHT}_R \bar{\mu}_R \sigma^{\mu\nu} e F_{\mu\nu} + \sum_{q=u,d}\Big(g^{\rm LHT}_{Ll(q)}(\bar{\mu}_L\gamma^\mu e_L)(\bar{q}_L\gamma_\mu q_L) + g^{\rm LHT}_{Lr(q)}(\bar{\mu}_L\gamma^\mu e_L)(\bar{q}_R\gamma_\mu q_R)\Big) + \text{H.c.}\Big]. \tag{84}$$

The Wilson coefficients are obtained by replacing the lepton flavor indices $3(\tau)$ and $2(\mu)$ with $2(\mu)$ and $1(e)$ in Eqs. (37), (73) and (74).

We calculate the $\mu - e$ conversion rates following the method given in Ref. [22]. The $\mu - e$ conversion branching ratio in the LHT is written as

$$\mathrm{R}(\mu^- A \to e^- A)_{\rm LHT} = \frac{2G_F^2}{\omega_{\rm capt}}\Big|-A^{\rm LHT}_R D + 2(2g^{\rm LHT}_{Ll(u)} + 2g^{\rm LHT}_{Lr(u)} + g^{\rm LHT}_{Ll(d)} + g^{\rm LHT}_{Lr(d)})V^{(p)} + 2(g^{\rm LHT}_{Ll(u)} + g^{\rm LHT}_{Lr(u)} + 2g^{\rm LHT}_{Ll(d)} + 2g^{\rm LHT}_{Lr(d)})V^{(n)}\Big|^2, \tag{85}$$

where $\omega_{\rm capt}$ is the muon capture rate. D, $V^{(p)}$ and $V^{(n)}$ are the overlap integrals defined in Ref. [22]. For the reader's convenience we quote the values for Al, Ti, Au and Pb in Appendix A 6.

IV. NUMERICAL RESULTS

In this section we show numerical results for the LFV observables given in the previous section. We have to specify 19 parameters in order to calculate LFV observables in the LHT: the decay constant f, six masses of the T-odd fermions $m^i_{H\ell}$ and m^i_{Hq}, six mixing angles and six phases in the mixing matrices $V_{H\ell}$ and V_{Hd}. The value of f is constrained to $f \gtrsim 500$ GeV by the electroweak precision measurements [24]. Throughout the analysis in this paper, we fix f as $f = 500$ GeV. Since all the LFV amplitudes are proportional to f^{-2} as shown in Sec. III, the branching ratios scale as f^{-4}. We also assume that the T-odd quarks (except for the top partner) are degenerate in mass for simplicity. Under this assumption, T-odd particle loops do not induce additional contributions to the quark FCNC observables, and the mixing and the phase parameters in V_{Hd} are irrelevant. We fix the T-odd quark mass as 500 GeV. The top-partner quark mass is irrelevant for the LFV studied here. There remain nine free parameters in the T-odd lepton sector. We vary these parameters independently within the ranges 100 GeV $\leq m^i_{H\ell} \leq 1$ TeV ($i = 1,\ 2,\ 3$), $0 \leq \theta^\ell_{ij} < 2\pi$ [$(ij) = (12),\ (23),\ (13)$] and $0 \leq \delta^\ell_{ij} < 2\pi$ [$(ij) = (12),\ (23),\ (13)$]. For the type I and type II trilepton decays, we use following cutoff parameters:

$$\delta = \begin{cases} 3 \times 10^{-4} \sim 3\left(\frac{2m_e}{m_\mu}\right)^2 & : \mu^+ \to e^+e^+e^-, \\ 0.04 \sim 3\left(\frac{2m_\mu}{m_\tau}\right)^2 & : \tau^+ \to \mu^+\mu^+\mu^-,\ \tau^+ \to e^+\mu^+\mu^-, \\ 10^{-6} \sim 3\left(\frac{2m_e}{m_\tau}\right)^2 & : \tau^+ \to e^+e^+e^-,\ \tau^+ \to \mu^+e^+e^-. \end{cases} \tag{86}$$

For the type III modes we take $\delta = 0$ since there are no singularity in the differential widths.

We evaluate the observables explained in Sec. III for each model parameter set, and check if that set is allowed under current experimental constraints. At present, the upper limits of the branching ratios are available for various LFV processes. We use the values summarized in Table II.

A. μ LFV

The current experimental bounds of $\mu^+ \to e^+\gamma$ and $\mu^+ \to e^+e^+e^-$ are given by the MEGA [25] and SINDRUM I [26] collaborations, respectively. Also, the SINDRUM II collaboration provides us with upper limits on the $\mu - e$ conversion rates for titanium [27], gold [28],

Mode	Upper limit	Ref.
$\mu^+ \to e^+\gamma$	1.2×10^{-11}	[25]
$\mu^+ \to e^+e^+e^-$	1.0×10^{-12}	[26]
$\mu^-\mathrm{Ti} \to e^-\mathrm{Ti}$	4.3×10^{-12}	[27]
$\mu^-\mathrm{Au} \to e^-\mathrm{Au}$	0.7×10^{-12}	[28]
$\mu^-\mathrm{Pb} \to e^-\mathrm{Pb}$	4.6×10^{-11}	[29]

Mode	Upper limit	Ref.
$\tau^+ \to \mu^+\gamma$	4.4×10^{-8}	[30]
$\tau^+ \to \mu^+\mu^+\mu^-$	3.2×10^{-8}	[31]
$\tau^+ \to \mu^+e^+e^-$	2.7×10^{-8}	[31]
$\tau^+ \to \mu^+\pi^0$	1.1×10^{-7}	[32]
$\tau^+ \to \mu^+\eta$	6.5×10^{-8}	[33]
$\tau^+ \to \mu^+\eta'$	1.3×10^{-7}	[33]
$\tau^+ \to \mu^+\rho^0$	2.6×10^{-8}	[34]
$\tau^+ \to \mu^+\omega$	8.9×10^{-8}	[35]
$\tau^+ \to \mu^+\phi$	1.3×10^{-7}	[35]

Mode	Upper limit	Ref.
$\tau^+ \to e^+\gamma$	3.3×10^{-8}	[30]
$\tau^+ \to e^+e^+e^-$	3.6×10^{-8}	[31]
$\tau^+ \to e^+\mu^+\mu^-$	3.7×10^{-8}	[36]
$\tau^+ \to e^+\pi^0$	8.0×10^{-8}	[33]
$\tau^+ \to e^+\eta$	9.2×10^{-8}	[33]
$\tau^+ \to e^+\eta'$	1.6×10^{-7}	[33]
$\tau^+ \to e^+\rho^0$	4.6×10^{-8}	[34]
$\tau^+ \to e^+\omega$	1.1×10^{-7}	[37]
$\tau^+ \to e^+\phi$	3.1×10^{-8}	[34]

Mode	Upper limit	Ref.
$\tau^+ \to \mu^+\mu^+e^-$	2.3×10^{-8}	[31]
$\tau^+ \to e^+e^+\mu^-$	2.0×10^{-8}	[31]

TABLE II: Experimental upper bounds of various LFV branching ratios.

and lead [29]. The upper bounds given by these experiments are summarized in Table II. At present, the MEG experiment is ongoing in search for $\mu^+ \to e^+\gamma$, and an upper bound $\mathrm{Br}(\mu^+ \to e^+\gamma) < 1.5 \times 10^{-11}$ has been reported recently [38]. For $\mu - e$ conversions, COMET and Mu2e experiments are in preparation [39].

We present correlations among the branching ratios of $\mu^+ \to e^+\gamma$, $\mu^+ \to e^+e^+e^-$ and $\mu^-\mathrm{Al} \to e^-\mathrm{Al}$ in Fig. 3. The color of each dot represents the value of $\mathrm{Br}(\mu^+ \to e^+\gamma)$: black, red/gray and yellow/light-gray correspond to $10^{-12} < \mathrm{Br}(\mu^+ \to e^+\gamma) < 1.2 \times 10^{-11}$, $10^{-13} < \mathrm{Br}(\mu^+ \to e^+\gamma) \leq 10^{-12}$ and, $\mathrm{Br}(\mu^+ \to e^+\gamma) \leq 10^{-13}$, respectively. In all the scatter plots hereafter, we use the same color code. The current experimental upper limits

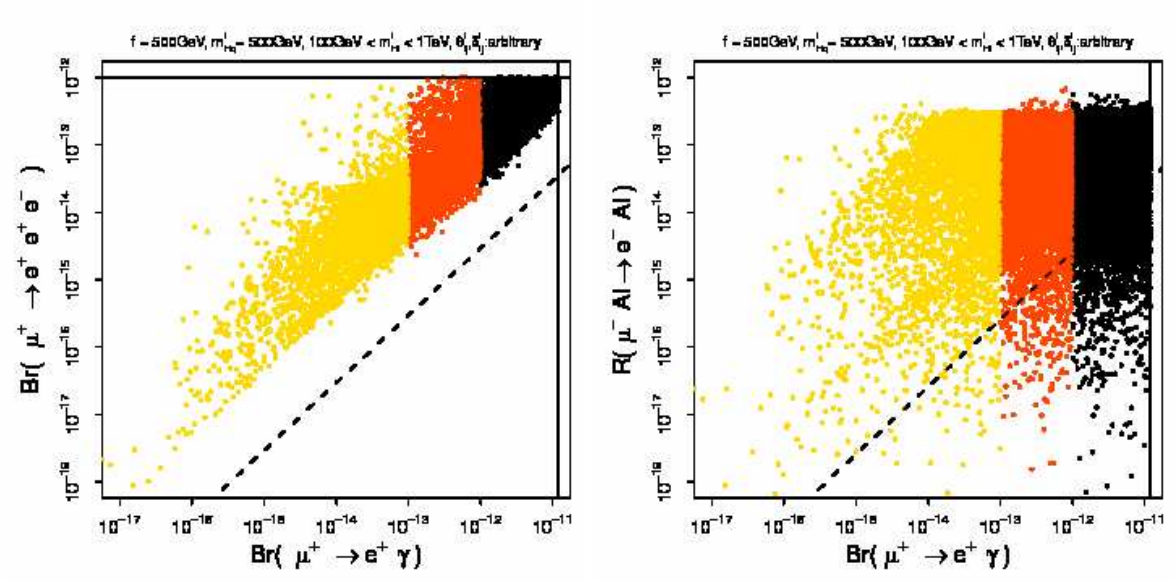

(a) (b)

(c)

FIG. 3: Correlations among the branching ratios of $\mu^+ \to e^+\gamma$, $\mu^+ \to e^+e^+e^-$ and $\mu^-\mathrm{Al} \to e^-\mathrm{Al}$ in the LHT, where the decay constant f is taken as 500 GeV. The T-odd lepton masses are varied in the range from 100 GeV to 1 TeV. The mixing angles and the phases in the mixing matrix $V_{H\ell}$ are also varied in the whole range. The T-odd quark masses are fixed as 500 GeV. The horizontal and vertical lines are experimental upper bounds. The dashed lines show the branching ratios calculated with the dipole contributions only. The color of each dot represents the value of $\mathrm{Br}(\mu^+ \to e^+\gamma)$: black, red/gray and yellow/light gray correspond to $10^{-12} < \mathrm{Br}(\mu^+ \to e^+\gamma) < 1.2 \times 10^{-11}$, $10^{-13} < \mathrm{Br}(\mu^+ \to e^+\gamma) \leq 10^{-12}$ and $\mathrm{Br}(\mu^+ \to e^+\gamma) \leq 10^{-13}$, respectively.

on $\mathrm{Br}(\mu^+ \to e^+\gamma)$ and $\mathrm{Br}(\mu^+ \to e^+e^+e^-)$ are shown by horizontal and vertical lines. The dashed lines show the branching ratios calculated with only the contributions from the dipole moment type operator $\bar{\mu}_R \sigma^{\mu\nu} e_L F_{\mu\nu}$. In a certain class of models, such as SUSY, it is known that the LFV effect dominantly appears in the dipole moment operator. In such a model, the branching ratios are predicted to be on the dashed lines in the correlation plots. In contrast with those models, the correlations in the LHT show that the contributions of the dipole moment operator are less significant than those from other four-Fermi interaction terms in $\mu^+ \to e^+e^+e^-$ and $\mu^-\mathrm{Al} \to e^-\mathrm{Al}$, as noted in Ref. [12]. We can see that there is rather strong correlation between the branching ratios of $\mu^+ \to e^+\gamma$ and $\mu^+ \to e^+e^+e^-$ whereas no correlation is observed in the branching ratios of $\mu^+ \to e^+\gamma$ and the conversion rate for Al.

We show the angular asymmetries of $\mu^+ \to e^+e^+e^-$ in Fig. 4. As explained in Sec. III B, A_Z and A_X are parity odd asymmetries and A_Y is a time-reversal asymmetry. We can see that A_Z is within the range from about -45% to $+30\%$, while A_X is within the range from about -10% to $+20\%$. There is a positive correlation between A_Z and A_X as shown in Fig. 4(c). Both asymmetries do not have correlations with the branching ratio. Possible value of the time-reversal asymmetry A_Y is in the range from about -10% to $+10\%$.

In Fig. 5, the $\mu - e$ conversion rates for Al, Ti, Au and Pb are plotted as functions of the mass of the first generation T-odd lepton $m^1_{H\ell}$ for $f = 500$ GeV. Here, we fix the parameters in the T-odd lepton sector as $m^2_{H\ell} = m^3_{H\ell} = 400$ GeV, $\theta^\ell_{12} = \pi/500$, $\theta^\ell_{23} = \theta^\ell_{13} = 0$ and $\delta^\ell_{ij} = 0$. T-odd quark masses are also fixed to 500 GeV, as in other scatter plots in this paper. The region $m^1_{H\ell} \gtrsim 500$ GeV is excluded since the branching ratio for Au exceeds the experimental upper limit. At $m^1_{H\ell} = 400$ GeV, all the three T-odd leptons are degenerate in mass, so that all the LFV amplitudes vanish. We can see that the conversion rates are suppressed also in a region between $m^1_{H\ell} = 100$ GeV and 200 GeV. In this region, cancellation among transition amplitudes occurs at different points for different nuclide.

We show correlation between the $\mu - e$ conversion rates for Al vs Ti (Au, Pb) in Fig. 6. We can see the ratios of the conversion rates vary within 1 order of magnitude in most of the parameter space. We also notice that, in some cases, the conversion rate for Ti, Au and Pb can be close to the experimental bounds even if the rate for Al is suppressed.

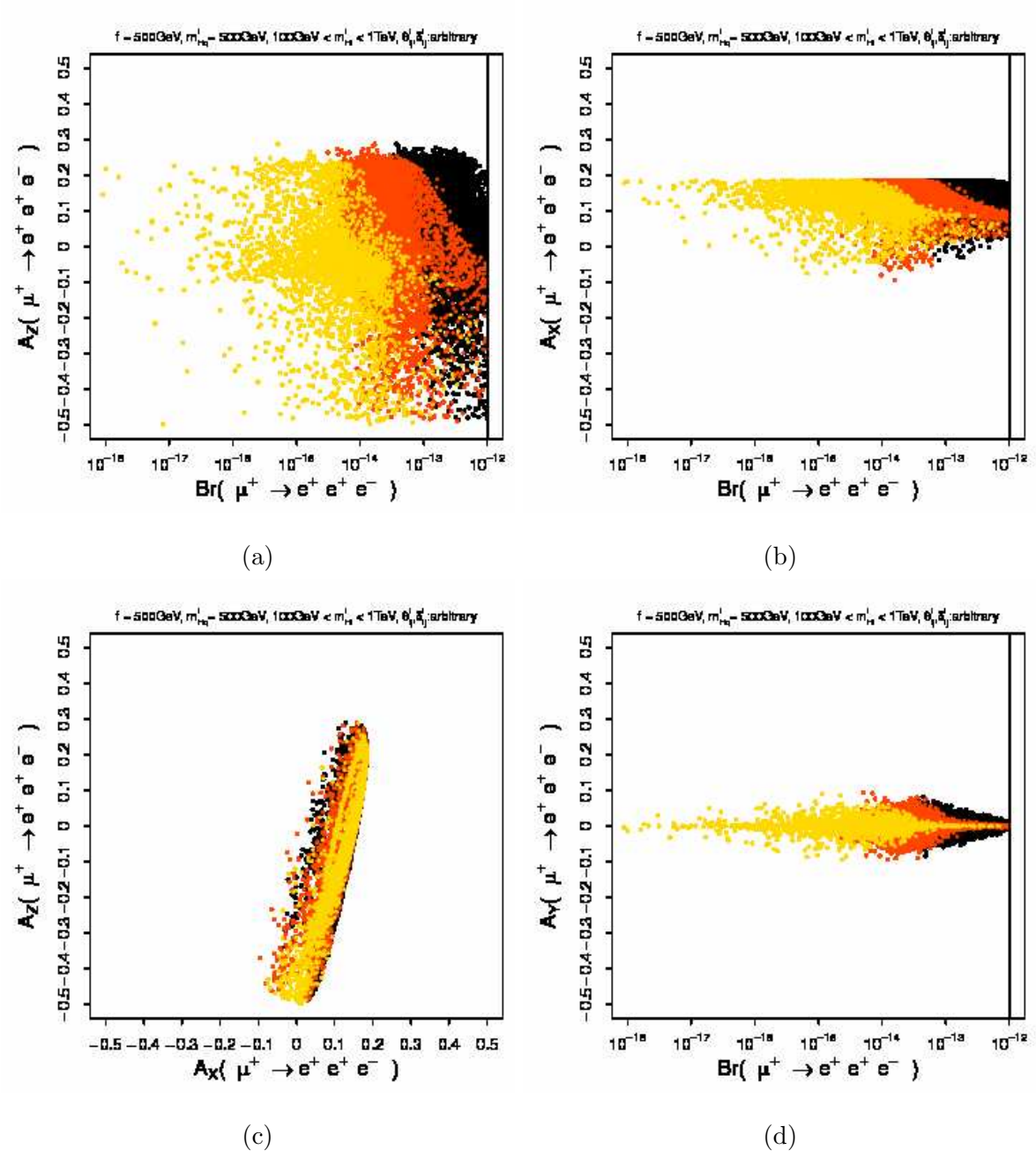

FIG. 4: Angular asymmetries of $\mu^+ \to e^+e^+e^-$ as functions of the branching ratio in the LHT for the same parameter set as in Fig. 3. The correlation between A_Z and A_X is also shown in (c). The vertical solid lines in (a), (b), and (d) is the experimental upper limit of $\mathrm{Br}(\mu^+ \to e^+e^+e^-)$. The color code is the same as in Fig. 3.

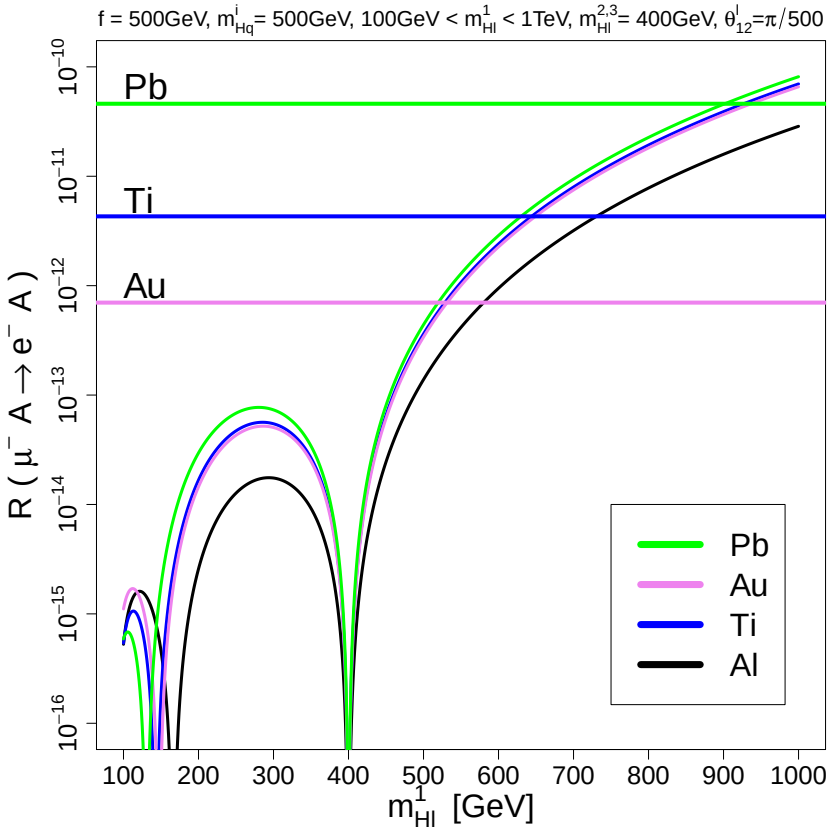

FIG. 5: $\mu - e$ conversion rates for lead, gold, titanium and aluminum as functions of the first generation T-odd lepton mass $m^1_{H\ell}$ for $f = 500$ GeV. Other parameters in the T-odd lepton sector are fixed as $m^2_{H\ell} = m^3_{H\ell} = 400$ GeV, $\theta^\ell_{12} = \pi/500$, $\theta^\ell_{23} = \theta^\ell_{13} = 0$ and $\delta^\ell_{ij} = 0$. The T-odd quark masses are also fixed as 500 GeV. The horizontal lines are the experimental upper bounds for Pb, Au and Ti.

B. τ LFV

The current upper bounds for τ-LFV decays are listed in Table II. These bounds are set by either the Belle and the Babar experiments. Improvements by 1 or 2 orders of magnitude are expected at future B-factories at KEK and in Italy [40].

In this subsection, we mainly present the results on the observables in $\tau \to \mu$ decays discussed in Sec. III. Quantities in $\tau \to e$ decay modes behave similarly to corresponding ones in $\tau \to \mu$ modes. Correlations between the observable quantities in $\tau \to \mu$ and $\tau \to e$ modes are discussed in Sec. IV C.

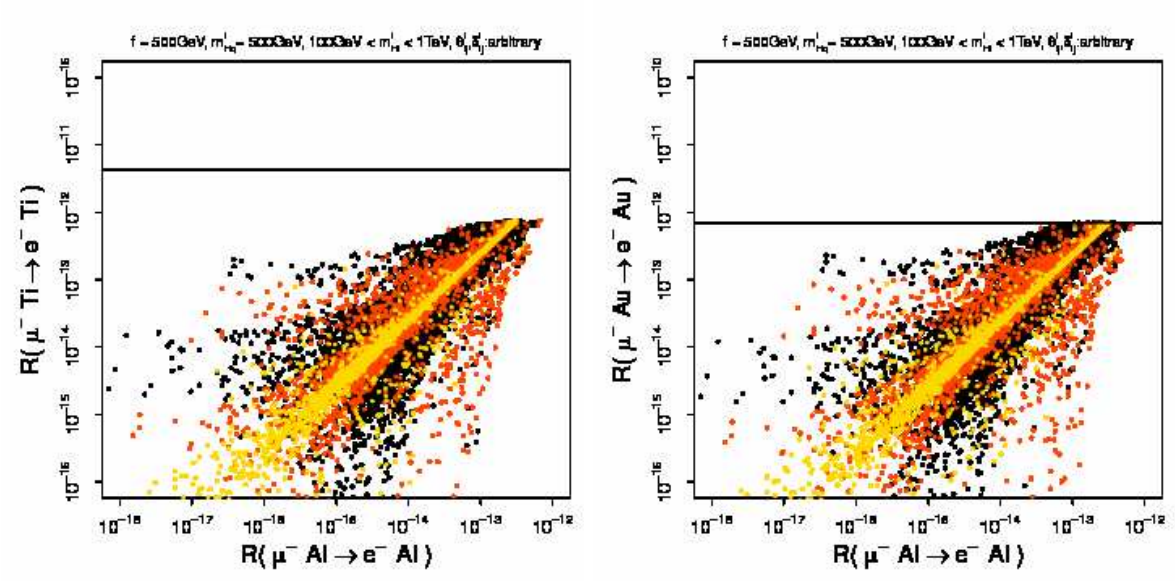

(a)

(b)

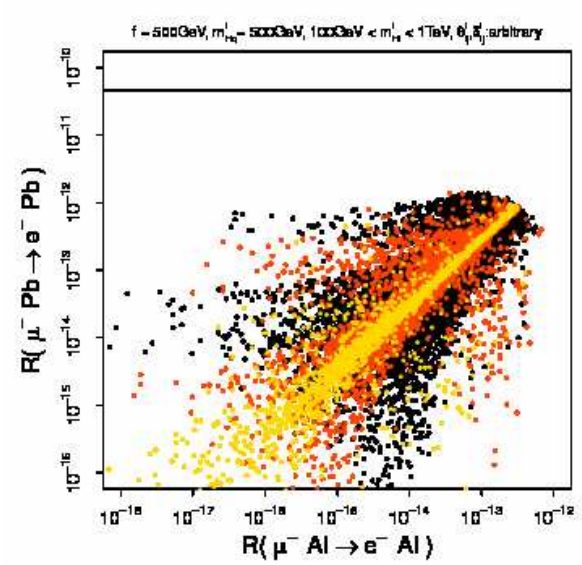

(c)

FIG. 6: Correlations among the $\mu - e$ conversion rates for Ti, Au, or Pb vs Al. The horizontal lines are experimental bounds. The input parameter set and the color code of the plots are the same as those in Fig. 3.

1. $\tau \to \mu\gamma$ and trilepton decay modes

In Fig. 7, we show correlations among the branching ratios of $\tau^+ \to \mu^+\gamma$, $\tau^+ \to \mu^+\mu^+\mu^-$, $\tau^+ \to \mu^+e^+e^-$ and $\tau^+ \to \mu^+\mu^+e^-$. We see that the branching ratio of $\tau^+ \to \mu^+\gamma$ can be

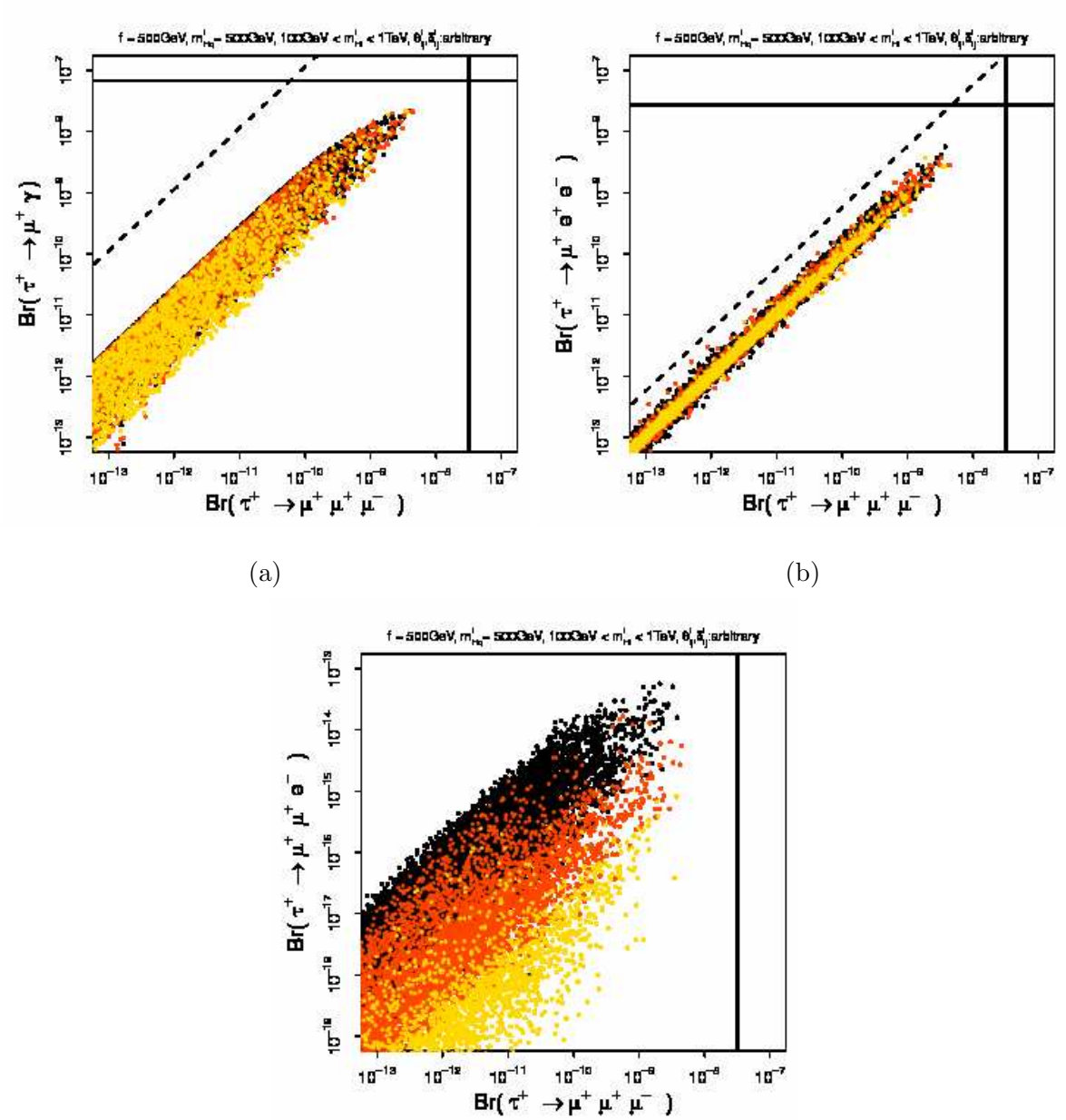

(a) (b)

(c)

FIG. 7: Branching ratios of $\tau^+ \to \mu^+\gamma$, $\tau^+ \to \mu^+e^+e^-$ and $\tau^+ \to \mu^+\mu^+e^-$ as functions of $\mathrm{Br}(\tau^+ \to \mu^+\mu^+\mu^-)$ for the same input parameter set as in Fig. 3. The horizontal and the vertical lines are the experimental bounds. The dashed lines show the branching ratios calculated with the dipole contributions only. The color code is the same as in Fig. 3.

as large as 10^{-8}, which is close to current experimental upper limit. For $\tau^+ \to \mu^+\mu^+\mu^-$ and $\tau^+ \to \mu^+e^+e^-$, the possible maximal values of the branching ratios are about 1 order of magnitude below the corresponding experimental limits. The behavior of the correlation between $\mathrm{Br}(\tau^+ \to \mu^+\gamma)$ and $\mathrm{Br}(\tau^+ \to \mu^+\mu^+\mu^-)$ shown in Fig. 7(a) is similar to the $\mu \to e$ case given in Fig. 3(a): $\mathrm{Br}(\tau^+ \to \mu^+\mu^+\mu^-)$ is larger than the prediction in the dipole-dominant case (dashed line) by 1 or 2 orders of magnitude. Since we take all the masses and the mixing angles/phases in the T-odd lepton sector as free parameters, there is no direct correlation between the $\tau \to \mu$ and $\mu \to e$ transition amplitudes. Therefore, the correlation plots among $\tau \to \mu$ processes do not change much even if the upper limit of $\mathrm{Br}(\mu \to e\gamma)$ is lowered. As shown in Fig. 7(c), the branching ratio of $\tau^+ \to \mu^+\mu^+e^-$ is highly suppressed because this process involves the $\mu \to e$ transition, whose magnitude is constrained by other $\mu \to e$ processes discussed in the previous subsection. We see that the suppression of $\mathrm{Br}(\tau^+ \to \mu^+\mu^+e^-)$ is stronger for a smaller value of $\mathrm{Br}(\mu^+ \to e^+\gamma)$. As for the other type III decay mode $\tau^+ \to e^+e^+\mu^-$, the correlation plot with $\mathrm{Br}(\tau^+ \to e^+e^+e^-)$ is almost the same as Fig. 7(c).

We show angular asymmetries of $\tau^+ \to \mu^+\mu^+\mu^-$ in Fig. 8. We find that the parity asymmetries are within the ranges $-25\% \lesssim A_Z \lesssim +25\%$ and $+5\% \lesssim A_X \lesssim +15\%$ irrespective of the branching ratio for $\mathrm{Br}(\tau^+ \to \mu^+\mu^+\mu^-) \gtrsim 10^{-13}$. The time-reversal asymmetry A_Y is very small for the same range of the branching ratio. Compared with Fig. 4, we can see that the possible ranges of the asymmetries for $\tau^+ \to \mu^+\mu^+\mu^-$ are narrower than those for $\mu^+ \to e^+e^+e^-$. This quantitative difference between the $\tau^+ \to \mu^+\mu^+\mu^-$ and $\mu^+ \to e^+e^+e^-$ cases is caused by the difference in the allowed ranges of the branching ratios. In the general scan in the parameter space of the T-odd lepton sector, the decay amplitudes for $\mu^+ \to e^+e^+e^-$, $\tau^+ \to \mu^+\mu^+\mu^-$ and $\tau^+ \to e^+e^+e^-$ behave in the same way. Consequently the distribution patterns of the asymmetries in the scatter plots such as Figs. 4 and 8 are similar if the experimental limits and differences of cutoff parameters are neglected. In fact, we have checked that the patterns of the scatter plots in Figs. 4 and 8 become the same if we draw all the sample points, including those excluded by the experimental limits as long as we take same cutoff parameters.

Figures. 9 and 10 show the asymmetries of the type II decay $\tau^+ \to \mu^+e^+e^-$. As given in Sec. III C, we define the seven asymmetries. We can see that the allowed ranges of the parity asymmetries A_Z, A_X, A_{ZFB} and A_{XFB} are almost independent of the branching ratio.

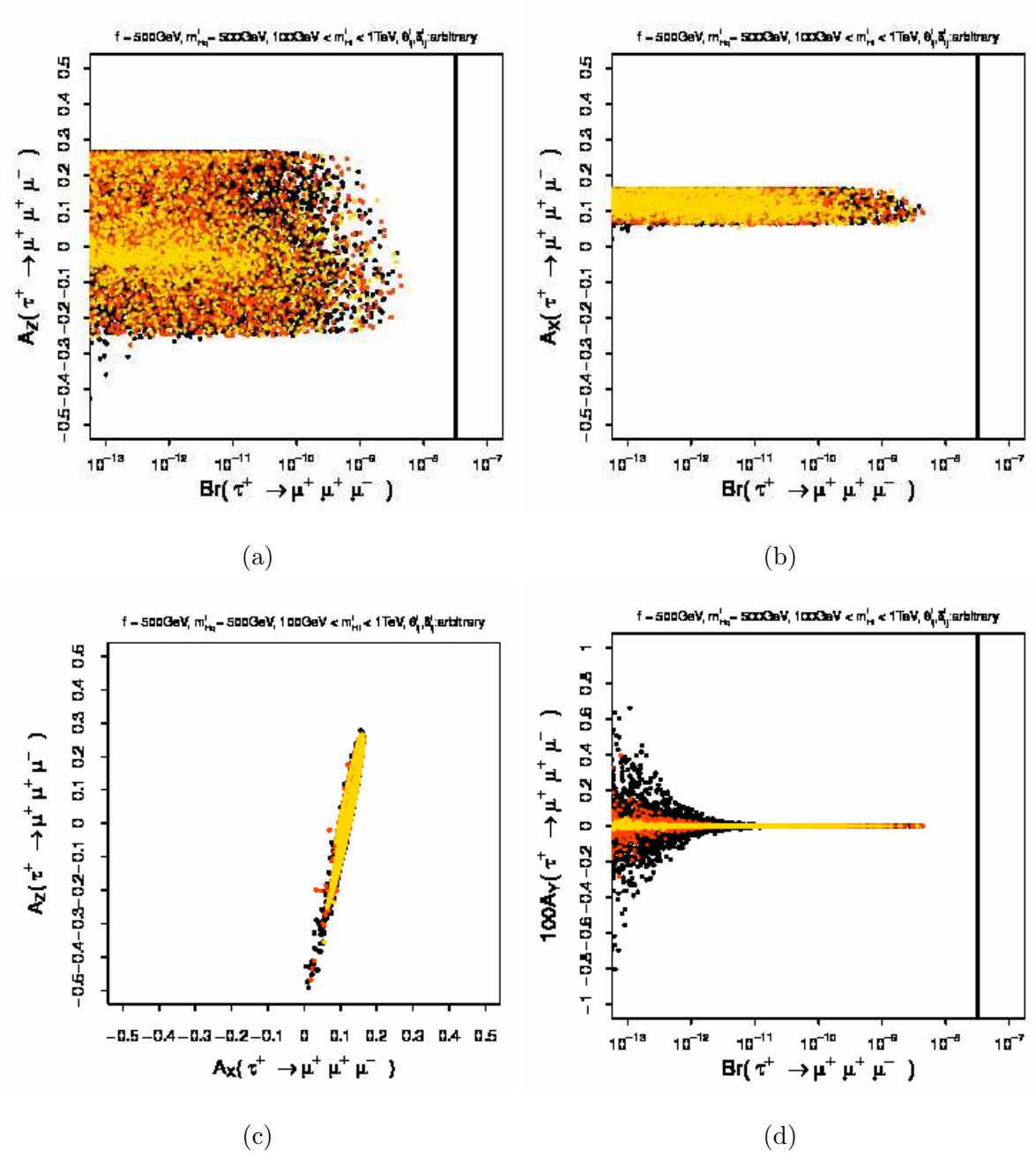

FIG. 8: Angular asymmetries of $\tau^+ \to \mu^+\mu^+\mu^-$ as functions of the branching ratio for the same parameter set as in Fig. 3. The correlation between A_Z and A_X is also shown in (c). A_Y is magnified by 100 in (d). The vertical solid lines in (a), (b) and (d) are the experimental upper limit of $\mathrm{Br}(\tau^+ \to \mu^+\mu^+\mu^-)$. The color code is the same as in Fig. 3.

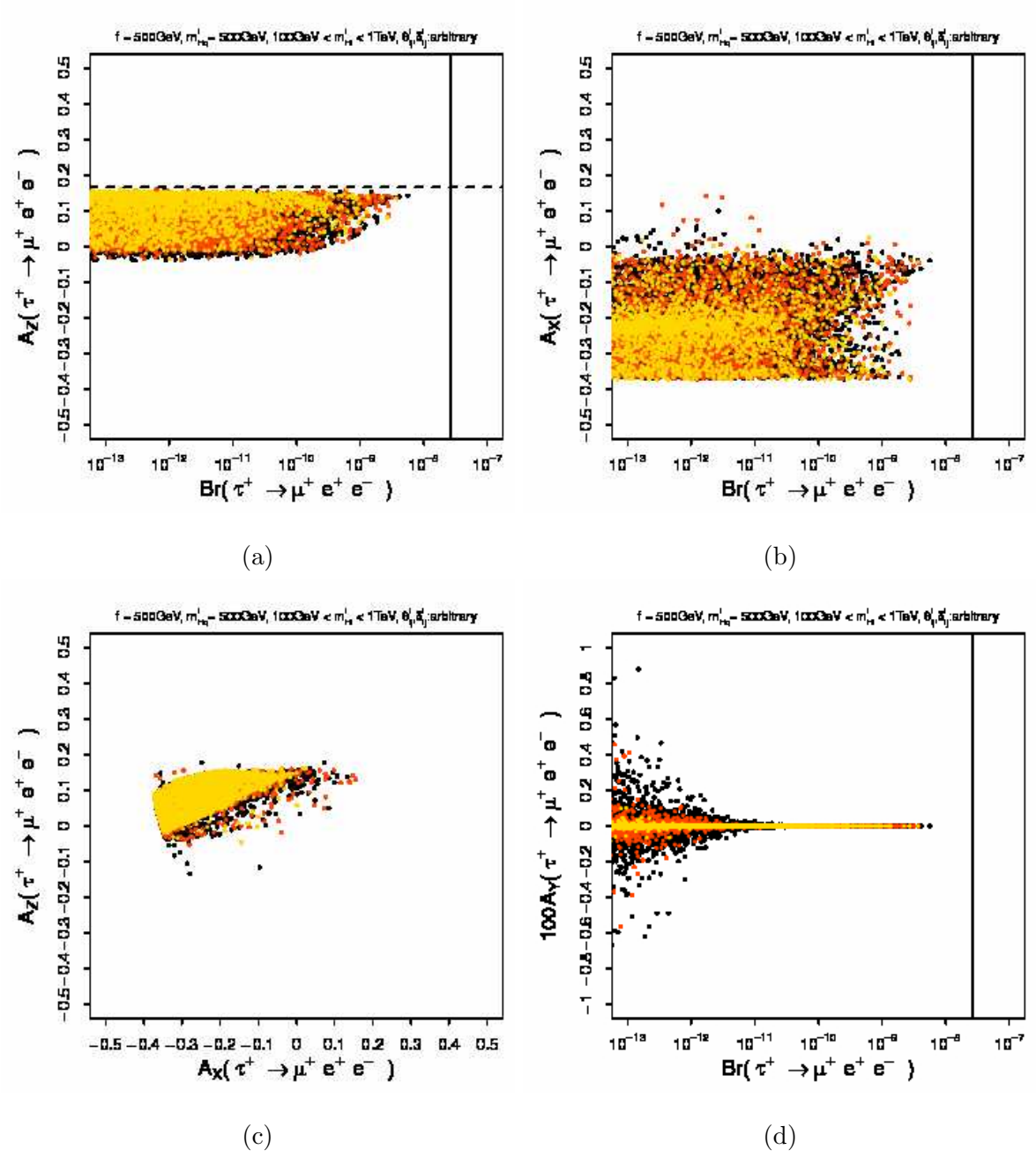

FIG. 9: Angular asymmetries of $\tau^+ \to \mu^+ e^+ e^-$ as functions of the branching ratio for the same parameter set as in Fig. 3. The correlation between A_Z and A_X is also shown in (c). A_Y is magnified by 100 in (d). The vertical solid lines in (a), (b), and (d) is the experimental upper limit of $\mathrm{Br}(\tau^+ \to \mu^+ e^+ e^-)$. The horizontal dashed line in (a) is the value in $A_R^{\mathrm{LHT}} \to 0$ limit. The color code is the same as in Fig. 3.

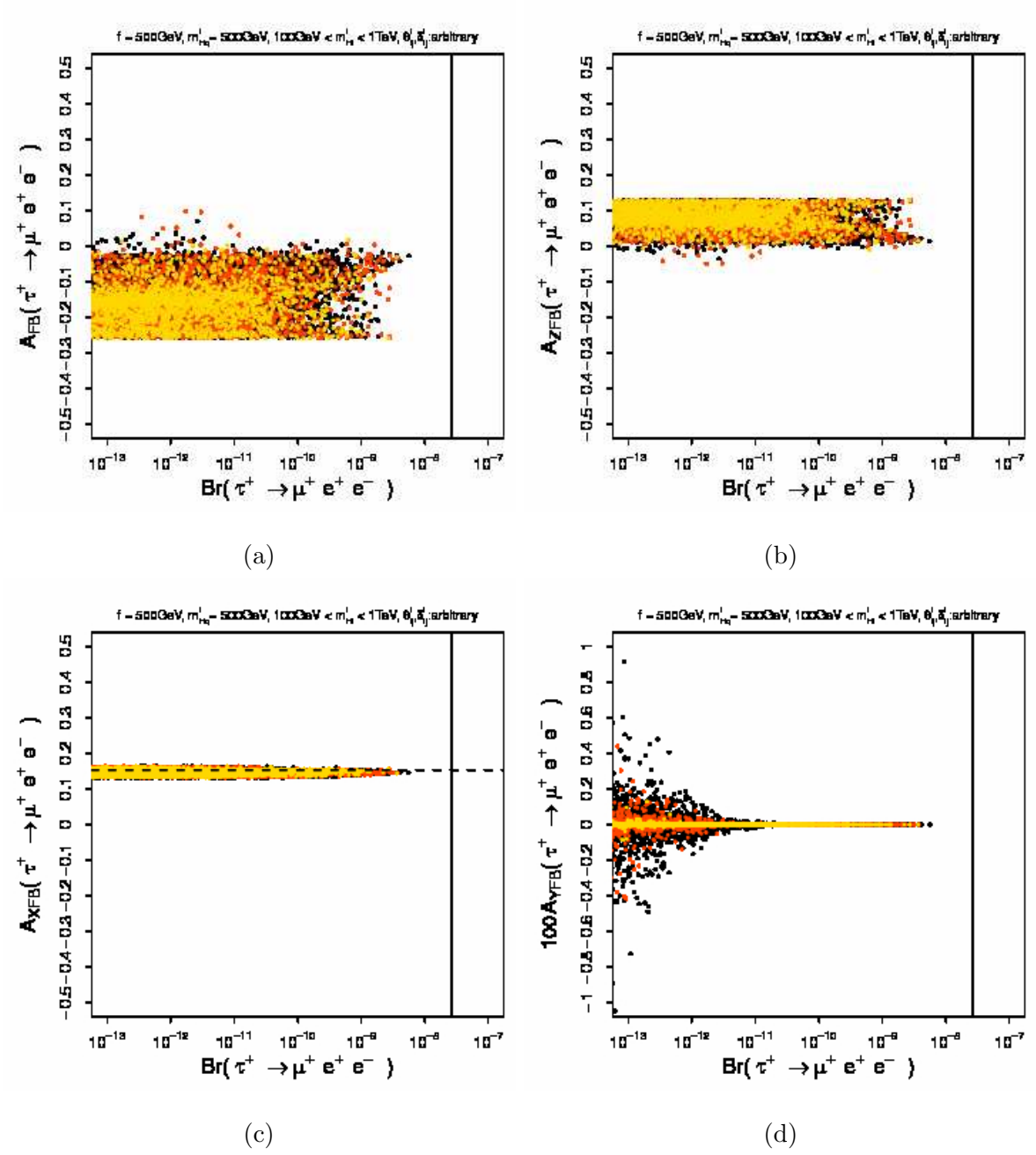

FIG. 10: Forward-backward asymmetry and forward-backward type angular asymmetries of $\tau^+ \to \mu^+e^+e^-$ as functions of the branching ratio for the same parameter set as in Fig. 3. A_{YFB} is magnified by 100 in (d). The vertical solid line in each plot is the experimental upper limit of $\mathrm{Br}(\tau^+ \to \mu^+e^+e^-)$. The horizontal dashed line in (c) is the value in $A_R^{\mathrm{LHT}} \to 0$ limit. The color code is the same as in Fig. 3.

Taking the $A_R^{\rm LHT} \to 0$ limit is informative to understand the behavior of the asymmetries, because the contribution of the dipole term in the LHT is relatively small. In this limit, values of A_Z and A_{XFB} are constants:

$$A_Z^{\rm II,LHT}(\delta \to 0)\Big|_{A_R^{\rm LHT}\to 0} = \frac{1}{6}, \tag{87}$$

$$A_{XFB}^{\rm II,LHT}(\delta \to 0)\Big|_{A_R^{\rm LHT}\to 0} = \frac{16}{105}. \tag{88}$$

Deviations from these values seen in Figs. 9(a) and 10(c) are identified as effects of the dipole term. This effect is larger in A_Z because the function D_5 in Eq. (62a) becomes logarithmically large for $\delta \to 0$ [see Eq. (A30e)], while the function E_4 in Eq. (A29c) does not have such an enhancement. On the other hand, $A_X^{\rm II,LHT}$ and $A_{ZFB}^{\rm II,LHT}$ depend on the relative magnitude of $g_{Ll}^{\rm II,LHT}$ and $g_{Lr}^{\rm II,LHT}$, so that these asymmetries depend on input parameters even if the dipole term is neglected. That is why $A_X^{\rm II,LHT}$ distributes within a wider range compared with $A_Z^{\rm II,LHT}$.

Since the $\tau^+ \to \mu^+e^+e^-$ decay in the LHT is described by only three Wilson coefficients, we can derive the following proportionality relation for $\delta \to 0$:

$$A_X : A_{FB} : A_{ZFB} = -\frac{4\pi}{35} : -\frac{1}{4} : \frac{1}{8}. \tag{89}$$

This relation holds for any values of $g_{Ll}^{\rm II,LHT}$, $g_{Lr}^{\rm II,LHT}$ and $A_R^{\rm LHT}$. Although A_{FB} is not a parity asymmetry, it is related to the parity asymmetries A_X and A_{ZFB} because of the restricted chirality structure of the LHT. We can see that Eq. (89) holds in a good approximation in Figs. 9(b), 10(a) and 10(b).

More relations characteristic to the LHT are discussed in Appendix C. When the LFV processes are precisely measured, these relations might be useful to determine whether or not the new physics is the LHT.

The time-reversal asymmetries A_Y and A_{YFB} are very small for $\mathrm{Br}(\tau^+ \to \mu^+e^+e^-) \gtrsim 10^{-13}$.

2. Semileptonic decay modes

The correlations between branching ratios of $\tau^+ \to \mu^+P$ ($P = \pi^0, \eta, \eta'$) and $\tau^+ \to \mu^+\mu^+\mu^-$ are shown in Fig. 11. These branching ratios are roughly of the same order of magnitude for each set of input parameters, because relevant Wilson coefficients $g_{Ll,r}^{\rm I,LHT}$ and

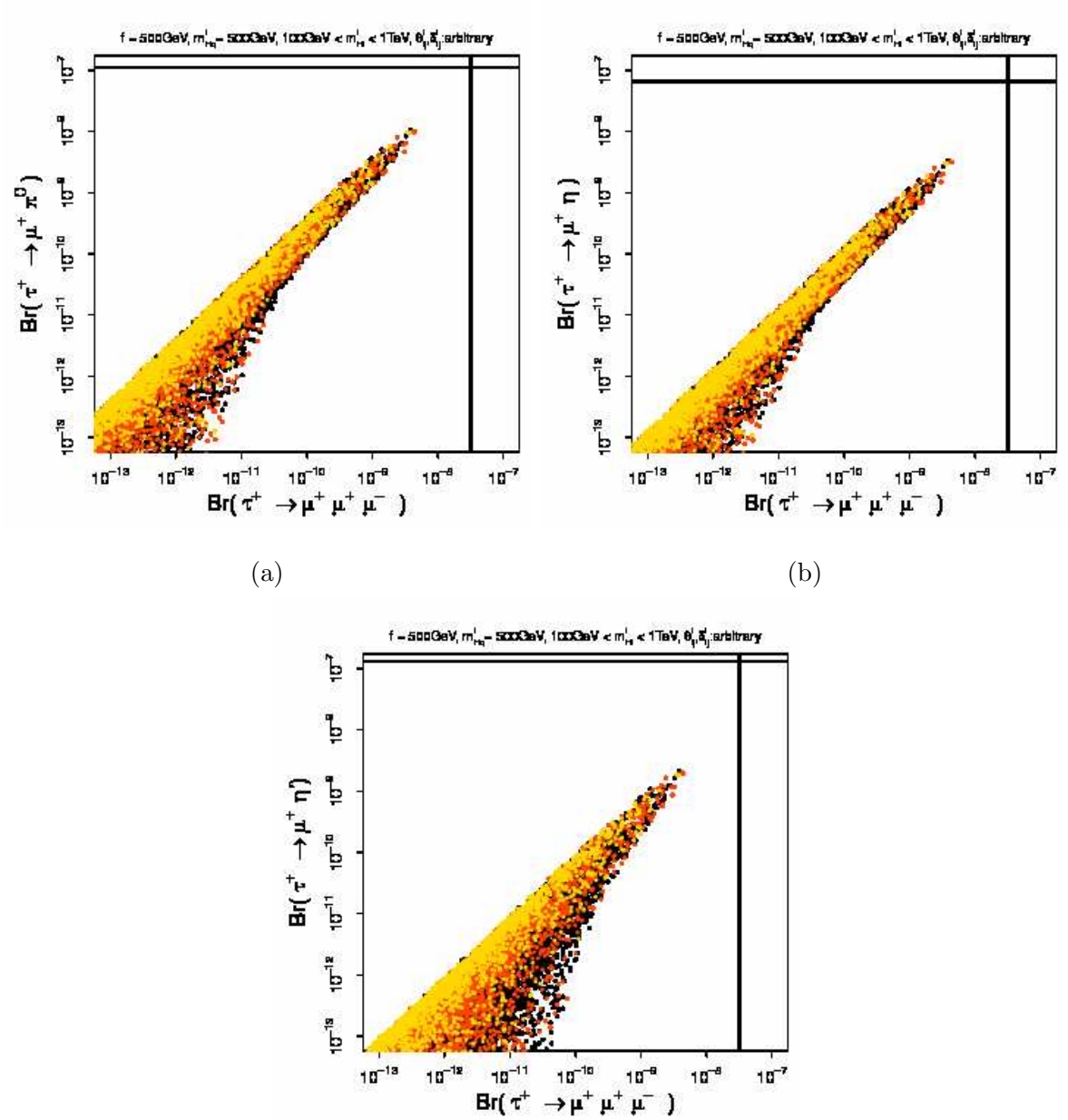

(a) (b)

(c)

FIG. 11: Correlations between $\mathrm{Br}(\tau^+ \to \mu^+ P)$ and $\mathrm{Br}(\tau^+ \to \mu^+\mu^+\mu^-)$ for $P = \pi^0$, η and η'. Input parameters are the same as those in Fig. 3. The vertical and the horizontal solid lines are the experimental upper limits. The color code is the same as in Fig. 3.

$g^{\mathrm{LHT}}_{Ll,r(q)}$ in Eqs. (45), (46), (73) and (74) are similar in magnitude and the effect of the dipole term (in $\tau^+ \to \mu^+\mu^+\mu^-$) on the branching ratio is small.

In Fig. 12 we show the branching ratios of $\tau^+ \to \mu^+ V$ ($V = \rho^0, \omega, \phi$) decays. The qualitative behavior of the correlations is the same as in the $\tau^+ \to \mu^+ P$ case. Polarization

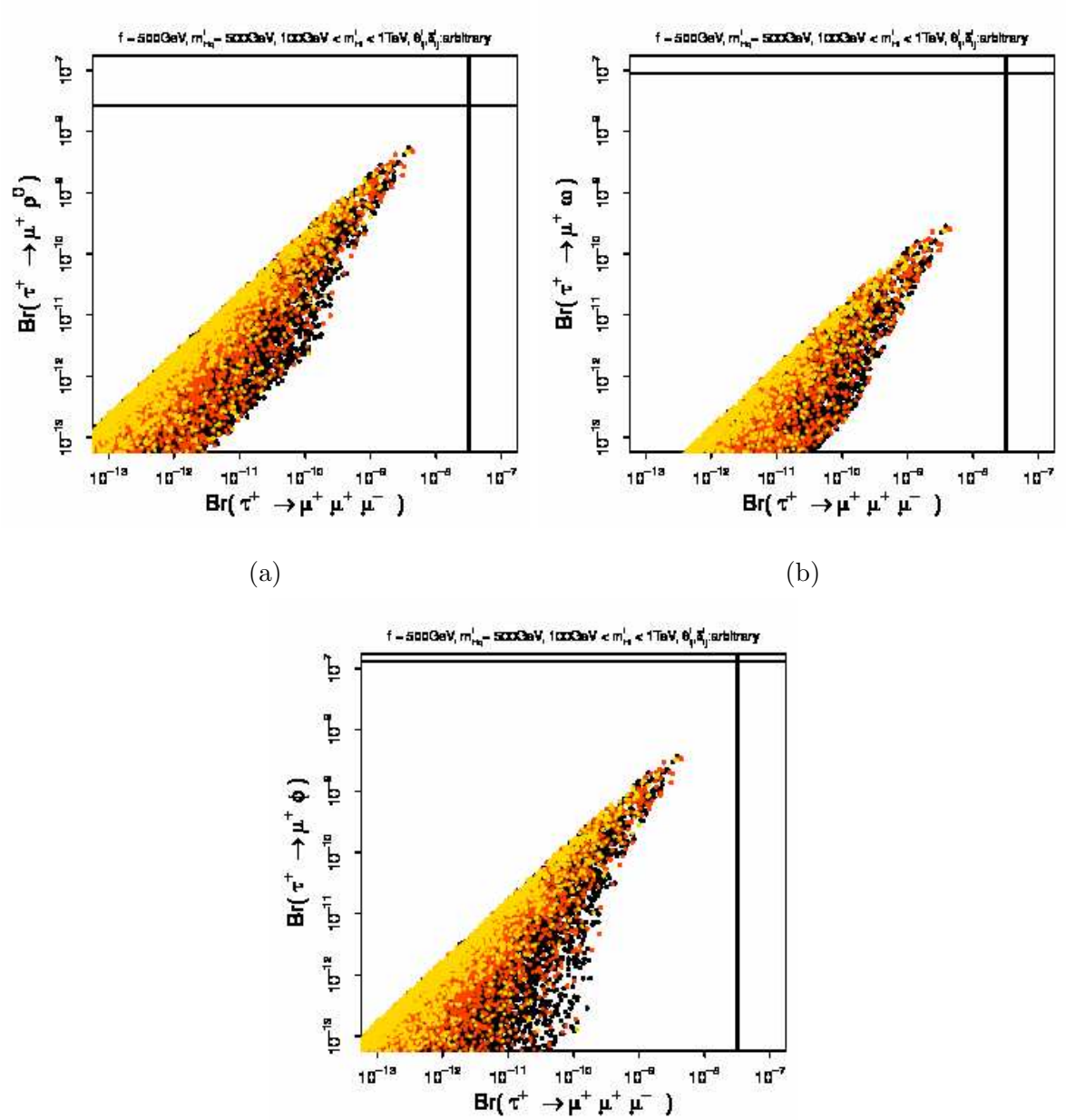

(a) (b)

(c)

FIG. 12: Correlations between $\mathrm{Br}(\tau^+ \to \mu^+ V)$ and $\mathrm{Br}(\tau^+ \to \mu^+\mu^+\mu^-)$ for $V = \rho^0$, ω and ϕ. Input parameters are the same as those in Fig. 3. The vertical and the horizontal solid lines are the experimental upper limits. The color code is the same as in Fig. 3.

asymmetries are shown in Fig. 13. The contribution of the dipole term in $\tau^+ \to \mu^+ V$ affects the polarization asymmetry though the effect on the branching ratio is small. In the

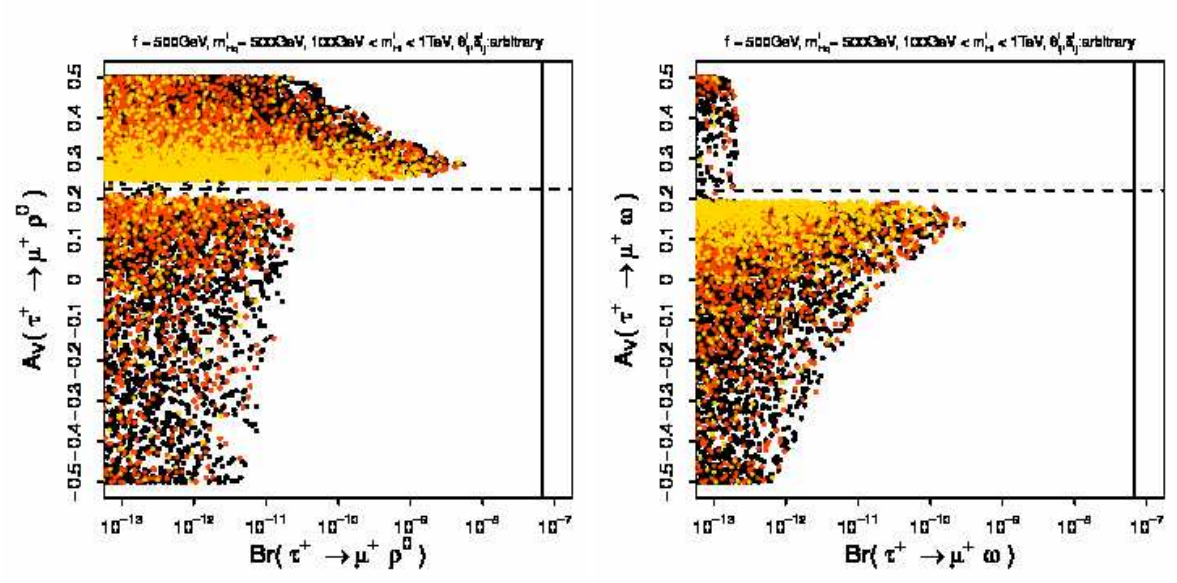

(a) (b)

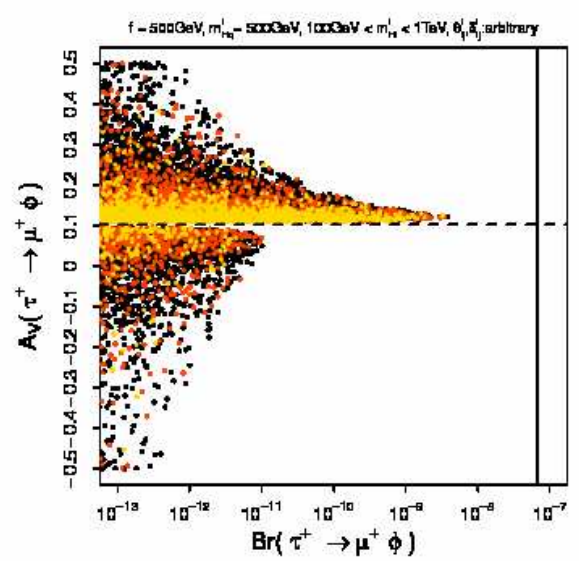

(c)

FIG. 13: Correlations between the polarization asymmetries and the branching ratios for $\tau^+ \to \mu^+ V$ ($V = \rho^0$, ω and ϕ) decay modes. Input parameters and the color code are the same as those in Fig. 3. The vertical solid lines are the experimental upper limits of the branching ratios. The dashed lines show asymmetries in $A_R^{\rm LHT} \to 0$ limit.

$A_R^{\rm LHT} \to 0$ limit, the asymmetry is determined as

$$A_V(\tau^+ \to \mu^+ V)_{\rm LHT}\big|_{A_R^{\rm LHT}\to 0} = \frac{1}{2}\frac{m_\tau^2 - 2m_V^2}{m_\tau^2 + 2m_V^2} \approx \begin{cases} 0.22 \ \text{ for } \ V = \rho^0,\, \omega, \\ 0.10 \ \text{ for } \ V = \phi. \end{cases} \tag{90}$$

The deviations from these values seen in Fig. 13 can be understood as effects of interferences

between the dipole and the four-Fermi terms. In particular, in the parameter region where the branching ratios are larger than 10^{-10}, contributions of the four-Fermi terms dominate the decay amplitude, so that values of A_V are not much different from those given in (90).

As in the case of trilepton modes, we can derive several relations among various branching ratios asymmetries of semileptonic modes, which is discussed in Appendix C.

C. Correlations among $\mu \to e$, $\tau \to \mu$, and $\tau \to e$ transitions

There are three classes of processes which change the lepton flavor by one: $\mu \to e$, $\tau \to \mu$, and $\tau \to e$ transitions. Here, we discuss correlations among different lepton flavor transitions.

We show correlations among branching ratios of $\mu^+ \to e^+\gamma$, $\tau^+ \to \mu^+\gamma$, and $\tau^+ \to e^+\gamma$ in Fig. 14. As can be seen in Fig. 14(a) and (b), there are no direct correlations between the branching ratios of $\mu^+ \to e^+\gamma$ and τ LFV decays, because we take the T-odd lepton masses $m^i_{H\ell}$ and parameters in the mixing matrix $V_{H\ell}$ as free parameters and vary them independently. On the other hand, in Fig. 14(c), we notice that a parameter region where both $\mathrm{Br}(\tau^+ \to \mu^+\gamma)$ and $\mathrm{Br}(\tau^+ \to e^+\gamma)$ are larger than 10^{-9} is not allowed. When both $\tau \to \mu$ and $\tau \to e$ transition amplitudes are large, the corresponding $\mu \to e$ amplitudes also become large so that the branching ratios of the $\mu \to e$ transition processes exceed the experimental bounds. In fact, we have checked that the branching ratios $\mathrm{Br}(\ell_1 \to \ell_2\gamma)/\mathrm{Br}(\ell_1 \to \ell_2\nu\bar{\nu})$ $[(\ell_1, \ell_2) = (\mu, e), (\tau, \mu)$ and $(\tau, e)]$ distribute within the same range ($\lesssim 10^{-7}$) when we ignore experimental constraints on $\mu \to e$ processes.

The correlations among the type I leptonic three-body decay branching ratios are shown in Fig. 15. The behavior of the correlations is the same as the case of Fig. 14.

V. CONCLUSION

We have calculated branching ratios and angular and forward-backward asymmetries of μ and τ-LFV processes in the LHT. We have obtained the following results:

- The branching ratios of three μ-LFV processes, $\mu^+ \to e^+\gamma$, $\mu^+ \to e^+e^+e^-$ and the $\mu - e$ conversion rates, can be close to the present experimental bounds. There is a rather strong correlation between the branching ratios of $\mu^+ \to e^+\gamma$ and $\mu^+ \to e^+e^+e^-$. This

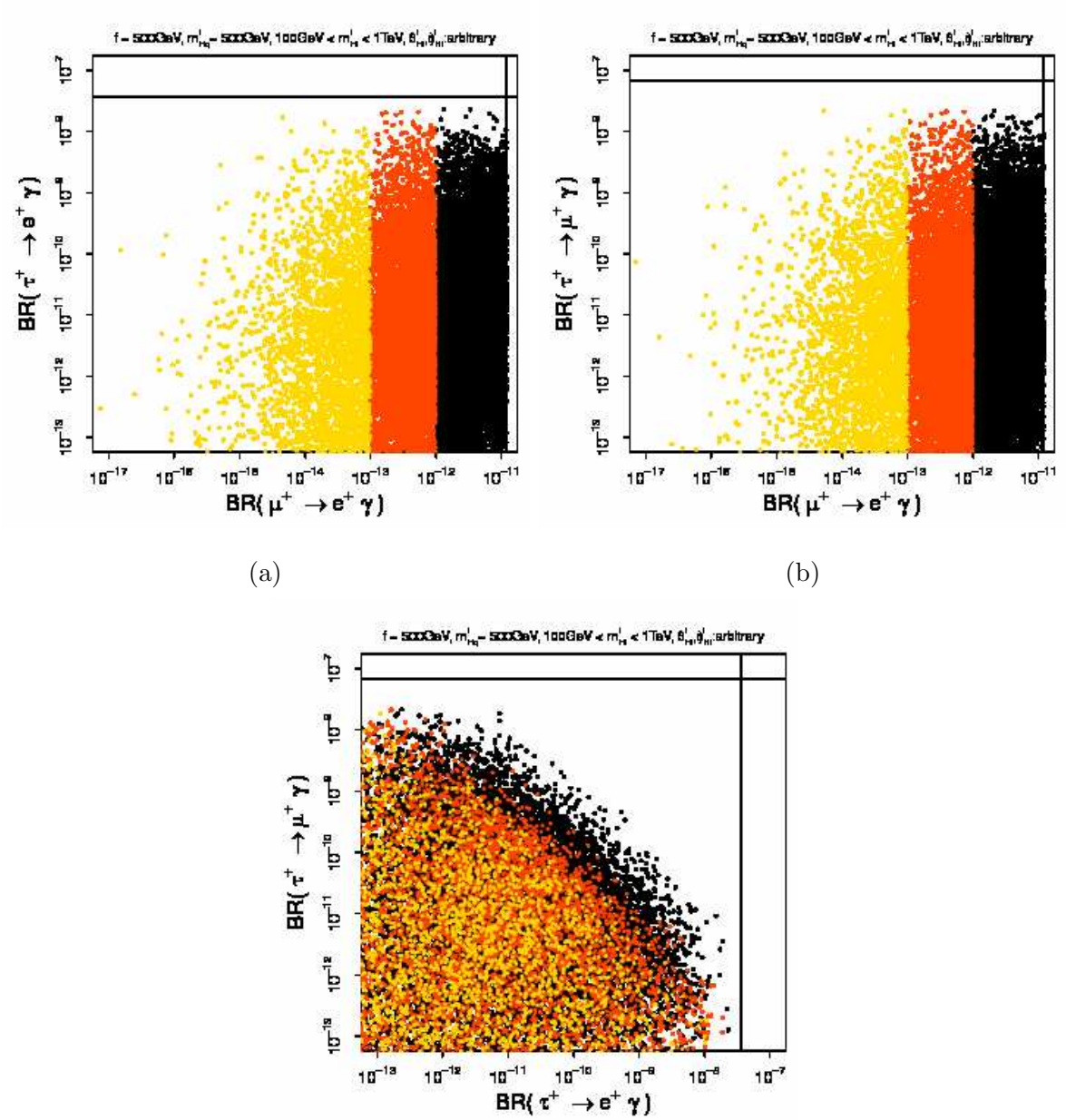

FIG. 14: Correlations among branching ratios of $\mu^+ \to e^+\gamma$, $\tau^+ \to \mu^+\gamma$ and $\tau^+ \to e^+\gamma$. Input parameters and the color code are the same as those in Fig. 3. The horizontal and the vertical lines are experimental upper bounds.

is in contrast to the case of $\mu^+ \to e^+\gamma$ and the $\mu - e$ conversion where no correlation is observed. These features are noted in Ref. [12]

- The parity asymmetry of $\mu^+ \to e^+\gamma$ is -1/2. For $\mu^+ \to e^+e^+e^-$, the parity asymmetries can be large, whereas the time-reversal asymmetry is within 10%.

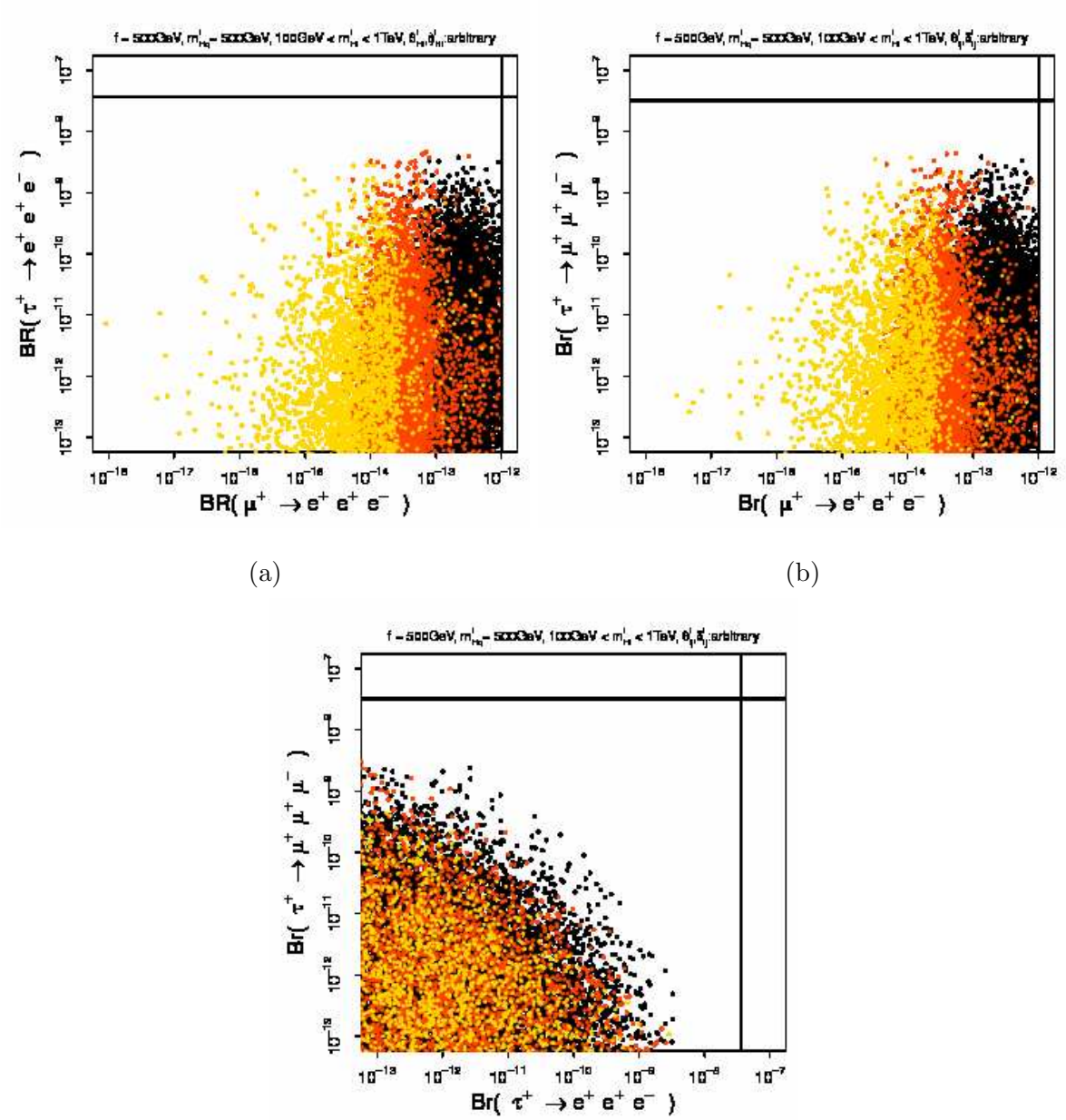

(a) (b)

(c)

FIG. 15: Correlations among branching ratios of $\mu^+ \to e^+e^+e^-$, $\tau^+ \to \mu^+\mu^+\mu^-$ and $\tau^+ \to e^+e^+e^-$. Input parameters and the color code are the same as those in Fig. 3. The horizontal and the vertical lines are experimental upper bounds.

- We have calculated the $\mu - e$ conversion rates for various muonic atoms: Al, Ti, Au and Pb. In most of the parameter space, ratios of the conversion rates are found within 1 order of magnitude. In some cases, however, the conversion rates for Ti, Au and Pb can be close to the experimental bounds even if the rate for Al is suppressed.

- The maximal values of the branching ratios for various τ-LFV processes are 10^{-9}–10^{-8} except for $O(10^{-10})$ for $\tau^+ \to \mu^+\omega$ and $\tau^+ \to e^+\omega$, and $O(10^{-13})$ for $\tau^+ \to \mu^+\mu^+e^-$ and $\tau^+ \to e^+e^+\mu^-$.

- The parity asymmetries of $\tau^+ \to \mu^+\gamma$ and $\tau^+ \to e^+\gamma$ are -1/2 and $\tau^+ \to \mu^+P$ and $\tau^+ \to e^+P$ are 1/2 reflecting the chirality structure. For $\tau^+ \to \mu^+V$ and $\tau^+ \to e^+V$, if branching ratios are larger than 10^{-10}, the asymmetries are about 0.3, 0.15, and 0.1 for ρ^0, ω, and ϕ, respectively.

- There are sizable parity asymmetries in $\tau^+ \to \mu^+\mu^+\mu^-$, $\tau^+ \to e^+e^+e^-$, $\tau^+ \to \mu^+e^+e^-$, and $\tau^+ \to e^+\mu^+\mu^-$. For $\tau^+ \to \mu^+e^+e^-$ and $\tau^+ \to e^+\mu^+\mu^-$, forward-backward asymmetries can be defined, and there is a relation among asymmetries as Eq. (89). The time-reversal asymmetries are found to be very suppressed.

The search for LFV in μ and τ decays has a complementary role to the new particle search at the LHC experiment to explore the TeV-scale physics. We have seen that branching ratios of these processes in the LHT can be within the reach of ongoing and planned experiments such as MEG, COMET and Mu2e for μ-LFV processes and τ rare decay searches at future B factories and the LHC. We have found that various asymmetries defined with the help of μ and τ polarizations reflect the characteristic chirality structure of the LHT. Experimental searches for LFV processes using polarization of initial leptons are important to identify this model among various candidates of TeV-scale physics models.

Acknowledgments

We thank S.Mihara for a helpful conversation. The work of T.G. and Y.O. is supported in part by Grant-in-Aid for Science Research, Japan Society for the Promotion of Science, No.20244037. The work of Y.O. is supported in part by Grant-in-Aid for Ministry of Education, Culture, Sports, Science and Technology Japan, No.16081211 and No.22244031. The work of Y.Y. is supported in part by Grant-in-Aid for JSPS Fellows, Japan Society for the Promotion of Science, No.22.3824.

Appendix A: General formulae of branching ratios and asymmetries

We present general formulae of the branching ratios and asymmetries in the LFV processes based on the general low energy Lagrangians. Some basic formulae can be found in Refs. [17, 18, 41].

1. $\mu^+ \to e^+\gamma$, $\tau^+ \to \mu^+\gamma$ and $\tau^+ \to e^+\gamma$

The Lagrangian of the radiative two-body decay is

$$\mathcal{L}_\gamma = -\frac{4G_F}{\sqrt{2}}[m_\tau A_R \bar{\tau}_R \sigma^{\mu\nu} \mu_L F_{\mu\nu} + m_\tau A_L \bar{\tau}_L \sigma^{\mu\nu} \mu_R F_{\mu\nu} + \text{H.c.}]. \tag{A1}$$

The differential decay width of $\tau^+ \to \mu^+\gamma$ is

$$\frac{d\text{Br}(\tau^+ \to \mu^+\gamma)}{d\cos\theta} = \tau_\tau \frac{G_F^2 m_\tau^5}{\pi}(|A_L|^2 + |A_R|^2 + (|A_L|^2 - |A_R|^2)\cos\theta). \tag{A2}$$

The branching ratio and the asymmetry defined in Eq. (40) are

$$\text{Br}(\tau^+ \to \mu^+\gamma) = \tau_\tau \frac{2G_F^2 m_\tau^5}{\pi}(|A_R|^2 + |A_L|^2), \tag{A3}$$

$$A_\gamma(\tau^+ \to \mu^+\gamma) = \frac{1}{2}\frac{|A_L|^2 - |A_R|^2}{|A_L|^2 + |A_R|^2}. \tag{A4}$$

2. $\mu^+ \to e^+e^+e^-$, $\tau^+ \to \mu^+\mu^+\mu^-$ and $\tau^+ \to e^+e^+e^-$

The Lagrangian of the type I leptonic three-body decay is

$$\begin{aligned}\mathcal{L}_\text{I} = -\frac{4G_F}{\sqrt{2}}\big[&m_\tau A_R \bar{\tau}_R \sigma^{\mu\nu} \mu_L F_{\mu\nu} + m_\tau A_L \bar{\tau}_L \sigma^{\mu\nu} \mu_R F_{\mu\nu} \\ &+ g^\text{I}_{Rs}(\bar{\tau}_R \mu_L)(\bar{\mu}_R \mu_L) + g^\text{I}_{Ls}(\bar{\tau}_L \mu_R)(\bar{\mu}_L \mu_R) \\ &+ g^\text{I}_{Rr}(\bar{\tau}_R \gamma^\mu \mu_R)(\bar{\mu}_R \gamma_\mu \mu_R) + g^\text{I}_{Ll}(\bar{\tau}_L \gamma^\mu \mu_L)(\bar{\mu}_L \gamma_\mu \mu_L) \\ &+ g^\text{I}_{Rl}(\bar{\tau}_R \gamma^\mu \mu_R)(\bar{\mu}_L \gamma_\mu \mu_L) + g^\text{I}_{Lr}(\bar{\tau}_L \gamma^\mu \mu_L)(\bar{\mu}_R \gamma_\mu \mu_R) + \text{H.c.}\big].\end{aligned} \tag{A5}$$

The differential partial decay width of $\tau^+ \to \mu^+\mu^+\mu^-$ can be written as

$$\begin{aligned}\frac{d^4\text{Br}(\tau^+ \to \mu^+\mu^+\mu^-)}{dx_b dx_c\, d\phi\, d\cos\theta} = \tau_\tau \frac{G_F^2 m_\tau^5}{128\pi^4}(&M^\text{I}_O(x_b, x_c) + M^\text{I}_Z(x_b, x_c)\cos\theta \\ &+ M^\text{I}_X(x_b, x_c)\sin\theta\cos\phi + M^\text{I}_Y(x_b, x_c)\sin\theta\sin\phi),\end{aligned} \tag{A6}$$

where

$$\begin{aligned}
M_O^{\mathrm{I}}(x_b,x_c) =&(C_{R1}^{\mathrm{I}}+C_{L1}^{\mathrm{I}})a_1(x_b,x_c)+(C_{R2}^{\mathrm{I}}+C_{L2}^{\mathrm{I}})a_2(x_b,x_c)\\
&+(C_{R3}^{\mathrm{I}}+C_{L3}^{\mathrm{I}})a_3(x_b,x_c)\\
&+(C_{J1}^{\mathrm{I}}+C_{J2}^{\mathrm{I}})a_4(x_b,x_c)+(C_{J3}^{\mathrm{I}}+C_{J4}^{\mathrm{I}})a_5(x_b,x_c), &\text{(A7a)}\\
M_Z^{\mathrm{I}}(x_b,x_c) =&(C_{R1}^{\mathrm{I}}-C_{L1}^{\mathrm{I}})b_1(x_b,x_c)+(C_{R2}^{\mathrm{I}}-C_{L2}^{\mathrm{I}})b_2(x_b,x_c)\\
&+(C_{R3}^{\mathrm{I}}-C_{L3}^{\mathrm{I}})a_3(x_b,x_c)\\
&-(C_{J1}^{\mathrm{I}}-C_{J2}^{\mathrm{I}})a_4(x_b,x_c)+(C_{J3}^{\mathrm{I}}-C_{J4}^{\mathrm{I}})a_5(x_b,x_c), &\text{(A7b)}\\
M_X^{\mathrm{I}}(x_b,x_c) =&(C_{R1}^{\mathrm{I}}-C_{L1}^{\mathrm{I}})c_1(x_b,x_c)+(C_{R2}^{\mathrm{I}}-C_{L2}^{\mathrm{I}})c_2(x_b,x_c)\\
&+(C_{J1}^{\mathrm{I}}-C_{J2}^{\mathrm{I}})c_3(x_b,x_c)+(C_{J3}^{\mathrm{I}}-C_{J4}^{\mathrm{I}})c_4(x_b,x_c), &\text{(A7c)}\\
M_Y^{\mathrm{I}}(x_b,x_c) =&C_{J5}^{\mathrm{I}}c_3(x_b,x_c)+C_{J6}^{\mathrm{I}}c_4(x_b,x_c), &\text{(A7d)}
\end{aligned}$$

where $C_{R1,\cdots}^{\mathrm{I}}$ are defined as

$$\begin{aligned}
C_{R1}^{\mathrm{I}} &= \left|eA_R\right|^2, & C_{L1}^{\mathrm{I}} &= \left|eA_L\right|^2, &\text{(A8a)}\\
C_{R2}^{\mathrm{I}} &= \left|g_{Rl}^{\mathrm{I}}\right|^2, & C_{L2}^{\mathrm{I}} &= \left|g_{Lr}^{\mathrm{I}}\right|^2, &\text{(A8b)}\\
C_{R3}^{\mathrm{I}} &= \frac{\left|g_{Rs}^{\mathrm{I}}\right|^2}{16}+\left|g_{Rr}^{\mathrm{I}}\right|^2, & C_{L3}^{\mathrm{I}} &= \frac{\left|g_{Ls}^{\mathrm{I}}\right|^2}{16}+\left|g_{Ll}^{\mathrm{I}}\right|^2, &\text{(A8c)}\\
C_{J1}^{\mathrm{I}} &= \mathrm{Re}[eA_R g_{Ll}^{\mathrm{I}*}], & C_{J2}^{\mathrm{I}} &= \mathrm{Re}[eA_L g_{Rr}^{\mathrm{I}*}], &\text{(A8d)}\\
C_{J3}^{\mathrm{I}} &= \mathrm{Re}[eA_R g_{Lr}^{\mathrm{I}*}], & C_{J4}^{\mathrm{I}} &= \mathrm{Re}[eA_L g_{Rl}^{\mathrm{I}*}], &\text{(A8e)}\\
C_{J5}^{\mathrm{I}} &= \mathrm{Im}[eA_R g_{Ll}^{\mathrm{I}*}+eA_L g_{Rr}^{\mathrm{I}*}], & C_{J6}^{\mathrm{I}} &= \mathrm{Im}[eA_R g_{Lr}^{\mathrm{I}*}+eA_L g_{Rl}^{\mathrm{I}*}]. &\text{(A8f)}
\end{aligned}$$

The functions are defined as follows:

$$\begin{aligned}
a_1(x_b,x_c) &= 8\frac{(1-x_b)(2x_b^2-2x_b+1)+(1-x_c)(2x_c^2-2x_c+1)}{(1-x_b)(1-x_c)}, &\text{(A9a)}\\
a_2(x_b,x_c) &= 2(x_b(1-x_b)+x_c(1-x_c)), &\text{(A9b)}\\
a_3(x_b,x_c) &= 8(2-x_a-x_b)(x_b+x_c-1), &\text{(A9c)}\\
a_4(x_b,x_c) &= 32(x_b+x_c-1), &\text{(A9d)}\\
a_5(x_b,x_c) &= 8(2-x_b-x_c), &\text{(A9e)}
\end{aligned}$$

$$\begin{aligned}
b_1(x_b,x_c) &= 8\Big(\frac{1-2x_b(1-x_b)}{1-x_c}+\frac{1-2x_c(1-x_c)}{1-x_b}-\frac{8(x_b+x_c-1)}{2-x_b-x_c}\Big), &\text{(A10a)}\\
b_2(x_b,x_c) &= 2\frac{(x_b+x_c)(x_b^2+x_c^2-3(x_b+x_c)+6)-4}{2-x_b-x_c}, &\text{(A10b)}
\end{aligned}$$

$$c_1(x_b,x_c) = -32\frac{(x_b-x_c)(x_b+x_c-1)}{2-x_b-x_c}\sqrt{\frac{x_b+x_c-1}{(1-x_b)(1-x_c)}}, \tag{A11a}$$

$$c_2(x_b,x_c) = -4\frac{x_b-x_c}{2-x_b-x_c}\sqrt{(1-x_b)(1-x_c)(x_b+x_c-1)}, \tag{A11b}$$

$$c_3(x_b,x_c) = -16(x_b-x_c)(x_b+x_c-1)\sqrt{\frac{x_b+x_c-1}{(1-x_b)(1-x_c)}}, \tag{A11c}$$

$$c_4(x_b,x_c) = -8(x_b-x_c)(2-x_b-x_c)\sqrt{\frac{x_b+x_c-1}{(1-x_b)(1-x_c)}}, \tag{A11d}$$

where x_b and x_c are defined in Eq. (47). The branching ratio and angular asymmetries defined as Eqs. (51a)–(51c) are

$$\mathrm{Br}(\tau^+\to\mu^+\mu^+\mu^-)(\delta) = \mathrm{Br}(\tau^+\to\bar{\nu}_\tau e^+\nu_e)B^{\mathrm{I}}(\delta), \tag{A12}$$

$$\begin{aligned} B^{\mathrm{I}}(\delta) =& (C^{\mathrm{I}}_{R1}+C^{\mathrm{I}}_{L1})A_1(\delta) + (C^{\mathrm{I}}_{R2}+C^{\mathrm{I}}_{L2})A_2(\delta) + (C^{\mathrm{I}}_{R3}+C^{\mathrm{I}}_{L3})A_3(\delta) \\ &+ (C^{\mathrm{I}}_{J1}+C^{\mathrm{I}}_{J2})A_4(\delta) + (C^{\mathrm{I}}_{J3}+C^{\mathrm{I}}_{J4})A_5(\delta), \end{aligned} \tag{A13}$$

$$\begin{aligned} A^{\mathrm{I}}_Z(\delta) =& \frac{1}{2B^{\mathrm{I}}(\delta)}\big((C^{\mathrm{I}}_{R1}-C^{\mathrm{I}}_{L1})B_1(\delta) - (C^{\mathrm{I}}_{R2}-C^{\mathrm{I}}_{L2})B_2(\delta) \\ &+ (C^{\mathrm{I}}_{R3}-C^{\mathrm{I}}_{L3})A_3(\delta) - (C^{\mathrm{I}}_{J1}-C^{\mathrm{I}}_{J2})A_4(\delta) \\ &+ (C^{\mathrm{I}}_{J3}-C^{\mathrm{I}}_{J4})A_5(\delta)\big), \end{aligned} \tag{A14a}$$

$$\begin{aligned} A^{\mathrm{I}}_X(\delta) =& \frac{1}{2B^{\mathrm{I}}(\delta)}\big(-(C^{\mathrm{I}}_{R1}-C^{\mathrm{I}}_{L1})C_1(\delta) - (C^{\mathrm{I}}_{R2}-C^{\mathrm{I}}_{L2})C_2(\delta) \\ &- (C^{\mathrm{I}}_{J1}-C^{\mathrm{I}}_{J2})C_3(\delta) + (C^{\mathrm{I}}_{J3}-C^{\mathrm{I}}_{J4})C_4(\delta)\big), \end{aligned} \tag{A14b}$$

$$A^{\mathrm{I}}_Y(\delta) = \frac{1}{2B^{\mathrm{I}}(\delta)}\big(-C^{\mathrm{I}}_{J5}C_3(\delta) + C^{\mathrm{I}}_{J6}C_4(\delta)\big). \tag{A14c}$$

Br, A^{I}_Z, A^{I}_X and A^{I}_Y extract the components M^{I}_O, M^{I}_Z, M^{I}_X and M^{I}_Y in Eq. (A6), respectively. Since the signs of $\cos\theta$, $\sin\theta\cos\phi$ and $\sin\theta\sin\phi$ are equal to $\vec{s}\cdot\vec{p}_a$, $\vec{s}\cdot((\vec{p}_a\times\vec{p}_b)\times\vec{p}_a)$ and $\vec{s}\cdot(\vec{p}_a\times\vec{p}_b)$, respectively (see Fig. 2), A^{I}_Z and A^{I}_X are parity odd asymmetries and A^{I}_Y is a time-reversal asymmetry. The following functions are introduced in the above formulae.

The cutoff parameter, δ, is defined in Sec.III for each of the processes.

$$A_1(\delta) = -16(1-\delta)(2-\delta+2\delta^2)\ln\left(\frac{\delta}{1-\delta}\right) - \frac{8}{3}(1-2\delta)(13-4\delta+4\delta^2), \tag{A15a}$$

$$A_2(\delta) = (1+2\delta-2\delta^2)(1-2\delta)^2, \tag{A15b}$$

$$A_3(\delta) = 2(1+2\delta)(1-2\delta)^3, \tag{A15c}$$

$$A_4(\delta) = 16(1-2\delta)^3, \tag{A15d}$$

$$A_5(\delta) = 8(1+\delta)(1-2\delta)^2, \tag{A15e}$$

$$\begin{aligned} B_1(\delta) =& -16(2+21\delta+3\delta^2-2\delta^3)\ln(2\delta) + 16(1-\delta)(2-\delta+2\delta^2)\ln(2(1-\delta)) \\ & - \frac{8}{3}(1-2\delta)(49+68\delta+4\delta^2), \end{aligned} \tag{A16a}$$

$$B_2(\delta) = \frac{1}{3}(1-2\delta)(1+8\delta-38\delta^2-12\delta^3) - 16\delta^3\ln(2\delta). \tag{A16b}$$

$$\begin{aligned} C_1(\delta) =& \frac{96}{5}(4+9\delta+\delta^2)\sqrt{1-2\delta} - 48\sqrt{\delta}(3+6\delta-\delta^2)\arccos\left(\frac{3\delta-1}{1-\delta}\right) \\ & + 384\delta\arccos\left(\frac{\delta}{1-\delta}\right), \end{aligned} \tag{A17a}$$

$$\begin{aligned} C_2(\delta) =& \frac{4}{105}(8+8\delta-93\delta^2-225\delta^3)\sqrt{1-2\delta} \\ & - 2\delta^{\frac{3}{2}}(1-6\delta-3\delta^2)\arccos\left(\frac{3\delta-1}{1-\delta}\right) - 16\delta^3\arccos\left(\frac{\delta}{1-\delta}\right), \end{aligned} \tag{A17b}$$

$$C_3(\delta) = \frac{8}{35}\sqrt{1-2\delta}(48-57\delta-68\delta^2+85\delta^3) - 12\sqrt{\delta}(1-\delta)^3\arccos\left(\frac{3\delta-1}{1-\delta}\right), \tag{A17c}$$

$$\begin{aligned} C_4(\delta) =& \frac{4}{35}\sqrt{1-2\delta}(64-41\delta+26\delta^2-85\delta^3) \\ & - 6\sqrt{\delta}(1-\delta-\delta^2+\delta^3)\arccos\left(\frac{3\delta-1}{1-\delta}\right). \end{aligned} \tag{A17d}$$

3. $\tau^+ \to \mu^+e^+e^-$ and $\tau^+ \to e^+\mu^+\mu^-$

The Lagrangian of type II leptonic decay is

$$\begin{aligned}\mathcal{L}_{\rm II} = -\frac{4G_F}{\sqrt{2}}\big[&m_\tau A_R \bar\tau_R \sigma^{\mu\nu}\mu_L F_{\mu\nu} + m_\tau A_L \bar\tau_L \sigma^{\mu\nu}\mu_R F_{\mu\nu}\\ &+ g^{II}_{Rs}(\bar\tau_R\mu_L)(\bar e_R e_L) + g^{II}_{Ls}(\bar\tau_L\mu_R)(\bar e_L e_R)\\ &+ g^{II}_{Rt}(\bar\tau_R e_L)(\bar e_R\mu_L) + g^{II}_{Lt}(\bar\tau_L e_R)(\bar e_L\mu_R)\\ &+ g^{II}_{Rr}(\bar\tau_R\gamma^\mu\mu_R)(\bar e_R\gamma_\mu e_R) + g^{II}_{Ll}(\bar\tau_L\gamma^\mu\mu_L)(\bar e_L\gamma_\mu e_L)\\ &+ g^{II}_{Rl}(\bar\tau_R\gamma^\mu\mu_R)(\bar e_L\gamma_\mu e_L) + g^{II}_{Lr}(\bar\tau_L\gamma^\mu\mu_L)(\bar e_R\gamma_\mu e_R)\\ &+ g^{II}_{Rx}(\bar\tau_R\gamma^\mu e_R)(\bar e_L\gamma_\mu\mu_L) + g^{II}_{Lx}(\bar\tau_L\gamma^\mu e_L)(\bar e_R\gamma_\mu\mu_R) + \text{H.c.}\big]. \end{aligned} \tag{A18}$$

The differential partial decay width of $\tau^+ \to \mu^+e^+e^-$ can be given as

$$\begin{aligned}\frac{d^4\text{Br}(\tau^+ \to \mu^+e^+e^-)}{dx_b dx_c\, d\phi\, d\cos\theta} = \tau_\tau \frac{G_F^2 m_\tau^5}{128\pi^4}(&M_O^{\rm II}(x_b,x_c) + M_Z^{\rm II}(x_b,x_c)\cos\theta\\ &+ M_X^{\rm II}(x_b,x_c)\sin\theta\cos\phi + M_Y^{\rm II}(x_b,x_c)\sin\theta\sin\phi), \end{aligned} \tag{A19}$$

where

$$\begin{aligned} M_O^{\rm II}(x_b,x_c) =&(C_{R1}^{\rm II} + C_{L1}^{\rm II})d_1(x_b,x_c) + (C_{R2}^{\rm II} + C_{L2}^{\rm II})d_2(x_b,x_c)\\ &+ (C_{R3}^{\rm II} + C_{L3}^{\rm II})d_3(x_b,x_c) + (C_{R4}^{\rm II} + C_{L4}^{\rm II})d_4(x_b,x_c)\\ &+ (C_{J1}^{\rm II} + C_{J2}^{\rm II})d_5(x_b,x_c) + (C_{J3}^{\rm II} + C_{J4}^{\rm II})d_6(x_b,x_c)\\ &+ (C_{J5}^{\rm II} + C_{J6}^{\rm II})d_7(x_b,x_c), \end{aligned} \tag{A20a}$$

$$\begin{aligned} M_Z^{\rm II}(x_b,x_c) =&(C_{R1}^{\rm II} - C_{L1}^{\rm II})e_1(x_b,x_c) + (C_{R2}^{\rm II} - C_{L2}^{\rm II})d_2(x_b,x_c)\\ &+ (C_{R3}^{\rm II} - C_{L3}^{\rm II})e_2(x_b,x_c) + (C_{R4}^{\rm II} - C_{L4}^{\rm II})e_3(x_b,x_c)\\ &+ (C_{J1}^{\rm II} - C_{J2}^{\rm II})e_4(x_b,x_c) + (C_{J3}^{\rm II} - C_{J4}^{\rm II})e_5(x_b,x_c)\\ &+ (C_{J5}^{\rm II} - C_{J6}^{\rm II})d_7(x_b,x_c), \end{aligned} \tag{A20b}$$

$$\begin{aligned} M_X^{\rm II}(x_b,x_c) =&(C_{R1}^{\rm II} - C_{L1}^{\rm II})f_1(x_b,x_c) + (C_{R3}^{\rm II} - C_{L3}^{\rm II})f_2(x_b,x_c)\\ &+ (C_{R4}^{\rm II} - C_{L4}^{\rm II})f_3(x_b,x_c)\\ &+ (C_{J1}^{\rm II} - C_{J2}^{\rm II})f_4(x_b,x_c) + (C_{J3}^{\rm II} - C_{J4}^{\rm II})f_5(x_b,x_c)\\ &+ (C_{J5}^{\rm II} - C_{J6}^{\rm II})f_6(x_b,x_c), \end{aligned} \tag{A20c}$$

$$M_Y^{\rm II}(x_b,x_c) = C_{J7}^{\rm II}g_1(x_b,x_c) + C_{J8}^{\rm II}g_2(x_b,x_c) + C_{J9}^{\rm II}f_6(x_b,x_c). \tag{A20d}$$

$C^{\rm II}_{R1,\cdots}$ are defined as

$$C^{\rm II}_{R1} = |eA_R|^2\,, \qquad C^{\rm II}_{L1} = |eA_L|^2\,, \tag{A21a}$$

$$C^{\rm II}_{R2} = \frac{|g_{Rs}|^2}{4} + |g_{Rx}|^2\,, \qquad C^{\rm II}_{L2} = \frac{|g_{Ls}|^2}{4} + |g_{Lx}|^2\,, \tag{A21b}$$

$$C^{\rm II}_{R3} = \frac{|g_{Rt}|^2}{4} + |g_{Rl}|^2\,, \qquad C^{\rm II}_{L3} = \frac{|g_{Lt}|^2}{4} + |g_{Lr}|^2\,, \tag{A21c}$$

$$C^{\rm II}_{R4} = |g_{Rr}|^2\,, \qquad C^{\rm II}_{L4} = |g_{Ll}|^2\,, \tag{A21d}$$

$$C^{\rm II}_{J1} = {\rm Re}[eA_R g^*_{Ll}], \qquad C^{\rm II}_{J2} = {\rm Re}[eA_L g^*_{Rr}], \tag{A21e}$$

$$C^{\rm II}_{J3} = {\rm Re}[eA_R g^*_{Lr}], \qquad C^{\rm II}_{J4} = {\rm Re}[eA_L g^*_{Rl}], \tag{A21f}$$

$$C^{\rm II}_{J5} = {\rm Re}[g_{Rs} g^*_{Rt}], \qquad C^{\rm II}_{J6} = {\rm Re}[g_{Ls} g^*_{Lt}], \tag{A21g}$$

$$C^{\rm II}_{J7} = {\rm Im}[eA_R g^*_{Ll} + eA_L g^*_{Rr}], \qquad C^{\rm II}_{J8} = {\rm Im}[eA_R g^*_{Lr} + eA_L g^*_{Rl}], \tag{A21h}$$

$$C^{\rm II}_{J9} = {\rm Im}[g_{Rs} g^*_{Rt} + g_{Ls} g^*_{Lt}]. \tag{A21i}$$

The functions, $d_i(x_b, x_c)$, $e_i(x_b, x_c)$, $f_i(x_b, x_c)$ and $g_i(x_b, x_c)$, are defined as

$$d_1(x_b, x_c) = 8\frac{x_b(1-x_c) + x_c(1-x_b)}{x_b + x_c - 1}, \tag{A22a}$$

$$d_2(x_b, x_c) = 2(2 - x_b - x_c)(x_b + x_c - 1), \tag{A22b}$$

$$d_3(x_b, x_c) = 2x_b(1-x_b), \tag{A22c}$$

$$d_4(x_b, x_c) = 2x_c(1-x_c), \tag{A22d}$$

$$d_5(x_b, x_c) = 8(1-x_c), \tag{A22e}$$

$$d_6(x_b, x_c) = 8(1-x_b), \tag{A22f}$$

$$d_7(x_b, x_c) = -(1-x_b)(x_b + x_c - 1), \tag{A22g}$$

$$e_1(x_b, x_c) = \frac{8}{x_b + x_c - 1}\left(x_b(1-x_c) + x_c(1-x_b) - 2\frac{(1-x_b)^2 + (1-x_c)^2}{2 - x_b - x_c}\right), \tag{A23a}$$

$$e_2(x_b, x_c) = 2\left(x_b(1-x_b) - \frac{2(1-x_b)(1-x_c)}{2 - x_b - x_c}\right), \tag{A23b}$$

$$e_3(x_b, x_c) = 2\left(x_c(1-x_c) - \frac{2(1-x_b)(1-x_c)}{2 - x_b - x_c}\right), \tag{A23c}$$

$$e_4(x_b, x_c) = -8\frac{(1-x_c)(x_b - x_c)}{2 - x_b - x_c}, \tag{A23d}$$

$$e_5(x_b, x_c) = 8\frac{(1-x_b)(x_b - x_c)}{2 - x_b - x_c}, \tag{A23e}$$

$$f_1(x_b,x_c) =16\frac{x_b-x_c}{2-x_b-x_c}\sqrt{\frac{(1-x_b)(1-x_c)}{x_b+x_c-1}}, \tag{A24a}$$

$$f_2(x_b,x_c) =4\frac{1-x_b}{2-x_b-x_c}\sqrt{(1-x_b)(1-x_c)(x_b+x_c-1)}, \tag{A24b}$$

$$f_3(x_b,x_c) =-4\frac{1-x_c}{2-x_b-x_c}\sqrt{(1-x_b)(1-x_c)(x_b+x_c-1)}, \tag{A24c}$$

$$f_4(x_b,x_c) =8\frac{(1-x_c)(x_b+x_c)}{2-x_b-x_c}\sqrt{\frac{(1-x_b)(1-x_c)}{x_b+x_c-1}}, \tag{A24d}$$

$$f_5(x_b,x_c) =-8\frac{(1-x_b)(x_b+x_c)}{2-x_b-x_c}\sqrt{\frac{(1-x_b)(1-x_c)}{x_b+x_c-1}}, \tag{A24e}$$

$$f_6(x_b,x_c) =-\sqrt{(1-x_b)(1-x_c)(x_b+x_c-1)}, \tag{A24f}$$

$$g_1(x_b,x_c) =-24(1-x_c)\sqrt{\frac{(1-x_b)(1-x_c)}{(x_b+x_c-1)}}, \tag{A25a}$$

$$g_2(x_b,x_c) =24(1-x_b)\sqrt{\frac{(1-x_b)(1-x_c)}{(x_b+x_c-1)}}. \tag{A25b}$$

The branching ratio and seven asymmetries defined in Eqs. (51a)–(51c) and (64)–(65c) are

$$\mathrm{Br}(\tau^+\to\mu^+e^+e^-)(\delta) =\mathrm{Br}(\tau^+\to\bar{\nu}_\tau e^+\nu_e)B^{\mathrm{II}}(\delta), \tag{A26}$$

$$\begin{aligned}B^{\mathrm{II}}(\delta) =&(C^{\mathrm{II}}_{R1}+C^{\mathrm{II}}_{L1})D_1(\delta)+\left(C^{\mathrm{II}}_{R2}+C^{\mathrm{II}}_{L2}-\frac{1}{4}(C^{\mathrm{II}}_{J5}+C^{\mathrm{II}}_{J6})\right)D_2(\delta)\\ &+(C^{\mathrm{II}}_{R3}+C^{\mathrm{II}}_{L3}+C^{\mathrm{II}}_{R4}+C^{\mathrm{II}}_{L4})D_3(\delta)+(C^{\mathrm{II}}_{J1}+C^{\mathrm{II}}_{J2}+C^{\mathrm{II}}_{J3}+C^{\mathrm{II}}_{J4})D_4(\delta),\end{aligned} \tag{A27}$$

$$A_Z^{\mathrm{II}}(\delta) = \frac{1}{2B^{\mathrm{II}}(\delta)}\Bigg(-(C_{R1}^{\mathrm{II}} - C_{L1}^{\mathrm{II}})D_5(\delta) + \Big(C_{R2}^{\mathrm{II}} - C_{L2}^{\mathrm{II}} - \frac{1}{4}(C_{J5}^{\mathrm{II}} - C_{J6}^{\mathrm{II}})\Big)D_2(\delta) - (C_{R3}^{\mathrm{II}} - C_{L3}^{\mathrm{II}} + C_{R4}^{\mathrm{II}} - C_{L4}^{\mathrm{II}})D_6(\delta) - \frac{1}{3}(C_{J1}^{\mathrm{II}} - C_{J2}^{\mathrm{II}} + C_{J3}^{\mathrm{II}} - C_{J4}^{\mathrm{II}})D_4(\delta)\Bigg), \tag{A28a}$$

$$A_X^{\mathrm{II}}(\delta) = \frac{\pi}{2B^{\mathrm{II}}(\delta)}\Bigg(\Big(C_{R3}^{\mathrm{II}} - C_{L3}^{\mathrm{II}} - C_{R4}^{\mathrm{II}} + C_{L4}^{\mathrm{II}} - \frac{1}{2}(C_{J5}^{\mathrm{II}} - C_{J6}^{\mathrm{II}})\Big)E_1(\delta) + (C_{J1}^{\mathrm{II}} - C_{J2}^{\mathrm{II}} - C_{J3}^{\mathrm{II}} + C_{J4}^{\mathrm{II}})E_2(\delta)\Bigg), \tag{A28b}$$

$$A_Y^{\mathrm{II}}(\delta) = \frac{\pi}{2B^{\mathrm{II}}(\delta)}\Bigg(-(C_{J7}^{\mathrm{II}} - C_{J8}^{\mathrm{II}})E_3(\delta) - \frac{1}{2}C_{J9}^{\mathrm{II}}E_1(\delta)\Bigg), \tag{A28c}$$

$$A_{FB}^{\mathrm{II}}(\delta) = \frac{1}{B^{\mathrm{II}}(\delta)}\Bigg(-\frac{1}{4}\Big(C_{R3}^{\mathrm{II}} + C_{L3}^{\mathrm{II}} - C_{R4}^{\mathrm{II}} - C_{L4}^{\mathrm{II}} - \frac{1}{2}(C_{J5}^{\mathrm{II}} + C_{J6}^{\mathrm{II}})\Big)D_2(\delta) + \frac{1}{2}(C_{J1}^{\mathrm{II}} + C_{J2}^{\mathrm{II}} - C_{J3}^{\mathrm{II}} - C_{J4}^{\mathrm{II}})D_4(\delta)\Bigg), \tag{A29a}$$

$$A_{ZFB}^{\mathrm{II}}(\delta) = \frac{1}{2B^{\mathrm{II}}(\delta)}\Bigg(-\frac{1}{4}\Big(C_{R3}^{\mathrm{II}} - C_{L3}^{\mathrm{II}} - C_{R4}^{\mathrm{II}} + C_{L4}^{\mathrm{II}} - \frac{1}{2}(C_{J5}^{\mathrm{II}} - C_{J6}^{\mathrm{II}})\Big)D_2(\delta) - \frac{1}{2}(C_{J1}^{\mathrm{II}} - C_{J2}^{\mathrm{II}} - C_{J3}^{\mathrm{II}} + C_{J4}^{\mathrm{II}})D_4(\delta)\Bigg), \tag{A29b}$$

$$A_{XFB}^{\mathrm{II}}(\delta) = \frac{1}{2B^{\mathrm{II}}(\delta)}\Bigg((C_{R1}^{\mathrm{II}} - C_{L1}^{\mathrm{II}})E_4(\delta) - \frac{4}{3}(C_{R3}^{\mathrm{II}} - C_{L3}^{\mathrm{II}} + C_{R4}^{\mathrm{II}} - C_{L4}^{\mathrm{II}})E_1(\delta) + \frac{4}{3}(C_{J1}^{\mathrm{II}} - C_{J2}^{\mathrm{II}} + C_{J3}^{\mathrm{II}} - C_{J4}^{\mathrm{II}})E_2(\delta)\Bigg), \tag{A29c}$$

$$A_{YFB}^{\mathrm{II}}(\delta) = \frac{1}{2B^{\mathrm{II}}(\delta)}\Bigg(-\frac{4}{3}(C_{J7}^{\mathrm{II}} + C_{J8}^{\mathrm{II}})E_3(\delta)\Bigg), \tag{A29d}$$

with

$$D_1(\delta) = \frac{16}{3}(-(1-\delta)(8-\delta-\delta^2) - 6\ln\delta), \tag{A30a}$$

$$D_2(\delta) = (1-\delta)^3(1+3\delta), \tag{A30b}$$

$$D_3(\delta) = (1-\delta)^3(1+\delta), \tag{A30c}$$

$$D_4(\delta) = 8(1-\delta)^3, \tag{A30d}$$

$$D_5(\delta) = \frac{16}{3}(-(1-\delta)(10-5\delta+\delta^2) - 6\ln\delta), \tag{A30e}$$

$$D_6(\delta) = \frac{1}{3}(1-\delta)^3(1-3\delta), \tag{A30f}$$

$$E_1(\delta) = \frac{1}{35}(1-\delta^{1/2})^3(8+24\delta^{1/2}+48\delta+45\delta^{3/2}+15\delta^2), \tag{A31a}$$

$$E_2(\delta) = \frac{2}{35}(1-\delta^{1/2})^3(64+87\delta^{1/2}+69\delta+45\delta^{3/2}+15\delta^2), \tag{A31b}$$

$$E_3(\delta) = \frac{6}{35}(1-\delta^{1/2})^4(16+29\delta^{1/2}+20\delta+5\delta^{3/2}), \tag{A31c}$$

$$E_4(\delta) = \frac{32}{15}(1-\delta^{1/2})^3(8+9\delta^{1/2}+3\delta). \tag{A31d}$$

4. $\tau^+ \to \mu^+\mu^+e^-$ and $\tau^+ \to e^+e^+\mu^-$

The effective Lagrangian of type III leptonic decay is

$$\begin{aligned}\mathcal{L}_{\rm III} = -\frac{4G_F}{\sqrt{2}}\big[&g^{III}_{Rs}(\bar\tau_R\mu_L)(\bar e_R\mu_L) + g^{III}_{Ls}(\bar\tau_L\mu_R)(\bar e_L\mu_R)\\ &+ g^{III}_{Rr}(\bar\tau_R\gamma^\mu\mu_R)(\bar e_R\gamma_\mu\mu_R) + g^{III}_{Ll}(\bar\tau_L\gamma^\mu\mu_L)(\bar e_L\gamma_\mu\mu_L)\\ &+ g^{III}_{Rl}(\bar\tau_R\gamma^\mu\mu_R)(\bar e_L\gamma_\mu\mu_L) + g^{III}_{Lr}(\bar\tau_L\gamma^\mu\mu_L)(\bar e_R\gamma_\mu\mu_R) + \text{H.c.}\big],\end{aligned} \tag{A32}$$

The differential partial decay width of $\tau^+ \to \mu^+\mu^+e^-$ is written as

$$\begin{aligned}\frac{d^4\text{Br}(\tau^+\to\mu^+\mu^+e^-)}{dx_b dx_c\, d\phi\, d\cos\theta} = \tau_\tau\frac{G_F^2 m_\tau^5}{128\pi^4}&(M^{\rm III}_O(x_b,x_c) + M^{\rm III}_Z(x_b,x_c)\cos\theta\\ &+ M^{\rm III}_X(x_b,x_c)\sin\theta\cos\phi + M^{\rm III}_Y(x_b,x_c)\sin\theta\sin\phi),\end{aligned} \tag{A33}$$

where

$$M_O^{\rm III}(x_b,x_c) =(C_{R2}^{\rm III}+C_{L2}^{\rm III})a_2(x_b,x_c)+(C_{R3}^{\rm III}+C_{L3}^{\rm III})a_3(x_b,x_c), \tag{A34a}$$

$$M_Z^{\rm III}(x_b,x_c) =(C_{R2}^{\rm III}-C_{L2}^{\rm III})b_2(x_b,x_c)+(C_{R3}^{\rm III}-C_{L3}^{\rm III})a_3(x_b,x_c), \tag{A34b}$$

$$M_X^{\rm III}(x_b,x_c) =(C_{R2}^{\rm III}-C_{L2}^{\rm III})c_2(x_b,x_c), \tag{A34c}$$

$$M_Y^{\rm III}(x_b,x_c) =0. \tag{A34d}$$

Integrating them in x_b-x_c plane, branching ratio and parity asymmetries are given as

$$\mathrm{Br}(\tau\to\mu^+\mu^+e^-)(\delta) =\mathrm{Br}(\tau^+\to\bar\nu_\tau e^+\nu_e)((C_{R2}^{\rm III}+C_{L2}^{\rm III})A_2(\delta)+(C_{R3}^{\rm III}+C_{L3}^{\rm III})A_3(\delta)), \tag{A35}$$

$$A_Z^{\rm III}(\delta) =\frac{1}{2}\frac{-(C_{R2}^{\rm III}-C_{L2}^{\rm III})B_2(\delta)+(C_{R3}^{\rm III}-C_{L3}^{\rm III})A_3(\delta)}{(C_{R2}^{\rm III}+C_{L2}^{\rm III})A_2(\delta)+(C_{R3}^{\rm III}+C_{L3}^{\rm III})A_3(\delta)}, \tag{A36}$$

$$A_X^{\rm III}(\delta) =\frac{1}{2}\frac{(C_{R2}^{\rm III}-C_{L2}^{\rm III})C_2(\delta)}{(C_{R2}^{\rm III}+C_{L2}^{\rm III})A_2(\delta)+(C_{R3}^{\rm III}+C_{L3}^{\rm III})A_3(\delta)}, \tag{A37}$$

$$A_Y^{\rm III}(\delta) =0, \tag{A38}$$

where coefficients $C_i^{\rm III}$s are given by replacement of I with III in coefficients of the type I, Eqs. (A8a)–(A8f). In this type, time-reversal asymmetry, A_Y, does not appear.

5. Semileptonic decays of τ

The effective Lagrangian of semileptonic τ decays is

$$\begin{aligned}\mathcal{L}_{\rm had} = -\frac{4G_F}{\sqrt{2}}\Big[&m_\tau A_R\bar\tau_R\sigma^{\mu\nu}\mu_L F_{\mu\nu}+m_\tau A_L\bar\tau_L\sigma^{\mu\nu}\mu_R F_{\mu\nu}\\ &+\sum_{q=u,d,s}\big(g_{Rs(q)}(\bar\tau_R\mu_L)(\bar q_R q_L)+g_{Ls(q)}(\bar\tau_L\mu_R)(\bar q_L q_R)\\ &\quad+g_{Rt(q)}(\bar\tau_R\mu_L)(\bar q_L q_R)+g_{Lt(q)}(\bar\tau_L\mu_R)(\bar q_R q_L)\\ &\quad+g_{Rr(q)}(\bar\tau_R\gamma^\mu\mu_R)(\bar q_R\gamma_\mu q_R)+g_{Ll(q)}(\bar\tau_L\gamma^\mu\mu_L)(\bar q_L\gamma_\mu q_L)\\ &\quad+g_{Rl(q)}(\bar\tau_R\gamma^\mu\mu_R)(\bar q_L\gamma_\mu q_L)+g_{Lr(q)}(\bar\tau_L\gamma^\mu\mu_L)(\bar q_R\gamma_\mu q_R)\\ &\quad+g_{RT(q)}(\bar\tau_R\sigma^{\mu\nu}\mu_L)(\bar q_R\sigma_{\mu\nu}q_L)+g_{LT(q)}(\bar\tau_L\sigma^{\mu\nu}\mu_R)(\bar q_L\sigma_{\mu\nu}q_R)+\mathrm{H.c.}\big)\Big].\end{aligned} \tag{A39}$$

The branching ratios and asymmetries for $\tau^+\to\mu^+P$ decays are

$$\mathrm{Br}(\tau^+\to\mu^+P)=\tau_\tau\frac{G_F^2m_\tau^3}{4\pi}\left(1-\frac{m_P^2}{m_\tau^2}\right)^2(|G_{RP}|^2+|G_{LP}|^2), \tag{A40}$$

$$A_P(\tau^+\to\mu^+P)=\frac{1}{2}\frac{|G_{RP}|^2-|G_{LP}|^2}{|G_{RP}|^2+|G_{LP}|^2}. \tag{A41}$$

Here, G_{RP} and G_{LP} for $P = \pi$ and η are given by

$$G_{R\pi} = \frac{f_\pi}{2\sqrt{2}}\Big(g_{Lr(u)} - g_{Lr(d)} - g_{Ll(u)} + g_{Ll(d)} - \frac{m_\pi^2}{2m_q m_\tau}(g_{Rt(u)} - g_{Rt(d)} - g_{Rs(u)} + g_{Rs(d)})\Big), \tag{A42a}$$

$$G_{L\pi} = \frac{f_\pi}{2\sqrt{2}}\Big(g_{Rr(u)} - g_{Rr(d)} - g_{Rl(u)} + g_{Rl(d)} + \frac{m_\pi^2}{2m_q m_\tau}(g_{Lt(u)} - g_{Lt(d)} - g_{Ls(u)} + g_{Ls(d)})\Big), \tag{A42b}$$

$$G_{R\eta} = \frac{1}{2}\Big(\frac{f_\eta^q}{\sqrt{2}}(g_{Lr(u)} + g_{Lr(d)} - g_{Ll(u)} - g_{Ll(d)}) + f_\eta^s(g_{Lr(s)} - g_{Ll(s)}) - \frac{h_\eta^q m_\eta^2}{2\sqrt{2}m_q m_\tau}(g_{Rt(u)} - g_{Rt(d)} - g_{Rs(u)} + g_{Rs}(d)) + \frac{h_\eta^s m_\eta^2}{2m_q m_\tau}(g_{Rt(s)} - g_{Rs(s)})\Big), \tag{A42c}$$

$$G_{L\eta} = \frac{1}{2}\Big(\frac{f_\eta^q}{\sqrt{2}}(g_{Rr(u)} + g_{Rr(d)} - g_{Rl(u)} - g_{Rl(d)}) + f_\eta^s(g_{Rr(s)} - g_{Rl(s)}) - \frac{h_\eta^q m_\eta^2}{2\sqrt{2}m_q m_\tau}(g_{Lt(u)} - g_{Lt(d)} - g_{Ls(u)} + g_{Ls(d)}) + \frac{h_\eta^s m_\eta^2}{2m_q m_\tau}(g_{Lt(s)} - g_{Ls(s)})\Big). \tag{A42d}$$

The expressions for η' are obtained by the replacement $\eta \to \eta'$ in the last two equations. To describe the decay constants for η and η', we used the formalism in Ref. [42]. We assume isospin symmetry so that $m_u = m_d = m_q$ in the following. The decay constants are

$$-if_\pi p^\mu = \langle 0|\frac{\bar{u}\gamma^\mu\gamma^5 u - \bar{d}\gamma^\mu\gamma^5 d}{\sqrt{2}}|\pi(p)\rangle, \tag{A43a}$$

$$-if_q p^\mu = \langle 0|\frac{\bar{u}\gamma^\mu\gamma^5 u + \bar{d}\gamma^\mu\gamma^5 d}{\sqrt{2}}|\eta_q(p)\rangle, \tag{A43b}$$

$$-if_s p^\mu = \langle 0|\bar{s}\gamma^\mu\gamma^5 s|\eta_s(p)\rangle, \tag{A43c}$$

$$\frac{ih_q}{2m_q} = \langle 0|\frac{\bar{u}\gamma^5 u + \bar{d}\gamma^5 d}{\sqrt{2}}|\eta_q(p)\rangle, \tag{A43d}$$

$$\frac{ih_s}{2m_s} = \langle 0|\bar{s}\gamma^5 s|\eta_s(p)\rangle, \tag{A43e}$$

For η and η', the decay constants, ${f_{\eta^{(\prime)}}}^{q,s}$ are ${h_{\eta^{(\prime)}}}^{q,s}$ are expressed by f_q, f_s and a mixing angle, ϕ_η, as follows.

$$\begin{pmatrix} f_\eta^q & f_\eta^s \\ f_{\eta'}^q & f_{\eta'}^s \end{pmatrix} = \begin{pmatrix} \cos\phi_\eta & -\sin\phi_\eta \\ \sin\phi_\eta & \cos\phi_\eta \end{pmatrix} \begin{pmatrix} f_q & 0 \\ 0 & f_s \end{pmatrix}, \tag{A44}$$

$$\begin{pmatrix} h_\eta^q & h_\eta^s \\ h_{\eta'}^q & h_{\eta'}^s \end{pmatrix} = \begin{pmatrix} \cos\phi_\eta & -\sin\phi_\eta \\ \sin\phi_\eta & \cos\phi_\eta \end{pmatrix} \begin{pmatrix} h_q & 0 \\ 0 & h_s \end{pmatrix}, \tag{A45}$$

where

$$h_q = f_q(m_\eta^2 \cos^2\phi_\eta + m_{\eta'}^2 \sin^2\phi_\eta) - \sqrt{2} f_s (m_{\eta'}^2 - m_\eta^2)\cos\phi_\eta \sin\phi_\eta \tag{A46a}$$

$$h_s = f_s(m_{\eta'}^2 \cos^2\phi_\eta + m_\eta^2 \sin^2\phi_\eta) - \frac{1}{\sqrt{2}} f_s (m_{\eta'}^2 - m_\eta^2)\cos\phi_\eta \sin\phi_\eta. \tag{A46b}$$

Similarly, for vector mesons, branching ratios and asymmetries are

$$\begin{aligned}\mathrm{Br}(\tau^+ \to \mu^+ V) =& \tau_\tau \frac{G_F^2 m_\tau^3}{\pi}\left(1 - \frac{m_V^2}{m_\tau^2}\right)^2 \\ & \times \left(C_{AV+}\frac{2m_\tau^2 + m_V^2}{m_\tau^2} + C_{V+}\frac{m_\tau^2 + 2m_V^2}{4m_V^2} - 3\mathrm{Re}[C_{IV+}]\right),\end{aligned} \tag{A47}$$

$$A_V(\tau^+ \to \mu^+ V) = \frac{1}{2}\frac{C_{AV-}(2m_\tau^2 - m_V^2)/m_\tau^2 + C_{V-}(m_\tau^2 - 2m_V^2)/(4m_V^2) + \mathrm{Re}[C_{IV-}]}{C_{AV+}(2m_\tau^2 + m_V^2)/m_\tau^2 + C_{V+}(m_\tau^2 + 2m_V^2)/(4m_V^2) - 3\mathrm{Re}[C_{IV+}]}, \tag{A48}$$

with

$$C_{AV+} = |G_{LAV}|^2 + |G_{RAV}|^2, \qquad C_{V+} = |G_{LV}|^2 + |G_{RV}|^2, \tag{A49a}$$

$$C_{AV-} = |G_{LAV}|^2 - |G_{RAV}|^2, \qquad C_{V-} = |G_{LV}|^2 - |G_{RV}|^2, \tag{A49b}$$

$$C_{IV+} = G_{RAV}G_{LV}^* + G_{LAV}G_{RV}^*, \qquad C_{IV-} = G_{RAV}G_{LV}^* - G_{LAV}G_{RV}^*. \tag{A49c}$$

The effective couplings G_{RAV}, G_{RV}, G_{LAV} and G_{LV} for $V = \rho^0$, ω and ϕ are

$$G_{RA\rho} = -\frac{f_\rho^T}{2}\frac{g_{RT(u)} - g_{RT(d)}}{\sqrt{2}} + f_\rho \frac{m_\tau}{m_\rho}\frac{Q_u - Q_d}{\sqrt{2}} eA_R, \tag{A50a}$$

$$G_{LA\rho} = -\frac{f_\rho^T}{2}\frac{g_{LT(u)} - g_{LT(d)}}{\sqrt{2}} + f_\rho \frac{m_\tau}{m_\rho}\frac{Q_u - Q_d}{\sqrt{2}} eA_L, \tag{A50b}$$

$$G_{R\rho} = \frac{f_\rho m_\rho}{2\sqrt{2}m_\tau}(g_{Rr(u)} - g_{Rr(d)} + g_{Rl(u)} - g_{Rl(d)}), \tag{A50c}$$

$$G_{L\rho} = \frac{f_\rho m_\rho}{2\sqrt{2}m_\tau}(g_{Ll(u)} - g_{Ll(d)} + g_{Lr(u)} - g_{Lr(d)}), \tag{A50d}$$

$$G_{RA\omega} = -\frac{f_\omega^T}{2}\frac{g_{RT(u)} + g_{RT(d)}}{\sqrt{2}} + f_\omega \frac{m_\tau}{m_\omega}\frac{Q_u + Q_d}{\sqrt{2}} eA_R, \tag{A50e}$$

$$G_{LA\omega} = -\frac{f_\omega^T}{2}\frac{g_{LT(u)} + g_{LT(d)}}{\sqrt{2}} + f_\omega \frac{m_\tau}{m_\omega}\frac{Q_u + Q_d}{\sqrt{2}} eA_L, \tag{A50f}$$

$$G_{R\omega} = \frac{f_\omega m_\omega}{2\sqrt{2}m_\tau}(g_{Rr(u)} + g_{Rr(d)} + g_{Rl(u)} + g_{Rl(d)}), \tag{A50g}$$

$$G_{L\omega} = \frac{f_\omega m_\omega}{2\sqrt{2}m_\tau}(g_{Ll(u)} + g_{Ll(d)} + g_{Lr(u)} + g_{Lr(d)}), \tag{A50h}$$

$$G_{RA\phi} = -\frac{f_\phi^T}{2} g_{RT(s)} + f_\phi \frac{m_\tau}{m_\phi} Q_s eA_R, \tag{A50i}$$

$$G_{LA\phi} = -\frac{f_\phi^T}{2} g_{LT(s)} + f_\phi \frac{m_\tau}{m_\phi} Q_s eA_L, \tag{A50j}$$

$$G_{R\phi} = \frac{f_\phi m_\phi}{2m_\tau}(g_{Rr(s)} + g_{Rl(s)}), \tag{A50k}$$

$$G_{L\phi} = \frac{f_\phi m_\phi}{2m_\tau}(g_{Ll(s)} + g_{Lr(s)}) \tag{A50l}$$

The decay constants f_V are defined as

$$m_\rho f_\rho \epsilon^\mu = \langle 0|\frac{\bar{u}\gamma^\mu u - \bar{d}\gamma^\mu d}{\sqrt{2}}|\rho(p)\rangle, \tag{A51a}$$

$$m_\omega f_\omega \epsilon^\mu = \langle 0|\frac{\bar{u}\gamma^\mu u + \bar{d}\gamma^\mu d}{\sqrt{2}}|\omega(p)\rangle, \tag{A51b}$$

$$m_\phi f_\phi \epsilon^\mu = \langle 0|\bar{s}\gamma^\mu s|\phi(p)\rangle, \tag{A51c}$$

where ϵ^μ is the polarization vector of the vector mesons. f_V^T are also defined with the same flavor combinations,

$$\langle 0|\bar{q}\sigma^{\mu\nu}q|V(p)\rangle = -if_V^T(p^\mu\epsilon^\nu - p^\nu\epsilon^\mu). \tag{A52}$$

Pseudoscalar		Vector	
f_π	130 MeV	f_ρ	221 MeV
f_q/f_π	1.07	f_ω	196 MeV
f_s/f_π	1.34	f_ϕ	228 MeV
ϕ_η	39.3°		

TABLE III: Decay constants of pseudoscalar and vector mesons.

f_V can be extracted from partial decay widths for e^+e^- decay modes,

$$f_\rho^2 = \frac{3m_\rho \Gamma_{\rho\to e^+e^-}}{2\pi\alpha^2}, \tag{A53a}$$

$$f_\omega^2 = \frac{27m_\omega \Gamma_{\omega\to e^+e^-}}{2\pi\alpha^2}, \tag{A53b}$$

$$f_\phi^2 = \frac{27m_\phi \Gamma_{\phi\to e^+e^-}}{4\pi\alpha^2}. \tag{A53c}$$

The values of the decay constants are listed in Table III.

6. $\mu - e$ conversion

The effective Lagrangian for μ-e conversion is obtained by the replacement of $\tau \to \mu$ and $\mu \to e$ in Eq. (A39). According to Ref.[22] the rates of coherent $\mu - e$ conversions are

$$\begin{aligned}\mathrm{R}(\mu^- A \to e^- A) =& \frac{2G_F^2}{\omega_{\rm capt}} \left| -A_R D + 2\sum_{N=p,n} \left((\tilde{g}_{Ls}^{(N)} + \tilde{g}_{Lt}^{(N)}) S^{(N)} + (\tilde{g}_{Ll}^{(N)} + \tilde{g}_{Lr}^{(N)}) V^{(N)} \right) \right|^2 \\ &+ (L \leftrightarrow R),\end{aligned} \tag{A54}$$

where $\omega_{\rm capt}$ is the muon capture rate of each atom and the p and n mean proton and neutron, respectively. $\tilde{g}_{Ls}^{(N)}, \cdots$ in the above equation are written in terms of the Wilson coefficients in the effective Lagrangian:

$$\tilde{g}_{Ls}^{(p)} + \tilde{g}_{Lt}^{(p)} = \sum_q G_S^{(q,p)} \big(g_{Ls(q)} + g_{Lt(q)} \big), \tag{A55a}$$

$$\tilde{g}_{Ls}^{(n)} + \tilde{g}_{Lt}^{(n)} = \sum_q G_S^{(q,n)} \big(g_{Ls(q)} + g_{Lt(q)} \big), \tag{A55b}$$

$$\tilde{g}_{Ll}^{(p)} + \tilde{g}_{Lr}^{(p)} = 2g_{Ll(u)} + 2g_{Lr(u)} + g_{Ll(d)} + g_{Lr(d)}, \tag{A55c}$$

$$\tilde{g}_{Ll}^{(n)} + \tilde{g}_{Lr}^{(n)} = g_{Ll(u)} + g_{Lr(u)} + 2g_{Ll(d)} + 2g_{Lr(d)}, \tag{A55d}$$

where $G_S^{(q,N)}$ are given in Ref. [22]:

$$G_S^{(u,p)} = G_S^{(d,n)} = 5.1, \tag{A56a}$$

$$G_S^{(d,p)} = G_S^{(u,n)} = 4.3, \tag{A56b}$$

$$G_S^{(s,p)} = G_S^{(s,n)} = 2.5. \tag{A56c}$$

D, $S^{(p)}$, $S^{(n)}$, $V^{(p)}$ and $V^{(n)}$, in Eq. (A54) are overlap integrals defined in Ref. [22]. They depend on nuclides. In this paper, we calculate the conversion rates for Al, Ti, Au and Pb using the numerical values listed in Table IV.

Nucleus	D	$S^{(p)}$	$V^{(p)}$	$S^{(n)}$	$V^{(n)}$	$\omega_{\rm capt}$
$^{27}_{13}$Al	0.0357	0.0153	0.0159	0.0163	0.0169	0.7054
$^{48}_{22}$Ti	0.0870	0.0371	0.0399	0.0462	0.0495	2.59
$^{197}_{79}$Au	0.167	0.0523	0.0859	0.0610	0.108	13.07
$^{208}_{82}$Pb	0.163	0.0493	0.0845	0.0686	0.120	13.45

TABLE IV: Values of overlap integrals and capture rates. They are taken from Table II for Al and Au, IV for Ti, VI for Pb and VIII in Ref.[22]. The integrals are in units of $m_\mu^{5/2}$ and rates are in units of 10^6/sec.

Appendix B: Functions used in the Wilson coefficients

The following functions are used to describe the Wilson coefficients in Sec.III:

$$N_{CM}(x) = \frac{x}{4(1-x)^3}\left(-1+5x+2x^2+\frac{6x^2}{1-x}\ln x\right), \tag{B1a}$$

$$N_{NM}(x) = \frac{x}{4(1-x)^3}\left(2+5x-x^2+\frac{6x}{1-x}\ln x\right), \tag{B1b}$$

$$P_\gamma(x) = -2\left(N_{CC}(x)+\frac{1}{2}N_{NC}(x)+\frac{1}{10}N_{NC}(x)\right), \tag{B1c}$$

$$N_{CC}(x) = \frac{x}{12(1-x)^3}\left(12+x-7x^2+(12-10x+x^2)\frac{2x}{1-x}\ln x\right), \tag{B1d}$$

$$N_{NC}(x) = \frac{x}{12(1-x)^3}\left(18-11x-x^2+(15-16x+4x^2)\frac{2x}{1-x}\ln x\right)-\frac{2}{3}\ln x, \tag{B1e}$$

$$P_Z(x) = -\frac{x}{1-x}\left(6-x+(2+3x)\frac{\ln x}{1-x}\right), \tag{B1f}$$

$$B_{(e)}(x,y) = \frac{1}{4}\left(B_{C(e)}(x,y) + B_N(x,y) + B_{NX}(x,y)\right), \tag{B2a}$$

$$B_{(u)}(x,y) = \frac{1}{4}\left(B_{C(u)}(x,y) + B_N(x,y) - B_{NX}(x,y)\right), \tag{B2b}$$

$$B_{(d)}(x,y) = \frac{1}{4}\left(B_{C(d)}(x,y) + B_N(x,y) + B_{NX}(x,y)\right), \tag{B2c}$$

$$B_{C(u)}(x,y) = (16+xy)B_X(x,y,1) - 8xyB_{XC}(x,y), \tag{B3a}$$

$$B_{C(d,e)}(x,y) = -(4+xy)B_X(x,y,1) + 8xyB_{XC}(x,y), \tag{B3b}$$

$$B_N(x,y) = 3\left(B_X(x,y,1) + \frac{\eta}{25}B_{X1}(x',y',1)\right), \tag{B3c}$$

$$B_{NX}(x,y) = \frac{6\eta}{5}B_X(x,y,\eta) \tag{B3d}$$

$$B_X(x,y,\eta) = -\frac{\eta^2\ln\eta}{(1-\eta)(\eta-x)(\eta-y)} + \frac{x^2\ln x}{(1-x)(\eta-x)(x-y)} + \frac{y^2\ln y}{(1-y)(\eta-y)(y-x)}, \tag{B3e}$$

$$B_{XC}(x,y) = \frac{1}{(1-x)(1-y)} + \frac{1}{x-y}\left(\frac{x\ln x}{(1-x)^2} - \frac{y\ln y}{(1-y)^2}\right), \tag{B3f}$$

where,

$$x = \frac{m_H^2}{m_{W_H}^2}, \quad x' = \frac{m_H^2}{m_{A_H}^2} = \frac{x}{\eta}, \quad \eta = \frac{\tan^2\theta_W}{5}. \tag{B4}$$

Appendix C: Consistency test of the LHT using LFV branching ratios and asymmetries

We introduce useful formulae to parametrize the various branching ratios and asymmetries in the LHT. Since the observables are expressed by a small number of parameters, we can obtain implicit relations among these quantities, which can be used for a consistency check of the model.

The nonzero elements of the Wilson coefficients are only of three types: $A_R^{\rm LHT}$, $g_{Lr}^{\rm LHT}$ and $g_{Ll}^{\rm LHT}$. Here we consider the $\tau \to \mu$ transition. Corresponding formulae for the $\tau \to e$ transition are also derived. According to Eqs. (45), (46), (58), (73) and (74), we can derive

the following parametrization:

$$\frac{g_{Lr}^{\mathrm{I,LHT}}}{eA_R^{\mathrm{LHT}}} = -\,z, \qquad \frac{g_{Ll}^{\mathrm{I,LHT}}}{eA_R^{\mathrm{LHT}}} = -\,z + \Delta^{\mathrm{I}}, \tag{C1a}$$

$$\frac{g_{Lr}^{\mathrm{II,LHT}}}{eA_R^{\mathrm{LHT}}} = -\,z, \qquad \frac{g_{Ll}^{\mathrm{II,LHT}}}{eA_R^{\mathrm{LHT}}} = -\,z + \Delta^{\mathrm{II}}, \tag{C1b}$$

$$\frac{g_{Lr(q)}^{\mathrm{LHT}}}{eA_R^{\mathrm{LHT}}} = Q_q\, z, \qquad \frac{g_{Ll(q)}^{\mathrm{LHT}}}{eA_R^{\mathrm{LHT}}} = Q_q\, z + \Delta_q. \tag{C1c}$$

z is a complex-valued function associated with photon penguin diagrams and a part of Z penguin diagrams.

In leptonic decays, the following formulae are obtained using the above parameters:

$$\begin{aligned}\frac{96\pi}{\alpha}\frac{\mathrm{Br}(\tau^+\to\mu^+\mu^+\mu^-)}{\mathrm{Br}(\tau^+\to\mu^+\gamma)} =& -8\left(4\ln(\delta)+\frac{13}{3}\right)+|z|^2+2\left|-z+\Delta^{\mathrm{I}}\right|^2\\ &+8\mathrm{Re}[-3z+2\Delta^{\mathrm{I}}],\end{aligned} \tag{C2a}$$

$$\begin{aligned}\frac{96\pi}{\alpha}\frac{\mathrm{BA}_Z(\tau^+\to\mu^+\mu^+\mu^-)}{\mathrm{Br}(\tau^+\to\mu^+\gamma)} =& -4\left(4\ln(\delta)+\frac{49}{3}\right)+\frac{1}{6}|z|^2-\left|-z+\Delta^{\mathrm{I}}\right|^2\\ &-4\mathrm{Re}[-z+2\Delta^{\mathrm{I}}],\end{aligned} \tag{C2b}$$

$$\frac{96\pi}{\alpha}\frac{\mathrm{BA}_X(\tau^+\to\mu^+\mu^+\mu^-)}{\mathrm{Br}(\tau^+\to\mu^+\gamma)} = \frac{64}{35}\left(-21+\frac{1}{12}|z|^2-\mathrm{Re}[-z+3\Delta^{\mathrm{I}}]\right), \tag{C2c}$$

$$\frac{96\pi}{\alpha}\frac{\mathrm{BA}_Y(\tau^+\to\mu^+\mu^+\mu^-)}{\mathrm{Br}(\tau^+\to\mu^+\gamma)} = \frac{64}{35}\mathrm{Im}[-z+3\Delta^{\mathrm{I}}], \tag{C2d}$$

$$\frac{96\pi}{\alpha}\frac{\mathrm{Br}(\tau^+\to\mu^+e^+e^-)}{\mathrm{Br}(\tau^+\to\mu^+\gamma)} = -32\left(\ln(\delta)+\frac{4}{3}\right)+|z|^2+\left|-z+\Delta^{\mathrm{II}}\right|^2+8\mathrm{Re}[-2z+\Delta^{\mathrm{II}}], \tag{C3a}$$

$$\frac{96\pi}{\alpha}\frac{\mathrm{BA}_Z(\tau^+\to\mu^+e^+e^-)}{\mathrm{Br}(\tau^+\to\mu^+\gamma)} = \frac{1}{6}\left(32(3\ln(\delta)+5)+|z|^2+\left|-z+\Delta^{\mathrm{II}}\right|^2-8\mathrm{Re}[-2z+\Delta^{\mathrm{II}}]\right), \tag{C3b}$$

$$\frac{96\pi}{\alpha}\frac{\mathrm{BA}_X(\tau^+\to\mu^+e^+e^-)}{\mathrm{Br}(\tau^+\to\mu^+\gamma)} = \frac{4\pi}{35}\left(-|z|^2+\left|-z+\Delta^{\mathrm{II}}\right|^2+16\mathrm{Re}[\Delta^{\mathrm{II}}]\right), \tag{C3c}$$

$$\frac{96\pi}{\alpha}\frac{\mathrm{BA}_Y(\tau^+\to\mu^+e^+e^-)}{\mathrm{Br}(\tau^+\to\mu^+\gamma)} = \frac{48\pi}{35}\mathrm{Im}[\Delta^{\mathrm{II}}], \tag{C3d}$$

$$\frac{96\pi}{\alpha}\frac{\mathrm{BA}_{FB}(\tau^+\to\mu^+e^+e^-)}{\mathrm{Br}(\tau^+\to\mu^+\gamma)} =\frac{1}{4}(-|z|^2+\left|-z+\Delta^{\mathrm{II}}\right|^2+16\mathrm{Re}[\Delta^{\mathrm{II}}]), \tag{C4a}$$

$$\frac{96\pi}{\alpha}\frac{\mathrm{BA}_{ZFB}(\tau^+\to\mu^+e^+e^-)}{\mathrm{Br}(\tau^+\to\mu^+\gamma)} =-\frac{1}{8}\left(-|z|^2+\left|-z+\Delta^{\mathrm{II}}\right|+16\mathrm{Re}[\Delta^{\mathrm{II}}]\right), \tag{C4b}$$

$$\frac{96\pi}{\alpha}\frac{\mathrm{BA}_{XFB}(\tau^+\to\mu^+e^+e^-)}{\mathrm{Br}(\tau^+\to\mu^+\gamma)} =\frac{16}{105}\left(56+|z|^2+\left|-z+\Delta^{\mathrm{II}}\right|^2+16\mathrm{Re}[-2z+\Delta^{\mathrm{II}}]\right), \tag{C4c}$$

$$\frac{96\pi}{\alpha}\frac{\mathrm{BA}_{YFB}(\tau^+\to\mu^+e^+e^-)}{\mathrm{Br}(\tau^+\to\mu^+\gamma)} =\frac{64}{35}\mathrm{Im}[-2z+\Delta^{\mathrm{II}}], \tag{C4d}$$

where BA_a ($a = Z$, X, Y, FB, ZFB, XFB and YFB) denotes asymmetry, A_a multiplied by the branching ratio. We take the limit $\delta \to 0$ except for logarithmically divergent terms in $A_1(\delta)$, $B_1(\delta)$, $D_1(\delta)$ and $D_5(\delta)$. The proportional relation (89) is found from Eqs. (C3c), (C4a) and (C4b). Furthermore, ten independent observables can be expressed by three complex functions.

Similarly, the following formulae are derived for semileptonic decays,

$$\frac{16}{\alpha}\frac{\mathrm{Br}(\tau^+\to\mu^+\pi^0)}{\mathrm{Br}(\tau^+\to\mu^+\gamma)} = \frac{\pi f_\pi^2}{m_\tau^2}(1-x_\pi)^2\left|\Delta_u-\Delta_d\right|^2, \tag{C5a}$$

$$\begin{aligned}\frac{1}{2\alpha}\frac{\mathrm{Br}(\tau^+\to\mu^+\rho^0)}{\mathrm{Br}(\tau^+\to\mu^+\gamma)} = \frac{\pi f_\rho^2}{m_\tau^2}(1-x_\rho)^2\Bigg(&\frac{(1-x_\rho)^2}{x_\rho(1+2x_\rho)}\\ &+\frac{1+2x_\rho}{32}\left|2z+\Delta_u-\Delta_d-\frac{12}{1+2x_\rho}\right|^2\Bigg),\end{aligned} \tag{C5b}$$

$$\begin{aligned}\frac{1}{\alpha}\frac{\mathrm{BA}(\tau^+\to\mu^+\rho^0)}{\mathrm{Br}(\tau^+\to\mu^+\gamma)} = \frac{\pi f_\rho^2}{m_\tau^2}(1-x_\rho)^2\Bigg(&-\frac{(1-x_\rho)^2}{x_\rho(1-2x_\rho)}\\ &+\frac{1-2x_\rho}{32}\left|2z+\Delta_u-\Delta_d+\frac{4}{1-2x_\rho}\right|^2\Bigg),\end{aligned} \tag{C5c}$$

$$\frac{8}{\alpha}\frac{\mathrm{Br}(\tau^+\to\mu^+\eta^{(\prime)})}{\mathrm{Br}(\tau^+\to\mu^+\gamma)} = \frac{\pi f_\pi^2}{m_\tau^2}(1-x_{\eta^{(\prime)}})^2\left|\frac{f^q_{\eta^{(\prime)}}}{\sqrt{2}f_\pi}(\Delta_u+\Delta_d)+\frac{f^s_{\eta^{(\prime)}}}{f_\pi}\Delta_s\right|^2, \tag{C6a}$$

$$\frac{1}{2\alpha}\frac{\mathrm{Br}(\tau^+\to\mu^+\omega)}{\mathrm{Br}(\tau^+\to\mu^+\gamma)} = \frac{\pi f_\omega^2}{m_\tau^2}(1-x_\omega)^2\left(\frac{1}{9}\frac{(1-x_\omega)^2}{x_\omega(1+x_\omega)} + \frac{1+2x_\omega}{32}\left|\frac{2}{3}z+\Delta_u+\Delta_d-\frac{4}{1+2x_\omega}\right|^2\right), \tag{C6b}$$

$$\frac{1}{2\alpha}\frac{\mathrm{Br}(\tau^+\to\mu^+\phi)}{\mathrm{Br}(\tau^+\to\mu^+\gamma)} = \frac{\pi f_\phi^2}{m_\tau^2}(1-x_\phi)^2\left(\frac{2}{9}\frac{(1-x_\phi)^2}{x_\phi(1+2x_\phi)} + \frac{1+2x_\phi}{16}\left|-\frac{2}{3}z+\Delta_s+\frac{4}{1+2x_\phi}\right|^2\right), \tag{C6c}$$

$$\frac{1}{\alpha}\frac{\mathrm{BA}(\tau^+\to\mu^+\omega)}{\mathrm{Br}(\tau^+\to\mu^+\gamma)} = \frac{\pi f_\omega^2}{m_\tau^2}(1-x_\omega)^2\left(-\frac{1}{9}\frac{(1-x_\omega)^2}{x_\omega(1-2x_\omega)} + \frac{1-2x_\omega}{32}\left|\frac{2}{3}z+\Delta_u+\Delta_d+\frac{4}{3(1-2x_\omega)}\right|^2\right), \tag{C6d}$$

$$\frac{1}{\alpha}\frac{\mathrm{BA}(\tau^+\to\mu^+\phi)}{\mathrm{Br}(\tau^+\to\mu^+\gamma)} = \frac{\pi f_\phi^2}{m_\tau^2}(1-x_\phi)^2\left(-\frac{2(1-x_\phi)^2}{9x_\phi(1-2x_\phi)} + \frac{1-2x_\phi}{16}\left|-\frac{2}{3}z+\Delta_s-\frac{4}{3(1-2x_\phi)}\right|^2\right), \tag{C6e}$$

where $x_a = m_a^2/m_\tau^2$. From the above expressions, we can see that various consistency tests are possible with complex functions z, $\Delta_u-\Delta_d$, $\Delta_u+\Delta_d$ and Δ_s.

---

[1] R. Barbieri and A. Strumia, Phys. Lett. B **462** (1999) 144 [arXiv:hep-ph/9905281].

[2] N. Arkani-Hamed, A. G. Cohen and H. Georgi, Phys. Lett. B **513** (2001) 232 [arXiv:hep-ph/0105239]; N. Arkani-Hamed, A. G. Cohen, T. Gregoire and J. G. Wacker, JHEP **0208** (2002) 020 [arXiv:hep-ph/0202089]; N. Arkani-Hamed, A. G. Cohen, E. Katz, A. E. Nelson, T. Gregoire and J. G. Wacker, JHEP **0208** (2002) 021 [arXiv:hep-ph/0206020].

[3] N. Arkani-Hamed, A. G. Cohen, E. Katz and A. E. Nelson, JHEP **0207** (2002) 034 [arXiv:hep-ph/0206021].

[4] C. Csaki, J. Hubisz, G. D. Kribs, P. Meade and J. Terning, Phys. Rev. D **67** (2003) 115002 [arXiv:hep-ph/0211124]; J. L. Hewett, F. J. Petriello and T. G. Rizzo, JHEP **0310** (2003) 062 [arXiv:hep-ph/0211218]; C. Csaki, J. Hubisz, G. D. Kribs, P. Meade and J. Terning, Phys. Rev. D **68** (2003) 035009 [arXiv:hep-ph/0303236].

[5] H. C. Cheng and I. Low, JHEP **0309** (2003) 051 [arXiv:hep-ph/0308199]; H. C. Cheng and I. Low, JHEP **0408** (2004) 061 [arXiv:hep-ph/0405243].

[6] N. Cabibbo, Phys. Rev. Lett. **10** (1963) 531; M. Kobayashi and T. Maskawa, Prog. Theor. Phys. **49** (1973) 652.

[7] B. Pontecorvo, Sov. Phys. JETP **6**, 429 (1957) [Zh. Eksp. Teor. Fiz. **33**, 549 (1957)]; Sov. Phys. JETP **7**, 172 (1958) [Zh. Eksp. Teor. Fiz. **34**, 247 (1957)]; Sov. Phys. JETP **26**, 984 (1968) [Zh. Eksp. Teor. Fiz. **53**, 1717 (1967)]; Z. Maki, M. Nakagawa and S. Sakata, Prog. Theor. Phys. **28** (1962) 870.

[8] J. Hubisz, S. J. Lee and G. Paz, JHEP **0606** (2006) 041 [arXiv:hep-ph/0512169]; M. Blanke, A. J. Buras, A. Poschenrieder, S. Recksiegel, C. Tarantino, S. Uhlig and A. Weiler, Phys. Lett. B **646** (2007) 253 [arXiv:hep-ph/0609284].

[9] M. Blanke, A. J. Buras, A. Poschenrieder, C. Tarantino, S. Uhlig and A. Weiler, JHEP **0612** (2006) 003 [arXiv:hep-ph/0605214]; M. Blanke, A. J. Buras, S. Recksiegel, C. Tarantino and S. Uhlig, Phys. Lett. B **657** (2007) 81 [arXiv:hep-ph/0703254]; M. Blanke, A. J. Buras, S. Recksiegel, C. Tarantino and S. Uhlig, JHEP **0706** (2007) 082 [arXiv:0704.3329 [hep-ph]]; M. Blanke, A. J. Buras, S. Recksiegel *et al.*, [arXiv:0805.4393 [hep-ph]].

[10] M. Blanke, A. J. Buras, A. Poschenrieder, S. Recksiegel, C. Tarantino, S. Uhlig and A. Weiler, JHEP **0701** (2007) 066 [arXiv:hep-ph/0610298].

[11] S. R. Choudhury, A. S. Cornell, A. Deandrea, N. Gaur and A. Goyal, Phys. Rev. D **75** (2007) 055011 [arXiv:hep-ph/0612327].

[12] M. Blanke, A. J. Buras, B. Duling, A. Poschenrieder and C. Tarantino, JHEP **0705** (2007) 013 [arXiv:hep-ph/0702136].

[13] T. Goto, Y. Okada and Y. Yamamoto, Phys. Lett. B **670** (2009) 378 [arXiv:0809.4753 [hep-ph]].

[14] F. del Aguila, J. I. Illana and M. D. Jenkins, JHEP **0901** (2009) 080 [arXiv:0811.2891 [hep-ph]].

[15] M. Blanke, A. J. Buras, B. Duling *et al.*, Acta Phys. Polon. **B41** (2010) 657-683. [arXiv:0906.5454 [hep-ph]].

[16] F. del Aguila, J. I. Illana, M. D. Jenkins, JHEP **1009** (2010) 040. [arXiv:1006.5914 [hep-ph]].

[17] Y. Okada, K. -i. Okumura, Y. Shimizu, Phys. Rev. **D61** (2000) 094001. [hep-ph/9906446].

[18] R. Kitano, Y. Okada, Phys. Rev. **D63** (2001) 113003. [hep-ph/0012040].

[19] S. Yamada, talk at the 8th International Workshop on Tau-Lepton Physics: http://meg.icepp.s.u-tokyo.ac.jp/docs/talks/s_yamada/tau04.shuei.yamada.ppt.

[20] M. Giffels, J. Kallarackal, M. Kramer, B. O'Leary and A. Stahl, Phys. Rev. **D77** (2008) 073010. [arXiv:0802.0049 [hep-ph]].

[21] J. Hubisz and P. Meade, Phys. Rev. D **71** (2005) 035016 [arXiv:hep-ph/0411264]; C. R. Chen, K. Tobe and C. P. Yuan, Phys. Lett. B **640** (2006) 263 [arXiv:hep-ph/0602211]; A. Belyaev, C. R. Chen, K. Tobe and C. P. Yuan, Phys. Rev. D **74** (2006) 115020 [arXiv:hep-ph/0609179].

[22] R. Kitano, M. Koike and Y. Okada, Phys. Rev. D **66**, 096002 (2002) [Erratum-ibid. D **76**, 059902 (2007)] [arXiv:hep-ph/0203110]; V. Cirigliano, R. Kitano, Y. Okada and P. Tuzon, Phys. Rev. **D80** (2009) 013002. [arXiv:0904.0957 [hep-ph]].

[23] C. Jarlskog, Phys. Rev. Lett. **55** (1985) 1039; C. Jarlskog, Z. Phys. **C29** (1985) 491-497.

[24] J. Hubisz, P. Meade, A. Noble *et al.*, JHEP **0601** (2006) 135. [hep-ph/0506042]; M. Asano, S. Matsumoto, N. Okada and Y. Okada, Phys. Rev. **D75** (2007) 063506. [hep-ph/0602157].

[25] M. L. Brooks *et al.* [MEGA Collaboration], Phys. Rev. Lett. **83** (1999) 1521 [arXiv:hep-ex/9905013].

[26] U. Bellgardt *et al.* [SINDRUM I Collaboration], Nucl. Phys. **299**, 1 (1988).

[27] C. Dohmen *et al.* [SINDRUM II Collaboration], Phys. Lett. B **317**, 631 (1993).

[28] W. H. Bertl *et al.* [SINDRUM II Collaboration], Eur. Phys. J. **C47** (2006) 337-346.

[29] W. Honecker *et al.* [SINDRUM II Collaboration], Phys. Rev. Lett. **76**, 200 (1996).

[30] B. Aubert *et al.* [BABAR Collaboration], Phys. Rev. Lett. **104** (2010) 021802. [arXiv:0908.2381 [hep-ex]].

[31] Y. Miyazaki *et al.* [Belle Collaboration], Phys. Lett. B **660** (2008) 154 [arXiv:0711.2189 [hep-ex]].

[32] B. Aubert *et al.* [BABAR Collaboration], Phys. Rev. Lett. **98** (2007) 061803 [arXiv:hep-ex/0610067].

[33] Y. Miyazaki *et al.* [BELLE Collaboration], Phys. Lett. B **648** (2007) 341 [arXiv:hep-ex/0703009].

[34] B. Aubert *et al.* [BABAR Collaboration], Phys. Rev. Lett. **103** (2009) 021801. [arXiv:0904.0339 [hep-ex]].

[35] Y. Nishio *et al.* [Belle Collaboration], Phys. Lett. B **664** (2008) 35 [arXiv:0801.2475 [hep-ex]].

[36] B. Aubert *et al.* [BABAR Collaboration], Phys. Rev. Lett. **99** (2007) 251803 [arXiv:0708.3650

[hep-ex]].

[37] B. Aubert *et al.* [BABAR Collaboration], Phys. Rev. Lett. **100** (2008) 071802 [arXiv:0711.0980 [hep-ex]].

[38] J. Adam *et al.* [MEG Collaboration], Nucl. Phys. **B834** (2010) 1-12. [arXiv:0908.2594 [hep-ex]]; R. Sawada, Proc. Sci. ICHEP2010 (2010) 263.

[39] Y. G. Cui *et al.* [COMET Collaboration], KEK Report 2009-10; R. M. Carey *et al.* [Mu2e Collaboration], fermilab-proposal-0973.

[40] T. Aushev, W. Bartel, A. Bondar *et al.*, [arXiv:1002.5012 [hep-ex]]; B. O'Leary *et al.* [SuperB Collaboration], [arXiv:1008.1541 [hep-ex]].

[41] A. Brignole and A. Rossi, Nucl. Phys. B **701** (2004) 3 [arXiv:hep-ph/0404211]; E. Arganda, M. J. Herrero and J. Portoles, JHEP **0806** (2008) 079 [arXiv:0803.2039 [hep-ph]].

[42] T. Feldmann, P. Kroll and B. Stech, Phys. Rev. D **58**, 114006 (1998) [arXiv:hep-ph/9802409]; T. Feldmann, P. Kroll and B. Stech, Phys. Lett. B **449**, 339 (1999) [arXiv:hep-ph/9812269].